Westshore Coastal Process Investigation

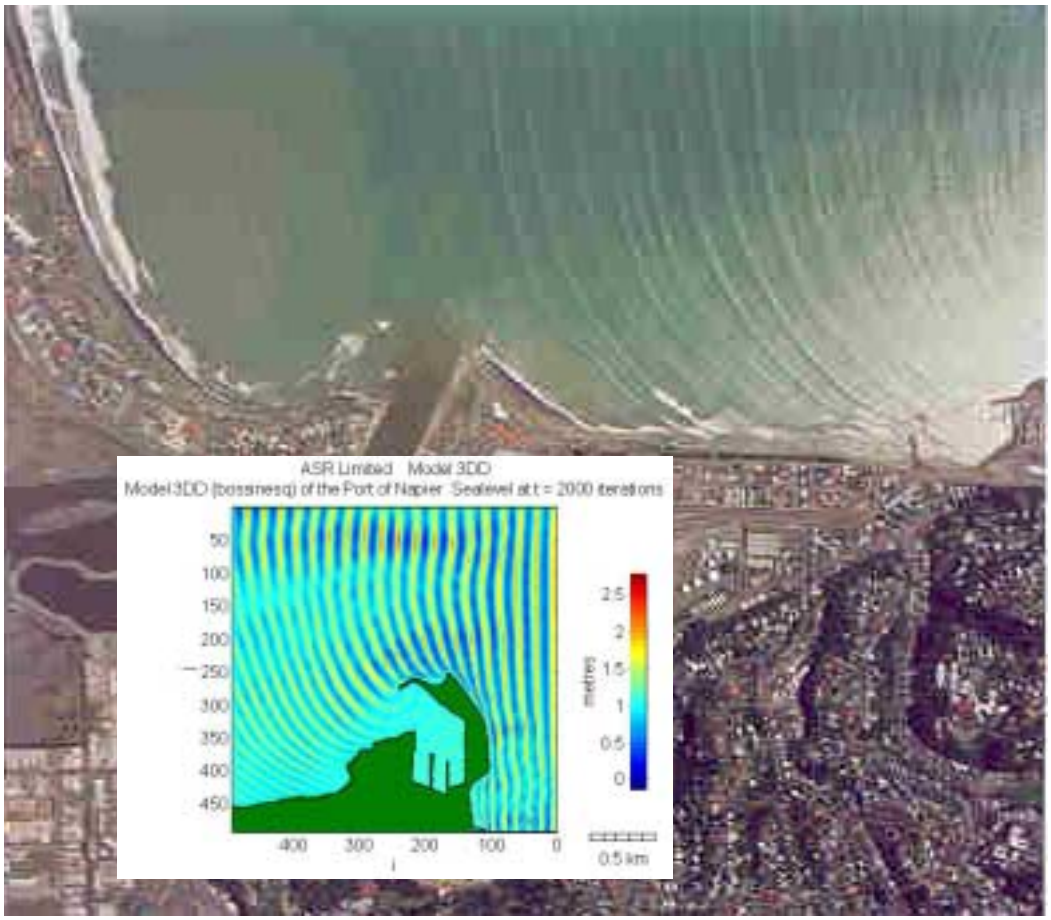

Prepared For Napier City Council

ASR

Marine and Freshwater Consultants

Cover: Aerial view of Westshore Beach and Ahuriri, showing the refraction pattern of waves moving into the bay. Inset, numerical model output of waves refracting past the Port of Napier.

Westshore Coastal Process Investigation

A Study to Determine the Coastal Processes in the Bay at Westshore and Provide a Long-Term Solution to Erosion Problems

Prepared for the
Napier City Council

By Shaw Mead, Kerry Black & Peter McComb (ASR Ltd)

September 2001

Marine and Freshwater Consultants
P.O. Box 13048, Hamilton, New Zealand. Ph. +64 7 834 8180,
Fax. +64 7 834 8188 E-mail enquiries@asrltd.co.nz Website www.asrltd.co.nz

Disclaimer

This project involves field data interpretation and numerical modelling of beaches, sediment transport and reefs. Care has been taken to calibrate the models and validate their behaviour and to interpret the field data in the light of existing knowledge of similar systems. The information in the report is provided to Napier City Council in good faith for their use and interpretation.

Intellectual Property

This project involves new design concepts developed by ASR Ltd. Copyright and intellectual property arising out of the design of artificial reefs or any other component of the recommended or constructed nearshore structures, as a result of this project, remains solely with ASR Ltd. Napier City Council retains the right to construct the recommended structure at Westshore Beach. No third party has the right to copy, duplicate or construct any part of the structure at other locations, without receiving the express permission of ASR Ltd. “Wave Rotating” components of the design have patent protection, registered by ASR Ltd (Patent No. PCT/NZ00/00250).

Executive Summary

Westshore Beach has been subject to erosion since the late 19th century due to a combination of human activities and natural events. In the past decade, the beach face above mean high water spring tides has been nourished annually (12,000 m^3/yr) to combat the continuing erosive trend. However, the question of long-term sustainability of renourishment, and whether it will continue to safeguard against erosion in the future has been raised.

To successfully protect a coastline from erosion, the processes that are causing the problem must first be identified so that the cause can be addressed, rather than the effects. Napier City Council commissioned the present study to determine the coastal processes that are influencing Westshore Beach. A field programme, with this aim in mind, was designed to collect data that were used together with numerical modelling to identify the processes operating in the Westshore Bay area and to form the basis for recommendations of remedial actions to combat the ongoing erosion problem. The field data and numerical modelling are supported by volumetric comparisons of bathymetric surveys between 1954 and 2000.

Three key mechanisms were identified in the Westshore Bay area;

1. **Equilibrium beach alignment**
2. **Compartmentalisation of sediment transport**
3. **The headland extension effect**

Mechanism 1 is idealised in Figure 1. The beaches in the area appear to be in balance with the wave climate, headland sheltering and sediment supply. The effect of the Port's extensions in this context are to increase the headland sheltering effect, i.e. to provide more shelter along Westshore Beach from the south. By this mechanism alone, the sheltering effect would cause the beach to accrete. While Mechanism 1 should lead to beach accretion, the other Mechanisms are expected to lead to erosion.

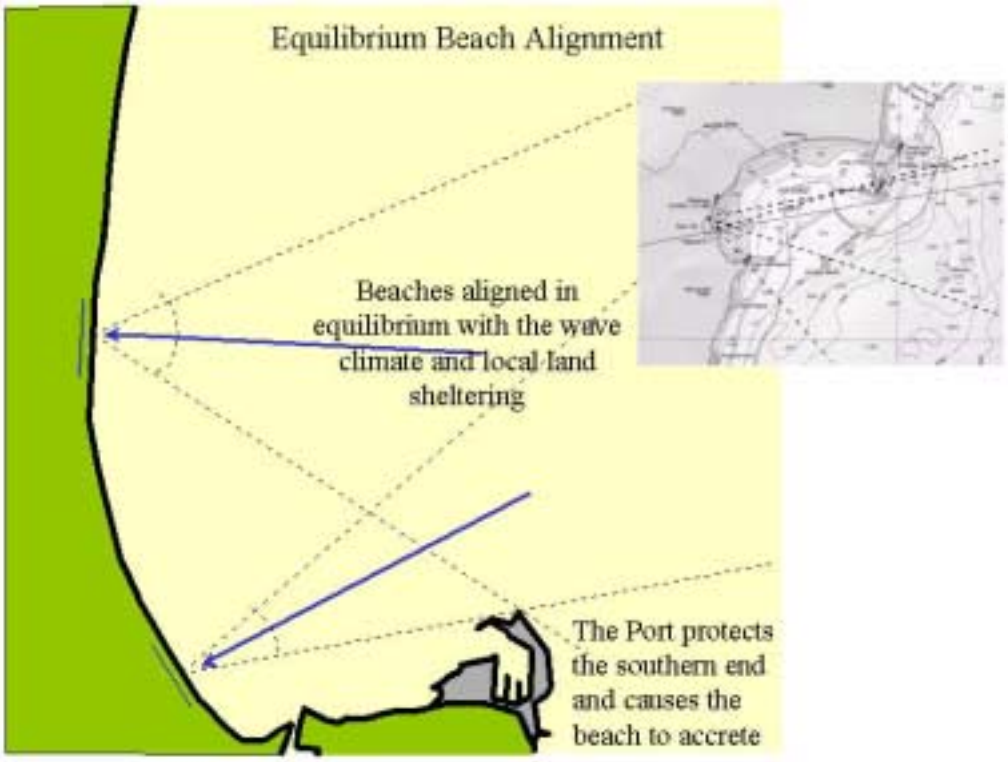

Figure 1. Idealised diagram of equilibrium beach alignment – **Mechanism #1**.

The present residual current patterns in the Westshore Bay result in the compartmentalisation of the area into 4 distinct compartments (Fig. 2):

- Northern beach
- Westshore sand fillet, which is a triangular wedge of sand in Westshore Bay
- Port and dredged channel
- Marine Parade Beach

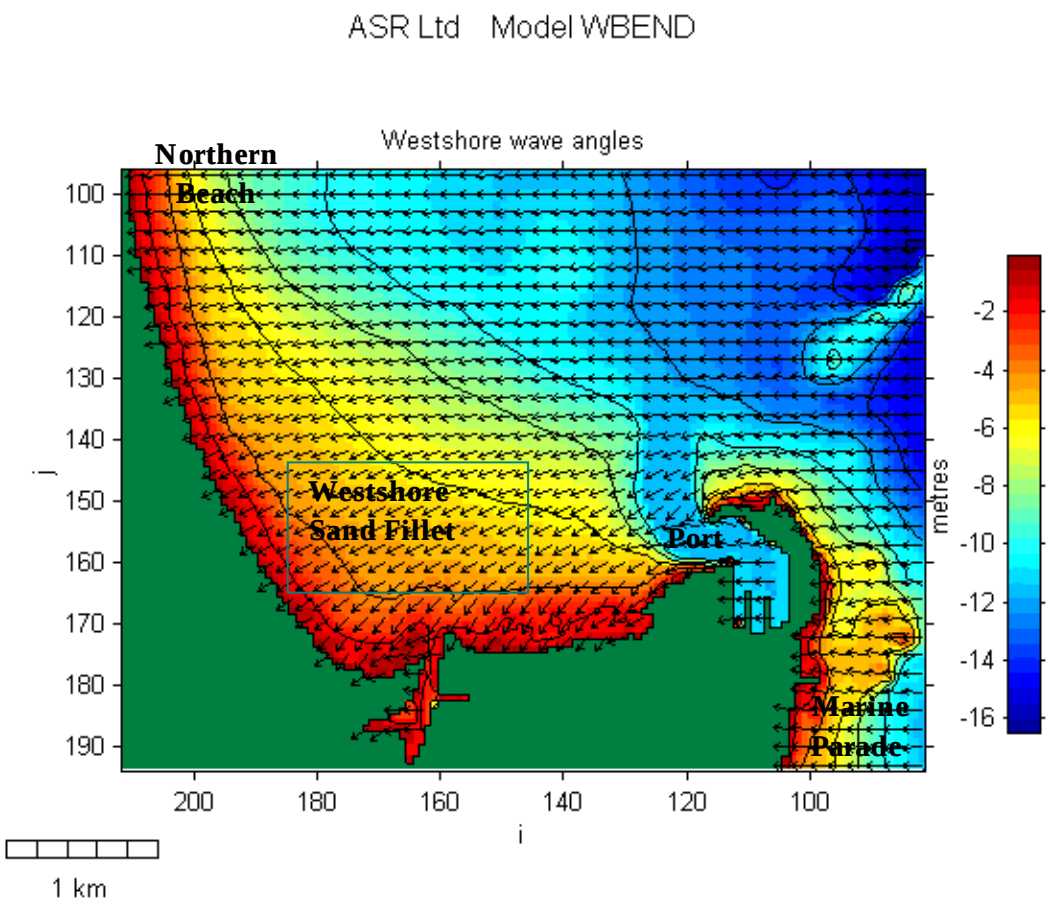

Figure 2. Bathymetry and wave angles at Westshore, showing the northern beach, Westshore sand fillet, Port and dredged channel and Marine Parade beach.

The Port and dredged channel are located at the eastern end, within the Westshore sand fillet. From the bathymetry, it can be seen that the sand fillet is a distinctive zone and that the beach is simply the upper level of this fillet. As such, the beach can be seen as residing within the sand fillet compartment. Notably, the Port and dredge channel are clearly also in this same compartment.

The important implications of the model results and data analysis are discernible as follows.

The flow oscillates at hourly, daily and weekly periods in Westshore Bay and the currents are often directed offshore, along the headland and across the Port's dredged channel. Consequently, sediment can be carried from the Westshore sand fillet into the channel and this material is being lost due to dredging. The dredging records show that about 11,000 m^3/yr (Hume *et* al., 1989) is dredged from the western side of the channel, and this has presumably come from the Westshore sand fillet.

There are also times when the currents are strong and directed north along the offshore side of the main Port breakwater. These flows are clearly able to transport sand into the channel, with the assistance of wave action to suspend the sands. The Port's maintenance dredging of 25,000 m^3/yr (Hume *et al.*, 1989) from the eastern side of the channel is evidence of this process.

Finally, the current vectors show that sand transported along the main Port breakwater can bypass the channel on the north-eastern side. Similar results have been obtained using tracers and numerical model studies at Port Taranaki (McComb and Black, 1999; Black and McComb, 1999). It was shown that while about 120,000 m3/yr collected in the tip shoal around the Port breakwater, an equally large amount was not trapped and continued to go past the Port.

These results provide the basis for an important mechanism that can result in shoreline erosion at Westshore. The Port is within the Westshore sand fillet compartment and so the Port's dredging, by removing sand and placing it offshore, will be degrading the volume in the fillet and thereby causing erosion of the beach. In other words,

- **the Port dredging operation is acting as a sediment sink in a recirculating sediment loop.**

Thus, it is essential that all sand dredgings from the Port are placed inshore, as recently agreed to by the Port and Regional Council. Mechanism 2 is idealised in Figure 2.

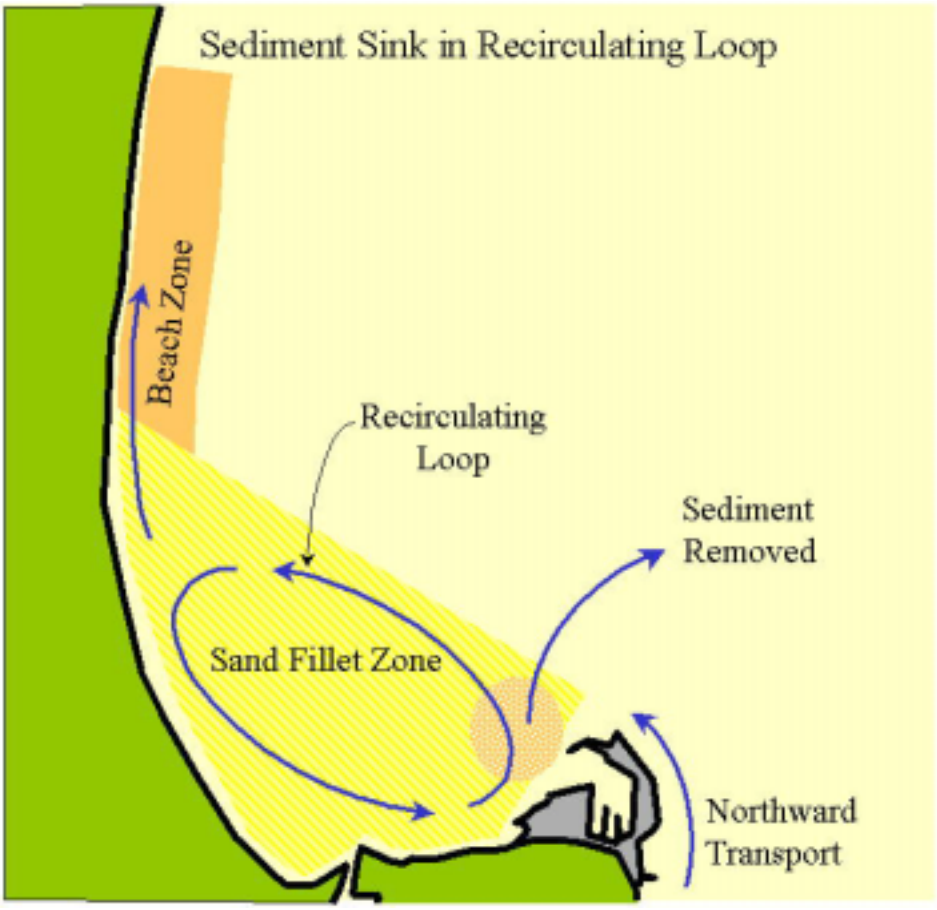

Figure 3. Idealised diagram of the sediment sink in the recirculating loop on the Westshore sand fillet – **Mechanism** #2.

Mechanism 3 is idealised in Figure 4. Modelling of Westshore Bay with and without the Port in place shows large differences in current circulation patterns. The presence of the Port diverts sand from its natural pathway around the coast, redirecting the sediment pathway into deeper water and therefore away from Westshore beach. Sand is deposited in deeper water and cannot easily find its way back to the beach due to the presence of the headland eddy directing flows offshore. The headland extension (the Port) disrupts the continuous recirculating sediment pathway over the Westshore sand fillet.

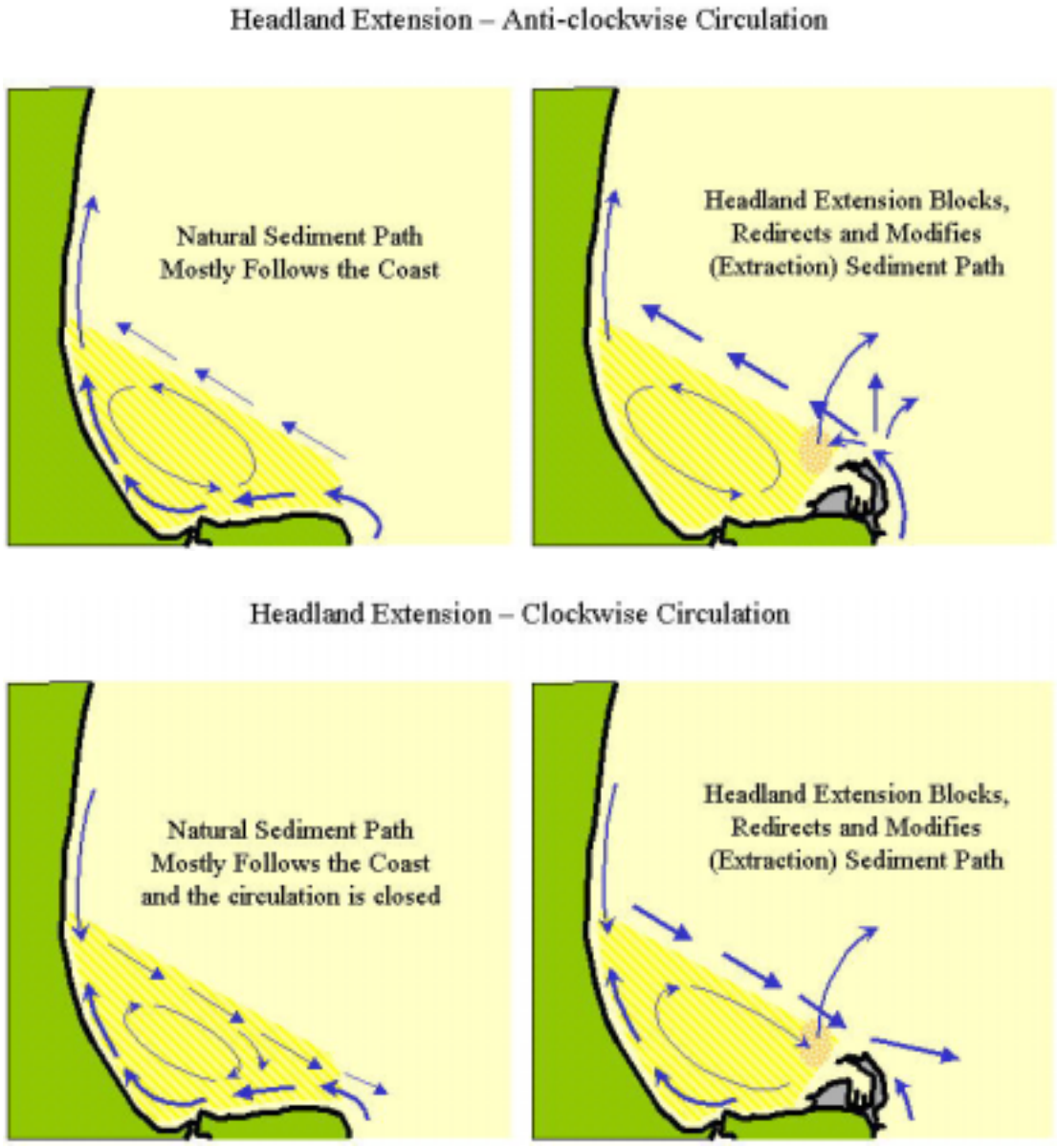

Figure 4. Idealised diagram of the effects of the headland extension (Port development) at Westshore Bay – **Mechanism #3**.

Mechanisms 2 and 3 at Westshore Bay indicate that sediment is constantly being lost out of the Westshore sand fillet. These losses were verified by volumetric comparisons of existing nautical charts and recent bathymetry surveys in the study area. The comparisons show the beach erosion observed at Westshore is symptomatic of a much larger problem, with volumes of around 131,000 m^3/yr being lost from the Westshore sand fillet. A new complete survey of the region is needed to confirm these findings and to record changes over the fillet in the last

20 years. However, the existing data shows a consistent erosionary trend. When the "beach compartment" at Westshore out to the 4 m depth contour is considered the average sediment loss was found to be 30,000 m^3/yr. Sediment fluxes in the Westshore Bay area are summarised in Figure 5.

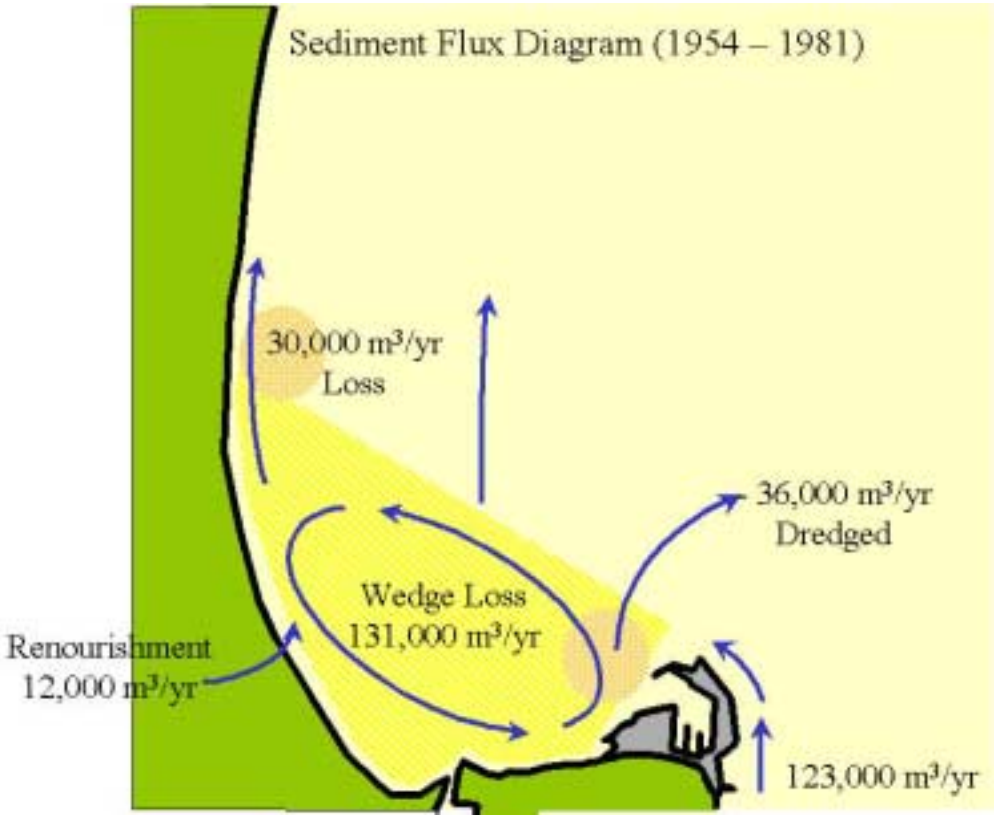

Figure 5. Summary of the sediment fluxes in Westshore Bay.

The recommended option for the mediation of the erosion occurring along Westshore Beach is shown in Figure 6. Due to the recent granting of resource consent, the Port can now use an inshore dump ground that is likely to positively impact on the beach erosion. While the total volume losses from the Westshore sand fillet are very large (131,000 m^3/yr between 1954 and 1981), the average annual volume of dredged sand that can now be dumped in the beach compartment (36,000 m^3/yr) is very similar to the amount of sand presently being lost (30,000 m^3/yr).

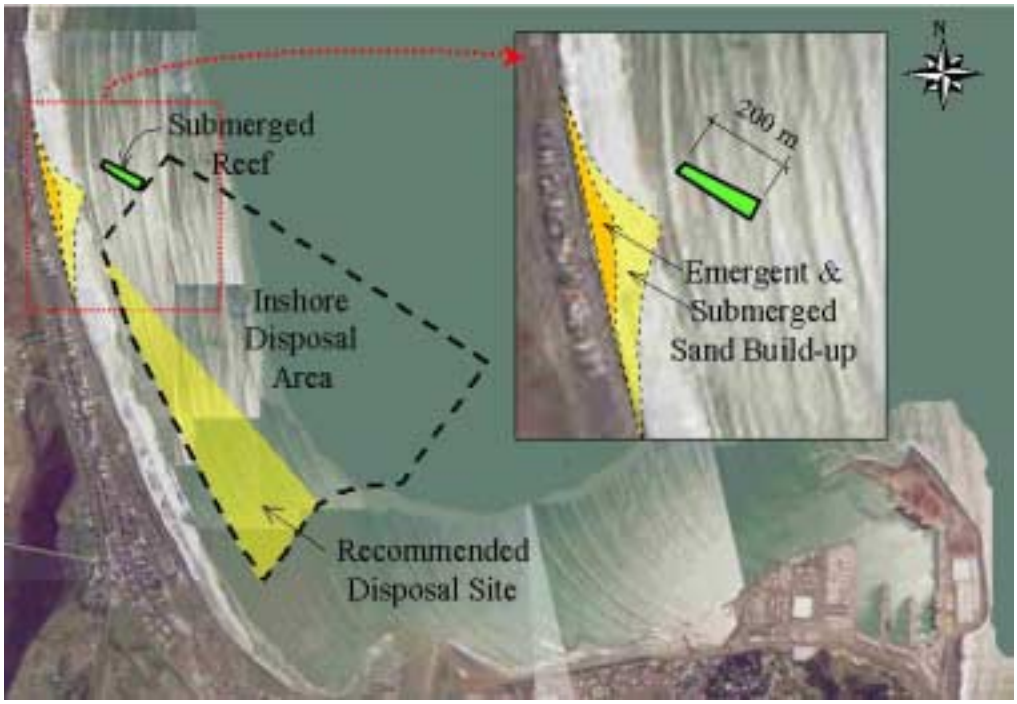

Figure 6. Recommended strategy for erosion remediation at Westshore.

Thus, the Port's dumping operations will have a major beneficial impact on the beach erosion if the Port's dredged sand is deposited as close as possible to the beach, and preferentially at the southern end of the beach in the allowable zone. This will ensure maximum benefit on the beach itself, even though offshore erosion is expected to continue. Thus, in order for the Port's dredging to provide optimal benefit, we recommended that:

- **The Port's dredged sand be preferentially placed within the beach compartment (shallower than the 5 m contour) in the zone marked in Figure 6;**
- **The orientation of the offshore side of this region is not parallel to the beach, but is set at an angle in order to rotate the waves as they cross the artificial sand bar and encourage longshore transport to the south, and;**

- **To gain further insight into whether the Port's operations alone will eradicate the beach erosion, the dredged sand will need to be monitored after placement, through bathymetric survey and using physical oceanographic methodologies.**

With respect to mitigation, the Port's inshore placement of dredged sand will provide security against severe erosion. However, the Port's dredging operations are sporadic and the volumes of dredge material vary, and thus beach protection cannot be guaranteed. In the years after a dredging campaign, the offshore dump mound will create a broad "over-full" sand bar that is likely to erode more rapidly than a beach with an equilibrium profile. Also, only a fraction of the sand will move onto the beach. In other years with no nourishment, the beach will be fully exposed to erosion.

In this context, more permanent protection would be beneficial to:

- **Act as a coastal control point;**
- **Smooth out the sporadic nature of the dredging events;**
- **Capture the sediment in a salient to act as a reservoir in the lean years;**
- **Optimise the benefits of the Port's "on-demand" dredging program; and**
- **Provide a sustainable solution to the beach erosion.**

After considering the various coastal protection options, we ultimately recommend an offshore, submerged reef at the northern end of the Port's inshore dump ground. The position is also centred on the area of worst erosion along the shoreline. Design of the submerged reef should also consider multi-purpose options such as optimising surfing conditions (an artificial surfing reef - ASR) and incorporation of habitat enhancement, which can greatly enhance the amenity and environmental values of coastal structures.

Recommended additional data collection and design studies are as follows:

- **A detailed bathymetric survey of the sand fillet and environs at Westshore to determine the rates of bed level adjustment over the last 20 years.**

- **Wave/current and sediment transport measurements at the proposed site of the ASR. Similar techniques to those used in the present study, amalgamated with the technical methods of Black and Vincent (2000), could be adopted.**
- **Monitoring of the dredge spoil and beach after placement, possibly including tracer experiments at the mound and around the Port.**
- **Detailed optimisation and design of the ASR. The estimated volume of the reef is 12,250 m^3 and the estimated inclusive cost of construction and additional studies is $1.1 million, based on a geotextile construction method and utilisation of the Port's dredge sand.**

TABLE OF CONTENTS

EXECUTIVE SUMMARY I

1 INTRODUCTION 1

1.1 BACKGROUND 1
1.2 STUDY BRIEF 3

2 METHODS AND NUMERICAL MODELLING 4

2.1 THE APPROACH 4
2.2 NUMERICAL WAVE REFRACTION MODELLING 5
2.3 CURRENT AND BOUSSINESQ NUMERICAL MODELLING 7
2.4 NUMERICAL MODEL GRID 8
2.5 SOURCES OF INFORMATION 10

3 HISTORICAL BACKGROUND 12

3.1 INTRODUCTION 12
3.2 EARLY HISTORY 12
3.3 THE CHANGING CHARACTER OF WESTSHORE BEACH – THE LAST 120 YEARS 13
3.4 DEVELOPMENT OF THE PORT OF NAPIER 17
3.5 SUMMARY 20

4 FIELD DATA COLLECTION AND ANALYSIS 21

4.1 INTRODUCTION 21
4.2 METHODS 21
4.2.1 Surficial sediments 23
4.2.2 Time-lapse video recording 25
4.3 WAVES AND CURRENTS 26
4.3.2 Wind and tide data 31
4.4 RESULTS 31
4.4.1 Surficial sediments 31
4.4.2 Wind, tide and barometric pressure 34
4.4.3 Waves 35
4.4.4 Currents 47
4.4.5 Suspended sediment concentrations 53
4.4.6 Tides 56
4.4.7 Seabed Description 56
4.4.8 Beach Profiles 57

5 NUMERICAL MODEL CALIBRATION 69

5.1 INTRODUCTION 69
5.2 THE PROCESS OF MODEL CALIBRATION 70
5.3 WAVE HEIGHT AND DIRECTION 71
5.4 BOUSSINESQ MODELLING 74
5.5 CALIBRATION OF THE 3DD DEPTH-AVERAGED CIRCULATION MODELING 76

5.5.1 Hydrodynamics *76*
5.6 CALIBRATION RESULTS 77

6 MECHANISMS IN OF THE BAY NORTH OF NAPIER 81

6.1 INTRODUCTION AND METHODOLOGY 81
6.2 THE ESTUARY AND THE EARTHQUAKE 81
6.3 MECHANISM #1 - EQUILIBRIUM BEACH ALIGNMENT 82
6.3.1 Hawke Bay shoreline shape *83*
6.3.2 Model GENIUS *83*
6.4 MECHANISM #2 – SEDIMENT TRANSPORT COMPARTMENTS 87
6.4.1 Bathymetry *88*
6.5 MECHANISM #3 - HEADLAND EXTENSION 97
6.5.1 Wind-Driven Circulation Patterns *108*
6.6 VOLUME CALCULATIONS 113
6.6.1 The Beach Compartment *115*

7 RECOMMENDATIONS FOR REMEDIAL WORKS 117

7.1 INTRODUCTION 117
7.2 PROTECTIVE WORKS OPTIONS 120
7.2.1 Beach Nourishment *120*
7.2.2 Sea Walls *121*
7.2.3 Groynes and Artificial Headlands *122*
7.2.4 Detached Breakwaters *123*
7.2.5 Submerged Reefs and Surfing Reefs *126*
7.2.6 Dune Management *130*
7.3 RECOMMENDED OPTION FOR THE MEDIATION OF THE EROSION OCCURRING ALONG WESTSHORE BEACH 130

ACKNOWLEDGEMENTS 133

REFERENCES 134

APPENDIX 1: WAVE REFRACTION MODEL WBEND

APPENDIX 2: HYDRODYNAMIC AND ADVECTION/DISPERSION MODEL 3DD

APPENDIX 3: SEDIMENT TRANSPORT MODEL GENIUS

APPENDIX 4: SUBMERGED REEFS FOR COASTAL PROTECTION

1 INTRODUCTION

1.1 Background

Westshore Beach is located to the north of Napier City, in Hawke Bay, on the East Coast of the North Island, New Zealand (Fig. 1.1.). Westshore Beach has been subject to erosion (and in some instances accretion) since the late 19th century due to a combination of human activities (building various coastal structures, redirection of rivers, etc.) and natural events (summarised on Chapter 3).

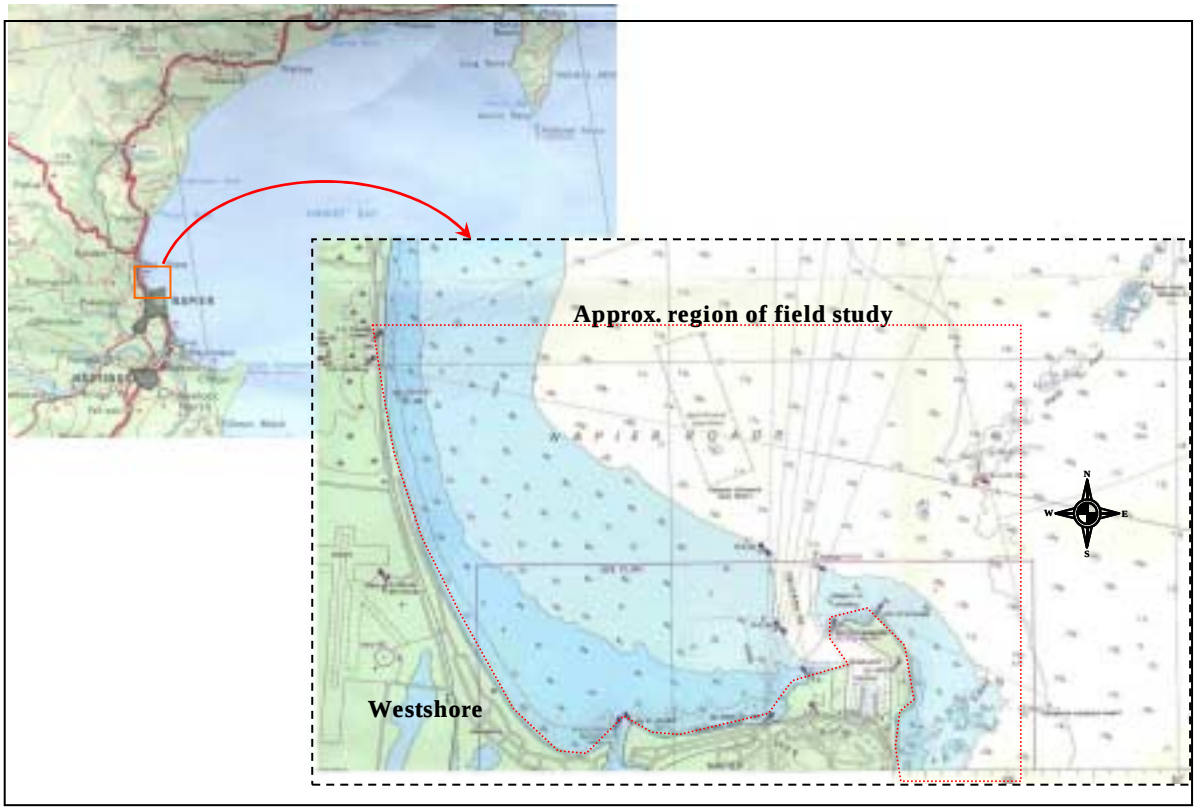

Figure 1.1. Location map.

In recent years, 12,000 m^3 of renourishment material (fine gravel and sand) has been placed annually along the beach at Westshore. This material is deposited in a manner that forms a wave uprush barrier, which to date has withstood intermittent storms, sustaining little or no damage. However, questions have been raised about the long-term sustainability of renourishment, and whether it will continue to safeguard against erosion in the future. In

addition, the renourishment does not fulfil the aspirations of the Westshore residents, who would like the beach to be user-friendly (the sand/gravel barrier is currently very steep and limits access to the seashore) and possibly a return to a past state, when a wide and gently sloping sandy beach was present (Fig. 1.2).

Figure 2.1. A selection of photographs of Westshore Beach showing a wide sandy beach from the late 1970's and early 1980's, the time commonly referred to as the beginning of the most recent erosion period. (Photographs courtesy of D. Foreman).

Napier City Council awarded ASR the Professional Services Contract No. 902 for the collection and analysis of oceanographic field data to determine the actions and/or reactions along the coastline of Hawke Bay having an influence on Westshore Beach. These data are used together with numerical modelling to identify the processes operating at Westshore Beach and offshore in the Bay to form the basis for recommendations of remedial actions to combat the ongoing erosion problem.

The name “Weshshore Bay” is used through the text of this report to describe the bay north of Napier, which incorporates, Westshore Beach, Ahuriri and the Port of Napier.

1.2 Study Brief

The principle objective of the study was to produce a high quality, in depth, assessment of the processes and patterns in Westshore Bay (Fig. 1.1) with respect to current, wave and wind conditions. This would incorporate the acquisition of sufficient field data to gain an understanding of coastal processes in the Westshore area and to provide calibration and validation of numerical model simulations. The data and modelling, when completed, would then enable a clear understanding of the coastal mechanisms at work and form the basis for recommendations for remedial/arresting actions or works.

In summary, the primary aims were to provide:

- high-quality oceanographic field data for the Westshore area including data on waves and currents, suspended sediment, tides, beach profiles, wind, air pressure and sediment particle size ;
- calibrated numerical models of the wave transformation and circulation processes in the bay north of Napier;
- a general picture of coastal processes and hydrodynamic circulation due to waves, wind and currents in the bay;
- formulate options and recommendations for the mediation/arrest of the erosion occurring along Westshore Beach, with accompanying cost estimates;

2 METHODS AND NUMERICAL MODELLING

2.1 The approach

The study aims were achieved through a series of stages as outlined here. A field programme was undertaken that incorporated a 4-week current/wave meter deployment and suspended sediment trapping, time-lapse video recording, beach profile surveys and surficial sediment sampling (Chapter 4). In addition, existing wave climate data, aerial photographs, nautical charts, wind data, atmospheric pressure data, tidal records, the results of other oceanographic and coastal studies of the Westshore Region of Hawke Bay and any other applicable metocean data were collected and analysed.

Specifically, fieldwork, data collection and analysis included:

- a literature search of the previous scientific and consulting work in the Westshore area of Hawke Bay that was relevant to the current study;
- digitising of nautical charts and Port of Napier soundings to establish grids for numerical modelling and volume comparisons;
- collection and analysis of 60 sediment samples to establish sediment grain size distributions over the study area;
- current/wave meter deployment at 4 sites within the study area for model calibration and tidal range;
- suspended sediment trapping at 8 sites in the study area (2 trap heights, 0.4 and 0.8 m);
- analysis of existing wave-rider buoy data to produce a short-term nearshore wave climate and numerical model calibration;
- fortnightly beach profile surveys at 14 sites during the field study;

- analysis of existing beach profile data;
- recording of time-lapse video (5 min every 1hr and 30 min during daylight during the field study);
- analysis of existing wind data to produce a wind climate for numerical wave modelling;
- analysis of historical aerial photographs to assess shoreline changes in the study area and assist with wave refraction model validation, and;
- analysis of existing tidal data for numerical wave modelling.

These data were used to establish a thorough understanding of the coastal processes in the Westshore area (Chapter 6), to calibrate and validate three numerical models (Chapter 5), and to present options and make recommendations for the mediation/arrest of the erosion occurring along Westshore Beach (Chapter 7).

Cost estimates for construction of an offshore geotextile reef were established by,

- establishing sources and costs of construction materials to fill the geotextile containers used for the reef structure;
- receiving cost estimates for geotextile containers, and;
- establishing the cost of mobilising construction equipment in the Hawke's Bay region.

2.2 Numerical Wave Refraction Modelling

The modelling was undertaken to identify the coastal processes operating in the Westshore area and assess remedial measures to prevent erosion. Three different models from the "3DD Computational Marine and Freshwater Laboratory" were used:

- WBEND – wave refraction and longshore transport modelling;
- GENIUS – long-term beach stability modelling; and
- 3DD – hydrodynamics and Boussinesq short-wave simulations

The model WBEND (Wave BENDing) (Black and Rosenberg, 1992a) is coupled to a full suite of hydrodynamic, dispersal and sediment transport models in the 3DD suite. WBEND is a 2-dimensional refraction and longshore sediment transport model for monochromatic or spectral inputs over variable topography (Appendix 1). The model applies an iterative, finite-difference solution to the wave action equations to rapidly solve for wave height and angle. Longshore sediment transport fluxes, bottom orbital currents, near-bed reference concentrations of suspended sediments, breakpoint location and breaker heights and angles are determined by the model.

Model WBEND has been applied to a broad range of physical environments and has been calibrated and shown to be accurate on many occasions. Moreover, the model has been successfully validated and used as one of the primary design tools for the beach process evaluation and submerged reef design for erosion prevention on the Gold Coast (Black *et al*., 1998) and Noosa Main Beach in Australia (Black *et al.*, 2001). WBEND has been validated in open coast conditions (Black *et al*., 1997, 1998; McComb *et al*., 1997), against field measurements (Black *et al.*, 1995; Hutt, 1997; Mead *et al*., 1998a; Mead and Black, 1999; Mead and Black, 2001a,b,c) and laboratory data (Black and Rosenberg, 1992a,b). Thus, WBEND was used for wave refraction tests at Westshore.

The aim of the WBEND refraction modelling was to gain better understanding of:

- wave height distribution from north to south along the shoreline as a function of input wave direction, with particular attention to sheltering of the bay caused by the headland and port breakwater;
- wave height transformation in the Westshore area;

- orientation of waves at the shoreline in relation to net sediment transport, and;
- to create an input file for Model 3DD to investigate current velocities and directions.

Wave/current meter measurements were used to calibrate the model.

2.3 Current and Boussinesq Numerical Modelling

Model 3DD (3-Dimensional Dynamics) contains 4 process models in a single computer code (Black, 1995) (Appendix 2). These are: (i) 2- and 3-dimensional hydrodynamics, (ii) advection/diffusion of salinity and/or temperature, (iii) surface gravity waves in shallow water using a Boussinesq approximation and (iv) ocean/atmosphere heat transfers. Because of its general capacity, 3DD has been applied to a wide range of vertically-stratified and homogeneous ocean, continental shelf and shallow-water environments (e.g. Young *et al*., 1993; Middleton and Black, 1994; Black *et al*., 2000a,b). Based around highly accurate mixed Eulerian/Lagrangian mathematical techniques, the model 3DD provides state-of-the-art- hydrodynamic and dispersal simulations. Developed and sustained by comprehensive field measurements and supplementary modelling support packages, the 3DD suite has been validated to achieve an unprecedented level of numerical refinement. High-quality animated graphics allow the model outputs to be easily interpreted by non-scientific people.

The aim of the 3DD hydrodynamic modelling was to:

- gain better understanding of wave and wind-driven currents, as these, in combination with wave action, are the dominant process controlling sediment movement and beach morphology, and thus;
- identify the coastal processes operating at Westshore and assess potential remedial measures to address the erosion problem along this stretch of the coast.

Calibration of the Model 3DD was carried out using the wave/current datasets that were collected during the field work (as described above), and validated with aerial photographs, previous field investigations, etc.

2.4 Numerical Model Grid

Several numerical modelling grids were developed by digitising nautical charts of "Napier Roads" (NZ 5712 – 1981; NZ 57 - 1953), Port of Napier bathymetry surveys and aerial photographs. Data were compiled into a bathymetry grids using Surfer© surface mapping system (Golden Software, Inc.). The Kriging method of interpolation was selected for grid creation. Kriging is a geostatistical gridding method that has proven useful and popular in many fields (Golden Software, Inc., 1996). This method produces contour and surface plots from irregularly spaced data such as that produced from digitising charts and bathymetry surveys. Kriging attempts to express trends that are suggested in the data, so that, for example, high points might be connected along a ridge, rather than isolated by bull's-eye type contours (Golden Software, Inc., 1996). Kriging is an exact interpolator, i.e. this method of gridding honours data points exactly when the data point coincides with the grid node being interpolated. Validation tests comparing survey data with grids created using Kriging have shown that the method is very accurate and that errors associated with grid creation are based on the accuracy of the depth sounding equipment (Mathew *et al.*, 2000), and in this case, the depths shown on the nautical chart and those recorded by the Port of Napier.

Aerial photographs of the bay north of Napier were also digitised and incorporated into the grids to verify the shoreline where survey data was absent and set the land boundaries for the bay.

A 211 x 207 cell grid was created from the compiled data (40 x 40 m cell size) and used for the majority of the numerical wave refraction modelling (Fig. 2.1). The grid extends from Bay View in the north to beyond Town Reef in the south (approximately 8.3 km and encompasses Pania Reef, extending to depths >20 m offshore (east). After the 180° rotation, the grid is oriented with the coast on the right hand side as required by WBEND. Thus, a wave direction of zero degrees denotes a wave heading due west (from the east). In the models, wave directions to the north of east are positive and wave directions to the south of

east are negative. For example, an angle in the model of –45° is at 135° True (southeast) and a model angle of +45° refers to 45°True (northeast). Note that due to grid rotation, this is opposite to standard directional convention.

For the circulation modelling, a grid of 120 m cells (using every 3rd cell from the 40 m grid) was adopted. This was also extended to the north and south to move the model boundaries away from the area of interest around Westshore Bay. A further grid was established by eliminating the Port and reclamation from the 120 m grid. Circulation modelling was then undertaken to examine the flow patterns without the Port, in order to isolate the Port's influence.

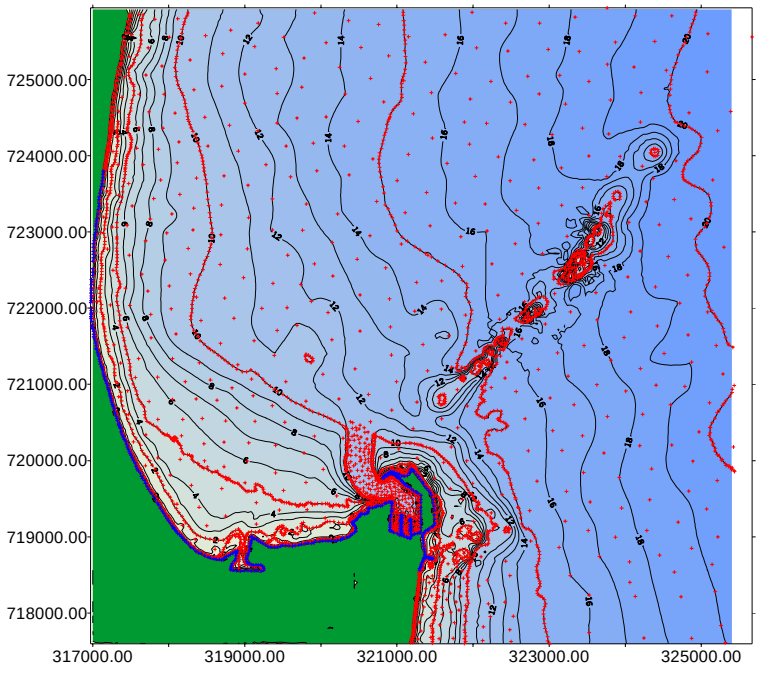

Figure 2.1. Contour map of bathymetry grid created from digitising the 1981 nautical chart NZ 5712 and aerial photographs for coast line positions (some digitised positions shown are as red and blue crosses).

A detailed 5 m by 5 m cell-sized grids was developed to validate the refraction patterns recorded by aerial photography around the Port and headland. This modelling was undertaken using Model 3DD in Boussinesq mode.

Two 10 m x 10 m cell-sized grids were created of the 1953 (NZ 57) and 1981 (NZ 5712) nautical charts. These grids were used for volumetric comparison to assess changes to the bathymetry to the bay north of Napier during the 25-year intervening period.

Two 10 m x 10 m cell-sized grids were also created of two areas that were covered by Port of Napier bathymetry surveys (one of the new inshore dump area for clean Fairway dredge spoil and another of the Port Fairway and dump site H) and plus an additional two of the same areas digitised from the 1981 (NZ 5712) nautical chart. These grids were used for volumetric comparisons to assess changes to the bathymetry in these areas since the 1981 chart survey (the Port surveys carried out in 2000). Table 2.1. summarises the cell-sizes, grid-sizes and areas covered for all of the grids that were created.

Table 2.1. Summary of bathymetry grids created.

Description	Cell Size (m)	Grid Size (no. of cells)
1981 Wave Hts and directions, and wind-driven currents	40	211x207
1981 Currents	120	71x69
1981 Currents minus the Port (1855)	120	71x69
1981 volume comparison	10	653x613
1954 volume comparison	10	653x613
1996 volume comparison	10	238x193
2000 volume comparison	10	304x190
Headland Refraction	5	477x477

2.5 Sources of Information

A variety of information sources were utilised in the present study including unpublished technical reports (e.g. O'Callahan, 1986; Smith, 1985; Hume *et al.,* 1989; Gibb, 1996) and theses (e.g. Ellison, 1995), scientific journal papers (e.g. Gibb, 1962; Black and Vincent, 2000), the Regional Coastal Plan (1999), aerial photographs, historical photographs and

reference publications (e.g. Stevenson, 1977), and a wide array of existing, measured and generated data (the metocean data sources are discussed in Chapter 4).

Smith (1985) and Gibb (1996) both give good summaries of the historical changes to Westshore Beach and beach profiles, which relate well to Hawke's Bay Regional Council records and summaries.

Field studies such as Ellison (1995), Hume *et al.* (1989), O'Callahan, etc., that contribute data, calculations of various study site variables (theoretical and actual) and offer insight into the processes that are operating in Westshore Bay were used to verify the findings of this study. Many good studies have been undertaken in the Westshore Bay area, although, apart from a few (e.g. Hume *et al*., 1989; Ellison, 1995; Black and Vincent, 2000), no actual measurements of hydrographical processes had previously been undertaken. Black and Vincent (2000) undertook a highly technical measurement study of sediment suspension at Westshore Beach in front of the Surf Lifesaving Club using modern acoustic sensors that measured sand concentration at 12 times per second in 5 mm vertical bins. The results of this study were used to obtain highly accurate calibration of the sediment transport model.

Aerial and other photographs provide verification of the historical descriptions of beach change in the area and numerical modelling simulations, and checks of the location of land features in the bathymetry grids used in the models.

3 HISTORICAL BACKGROUND

3.1 Introduction

The principle objective of the present study is to produce a high-quality assessment and interpretation of the processes and patterns presently operating in Westshore Bay (Section 1.2). Here, a brief history of the area is presented to highlight the large amount of change that has occurred, both human-induced and natural.

This summary of the historical changes to the coastline in the Westshore area has been compiled from a range of reports that have considered historical erosion/accretion along the Western Spit, in particular Smith (1985) and Gibb (1996).

3.2 Early History

The Westshore area was originally a sand and shingle barrier that separated Ahuriri Lagoon from the open sea, known as the Western Spit. This barrier is thought to have evolved over the last 7,000 to 7,500 years from the accretion of greywacke gravel and sand (Gibb, 1996). The sand and gravel that formed the Western Spit was originally supplied by the northerly transport of material eroded from the Kidnapper Cliffs and sporadically from rivers such as the Tukituki during flood (the present river mouth is located some 15 km to the south of Westshore), with relict gravel beds and the Tutaekuri River also supplying small amounts of sediment (Gibb, 1996; B. Crabbe, unpublished). Occasionally, after high seas and low flows, all 3 rivers, the Tutaekuri, Ngaruroro and Tukituki discharged into the Ahuriri Lagoon.

The first Maori settled in the Napier area around 700 years ago and, at that time, the entrance to Ahuriri Lagoon was located 6.5 km north of the present entrance, near the northern boundary of the present study site at Bay View (Fig. 1.1) (Harvey, 1948 – cited Gibb, 1996). The northern entrance, known as Keteketerau, was prone to closure as a result of storms, and was repeatedly re-opened by the local Maori until it became permanently closed in the

1760's (Harvey, 1948 – cited Gibb, 1996). During a flood caused by the closure of the Lagoon entrance in the 1760's, Tu Ahuriri was passing by with a large party of followers en route to Mahia. Tu Ahuriri and his party opened up a new entrance, which became known as the Ahuriri Entrance, in the position that is today the entrance to the inner harbour (Harvey, 1948 – cited Gibb, 1996).

3.3 The Changing Character of Westshore Beach – The Last 120 Years

Carr (1890, 1894 – cited Smith, 1985) summarized the early history of the coastal changes in the Ahuriri and Westshore area in a response to a petition from the residents of the Western Spit accusing the Harbour Board of being responsible for the erosion threat in the 1890's. From 1854 to 1876 the southern end of the Western Spit, as far north as the wreck of the Northumberland (the Beacons on the northern study boundary, Fig. 1.1) was gradually being eroded. Then, after construction of Ahuriri Entrance moles, the deposition of large quantities of dredge materials behind the western mole led to the rapid accretion of the spit. In 1888, the depositing of dredgings behind the Western mole was discontinued and the outer beach rapidly began to diminish, so much so that the freezing Company, located near the Western mole, had to run groynes out to protect their Works. Carr (1894 – cited Smith, 1985) noted that the beach had receded 200-240 m just west of the Freezing Works, but that no change had occurred north of the Northumberland wreck, which is near the northern boundary of the study area (Figure 1.1).

In addition, between 1887 and 1890 the shore-connected weather breakwater for the Port of Napier was constructed. It is most likely that this had a greater impact on Westshore Beach than the training mole at the harbour entrance. The water depth across the harbour entrance was stable at 2.7 to 3.0 m below LAT, which would have only partially blocked the northerly-directed sediment transport. Indeed, following the construction of the Port breakwater the depths at the Ahuriri Entrance increased to 4.27 m below LAT between 1887 and 1909 (Simpson, 1945 – cited Gibb, 1996), while the shoreline advanced 50 m on the southern side of the Port breakwater due to the trapping of the northerly drift of sand and gravel.

At Westshore, 91 m of erosion occurred between 1894 and 1900 (Hales, 1900 – cited Smith, 1996), which prompted protection works in the form of rock, timber, sheet piles and concrete blocks supplemented with dumped stones that were placed immediately to the west of the Freezing Works - more that 5,300 m^3 between 1911 and 1923 in the Whakarire Avenue to Charles Street area. Finch (1923 – cited Smith, 1996) reported that around 1320 m of beach was under constant threat of erosion during this time period and required protective work up until 1931. However, photographic evidence from the late 1930's show a large expanse of sandy beach just north at Westshore (known as the Joylands) with little evidence of erosion or protection works (Fig. 3.1).

Figure 3.1. Aerial perspective of Westshore Beach in the late 1920's. This area was a focal point for people visiting beach and became known as the "Joylands" where people would come to stroll and swim. (Photo courtesy of D. Foreman).

On 3 February 1931, the Hawke's Bay Earthquake uplifted the Westshore area by 1.8 m and resulted in the disappearance of most of the shallow Ahuriri Lagoon. After the 1931 earthquake, there are practically no references to erosion at Westshore. However, beach surveys were commenced in 1937 through until 1961. Other than the instantaneous advance of the high-water mark of between 20 and 66 m, the earthquake had a minimal visible effect on the Western Spit. Indeed, between 1937 and 1956 it seems there was a small amount of accretion, with the seafloor (which rose during the 1931 earthquake) as the probable source of material (Smith, 1985).

Since 1956, there has been general retreat at Westshore, which Smith (1985) attributed to the exhausting to the nearshore seabed material source, and by 1995 the protection works at Whakarire had been outflanked by erosion of up to 55 m (Gibb, 1996). Indeed, comparison of sounding profiles taken near the Ahuriri Entrance between 1882 and 1981 (1882, 1906, 1927, 1954 and 1981, as well as a 1931 profile generated from the 1927 soundings by raising them 1.8 m) shows this trend of erosion of the nearshore seabed (Gibb, 1996). Although this progressive record of profiles is confounded by the close proximity of the Ahuriri Entrance, which prior to the 1931 uplift had a tidal jet between the training moles of up to 7 knots, as well as the 1.8 m uplift in 1931 (which significantly diminished the tidal prism and consequently the tidal jet and disrupted the nearshore bar system), the erosive trend is clear (Fig. 3.2).

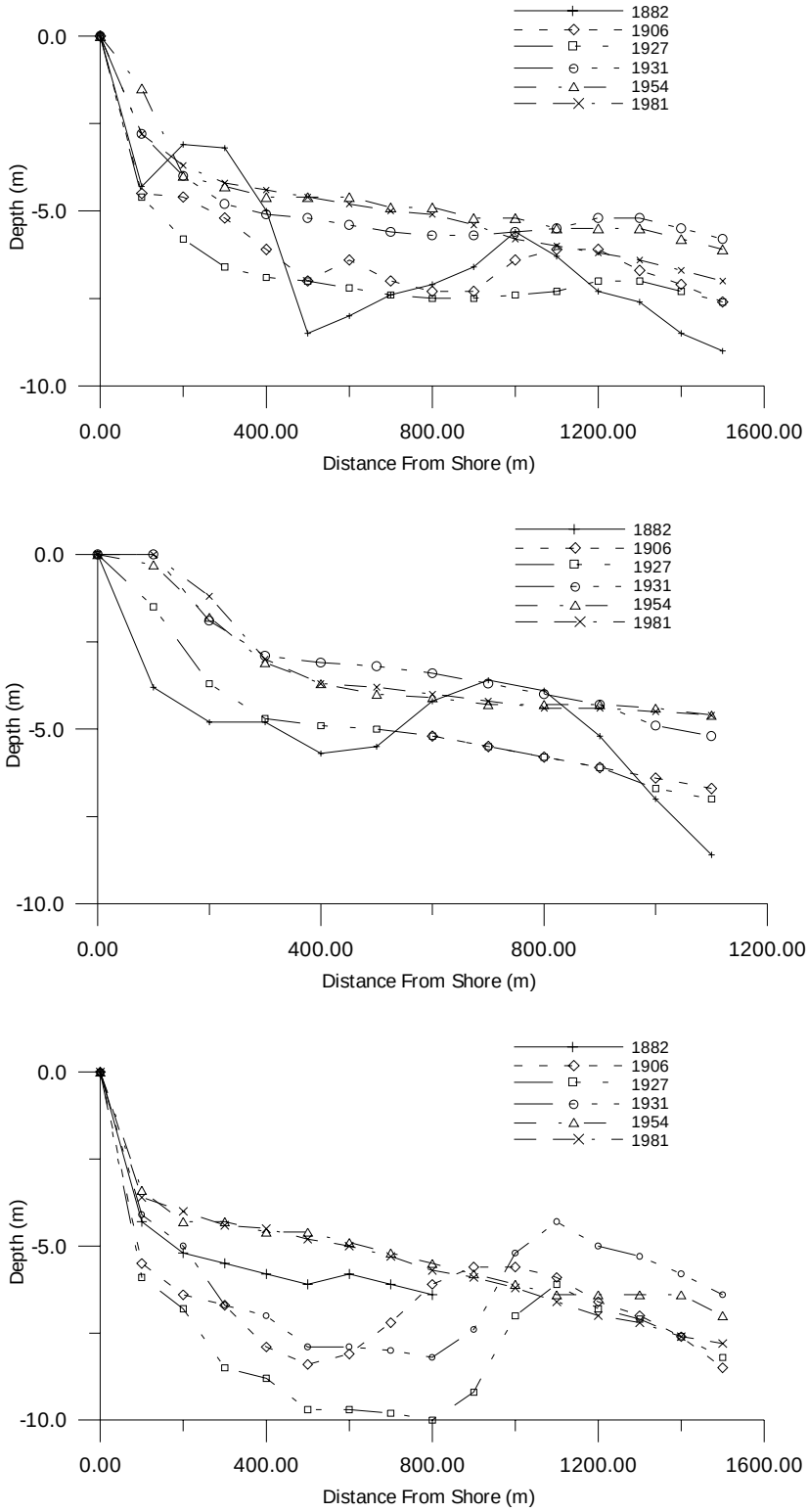

Figure 3.2. Time series of nearshore depth profiles off the Ahuriri Entrance. (Data from Gibb, 1996).

Since 1987, a beach replenishment programme has been conducted, involving the annual placement of between 4,500 and 24,500 m^3 of gravel and sand above the Mean High Water Spring tidemark. In recent years, 12,000 m^3 of renourishment material (fine gravel and sand) has been placed along the beach at Westshore on an annual basis. However, while the retreating crest of the beach has been maintained at its 1986 position along most of Westshore, questions remain concerning the long-term sustainability of renourishment, and whether it will continue to safeguard against erosion in the future. Indeed, the brief history above indicates that it is more than just the beach that is eroding; the nearshore seabed has also been following an erosive trend since the construction of first sections of the Port breakwater in the late 19th century. In addition, the gravel/sand renourishment results in a steep shoreface that limits access and diminishes the amenity value of Westshore. The investigation presented here is aimed at identifying the coastal processes in the northern Napier Bay area so that the potential for a long-term, user- and environmentally-friendly solution to the erosion problem can be properly addressed.

3.4 Development of the Port of Napier

The Port of Napier is a very prominent feature of the Napier headland (e.g. Fig. 2.1) that has been vital to the development of Napier City and, as described above, has influenced the Napier coastline since the late 1880's. Below is a brief chronology of the maritime works that have gone into the Port's development, extracted from 'Port and People' (Stevenson, 1977).

Breakwater construction;

- Work on the breakwater began in 1886.
- December 1888 the first section was completed 1200 feet.
- February 1889 a new section of 500 ft started.
- December 1889 the total length was 1024 feet.

- September 1890 the build up of material against the breakwater threatened to damage it.
- November 1890 the total length was 1138 feet.
- January 1891 the Port Engineer reported that the breakwater was causing the Western Spit (Westshore) to 'become denuded'.
- February 1891 storms saw the sea breaking across the Marine Parade and into houses and shops.
- December 1892 the breakwater was 1650 ft.
- February 1894 the breakwater was 2210 ft.
- September 1894 Consultant engineers Bell & Maxwell “I told you so” report on the effects of the breakwater on the denudation of Westshore. They recommended that the breakwater be extended further to push the effects further north away from the freezing works at what is now Whakarire Ave. They report that “the Western Spit problem was caused by the effect of the breakwater construction trapping the shingle. This would ultimately correct itself when the shingle build-up forced it around the end of the structure”.
- November 1906 a further 200 ft was added to bring the breakwater to 2410 ft.
- July 1925 big easterly storm created heavy damage at the freezing works breaking through the protection provided.
- 1931 The Hawk’s Bay Earthquake.
- 1934-40 breakwater extended by 424 ft to 2834 ft.

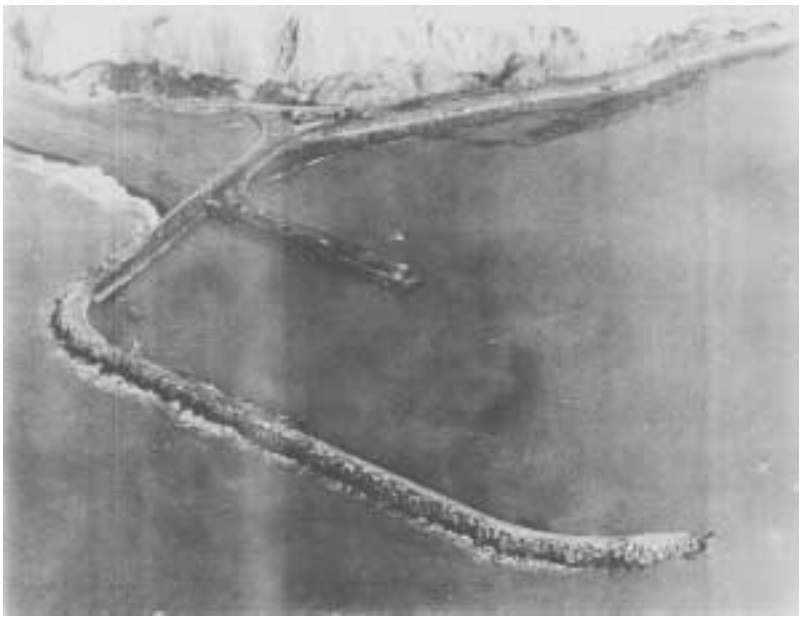

Figure 3.3. Early Port construction (circa 1933) – note the large build-up of shingle/sand on the southern side of the works (upper left-hand side).

- 1945-49 breakwater extended by another 500 ft to 3334ft.
- 1955-59 there is discussion of further extensions but no figures given.
- 1963-64 the breakwater was sealed to stop fine materials seeping through into the swing basin.
- December 1973-December 1974 a further extension of 900 ft completed.
- 1974-75 a further 744 ft extension added (total length >5000 ft or 1524 m, however, this is the perimeter of the arcing length not a linear dimension, which is a little over 1 km)

Fairway Development;

- The swingbasin was dredged after the earthquake to compensate for the rise in the sea floor.

- 1937 the swingbasin was dredged to 35 ft.
- Further swingbasin dredging occurred as each new wharf was constructed.
- 1940 the swingbasin and fairway were dredged to 30 ft.
- 1948 more major extensions of swing basin and fairway channel.
- 1973 the fairway was extended and dredged to the current depth of 12 metres

3.5 Summary

The northern Napier bay, comprising the Port of Napier, Ahuriri and Westshore, has undergone extensive morphological change since the late 19th century. The training of the entrance to Ahuriri Lagoon, development of the Port, redirection of the Tutaekuri River, the 1931 earthquake and various beach protection works, reclamations and renourishment have all impacted on the area. An erosive trend has been documented in the area since 1854 and the evidence suggests that this was exacerbated by the development of the Port of Napier since the late 1880's that effectively blocks the predominantly northerly drift of sediment into the Westshore area. The 1931 Hawke's Bay Earthquake resulted in an uplift of 1.8 m at Westshore, which probably masked the continual erosion. The present state indicates continued erosion from south of the Beacons to the Ahuriri Entrance.

4 FIELD DATA COLLECTION AND ANALYSIS

4.1 Introduction

A 30-day field measurement programme was specifically designed to provide a suitable database to resolve the dominant physical processes within the Westshore region and allow the calibration/validation of numerical models. This includes collecting data on waves and currents, and beach profile variability. The nature and magnitude of suspended sediments was required, along with the character of the surficial sediments within the Bay. Coastal processes are strongly affected by wind and tide level, so this data was also required.

This section provides a description of the field programme that was undertaken over the period 25th April to 24th May 2001, along with the analysis techniques applied to the data. The results of the measurement programme are also presented and discussed in this Chapter.

4.2 Methods

The key components of the measurement programme were:

- Measurement of waves and currents at an offshore site (adjacent to the Port of Napier waverider buoy) for 15 days.
- Measurement of waves and currents at 3 nearshore sites over the 30-day period
- Coincident wind, atmospheric pressure and tide measurements over the 30-day period.
- Time-lapse video monitoring of the nearshore environment.
- Sampling/analysis of the surficial sediments within the Bay.
- Measuring the time-averaged suspended sediment concentrations coincident with wave/current measurements at 4 sites and 4 additional sites.

- Fortnightly beach profile measurement (12 within the Bay and 2 on Marine Parade to the south east), 3 times at each profile.

The locations of the measurement sites are given in Table 4.1, and illustrated in Figure 4.1. The methodology employed for these components is discussed below.

Table 4.1. Locations of the measurement sites for the current meters (CM1-CM4) and sediment traps (ST1-ST4). Co-ordinates are given in the Hawke Bay local metric grid, and depths are referenced to Chart Datum (which is 0.043 m above the level of the Lowest Astronomical Tide).

Site	Easting(m)	Northing(m)	Depth (m)
CM1	322533.1	720329.9	15.93
CM2	319563.3	719407.2	5.64
CM3	318478.5	719754.1	5.15
CM4	317297.7	722130.9	4.79
ST1	321075.8	720297	10.9
ST3	318800.3	719379.5	7.4
ST2	319751.7	720193.2	4.3
ST4	318644.3	721903.9	10.4

It is interesting to note that when the above GPS coordinates are plotted onto the bathymetry map (i.e. nautical chart NZ 5712), the locations correspond to depths that are 0.3 – 0.8 m shallower than that recorded by the pressure sensors on the wave/current meters. This is most likely a combination of some sinking of the current meter frame through time. However, it suggests that the modern day seabed is actually considerably deeper than on the 1981 nautical chart.

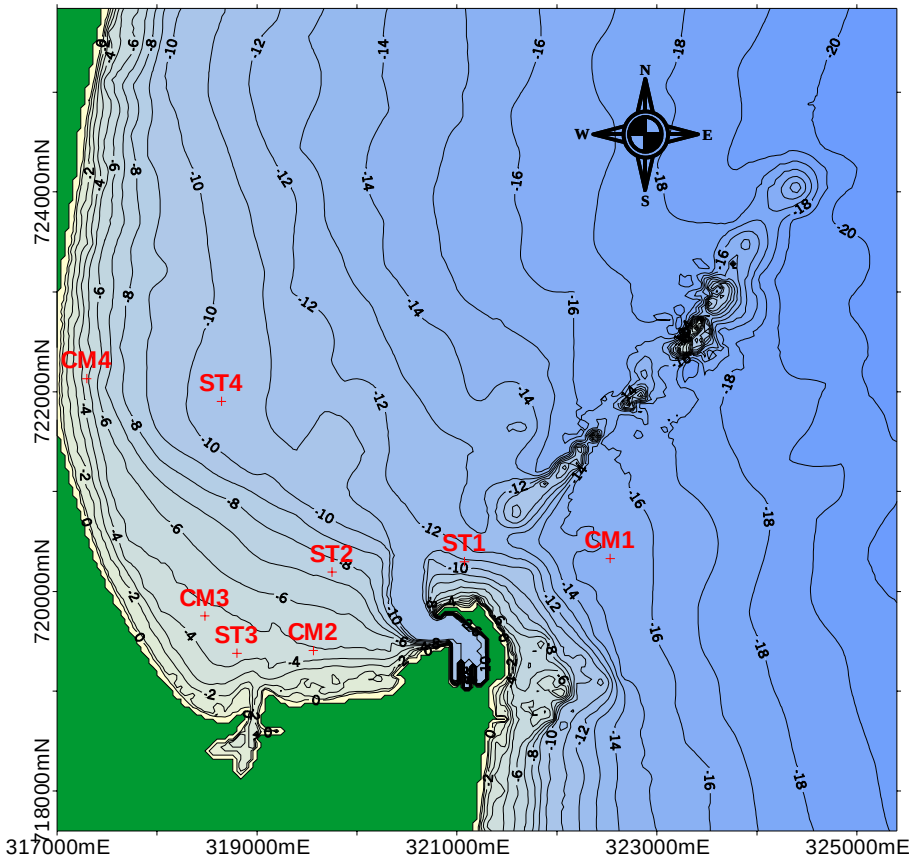

Figure 4.1. Bathymetric map of the study area showing the location of the measurement sites (CM1 - CM4), the Port of Napier waverider buoy, the sites of the sediment traps (ST1 - ST4; sediment traps were also located on each of the current meter sites) and the location of the 10 year wave hindcast. Water depths are marked in 1 m isobaths.

4.2.1 Surficial sediments

A total of 60 surfacial bed samples were collected on 25/5/01 in the positions shown in Figure 4.2 using a seabed sampling device (Fig. 4.3) for the subtidal sites, and by hand for the intertidal regions. These samples were analysed for particle grain size distributions using a Malvern Laser-Sizer (Fig. 4.4), and for settling velocity distributions using a Rapid Sediment Analyser (RSA). In the RSA, sediment samples are released at the top of the fall-tube and a mass balance at the bottom of the fall-tube measures the amount of sediment settling to the bottom over time. This allows the range of settling velocities to be determined.

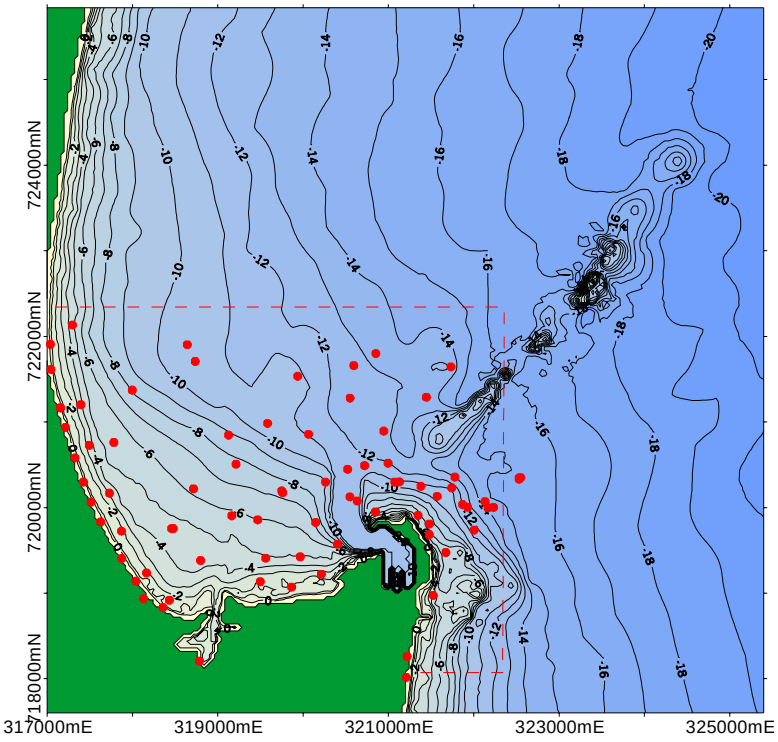

Figure 4.2. Bathymetry map showing the positions of surficial sediment samples (red dots).

Figure 4.3. Flared pipe used for collecting surficial sediments.

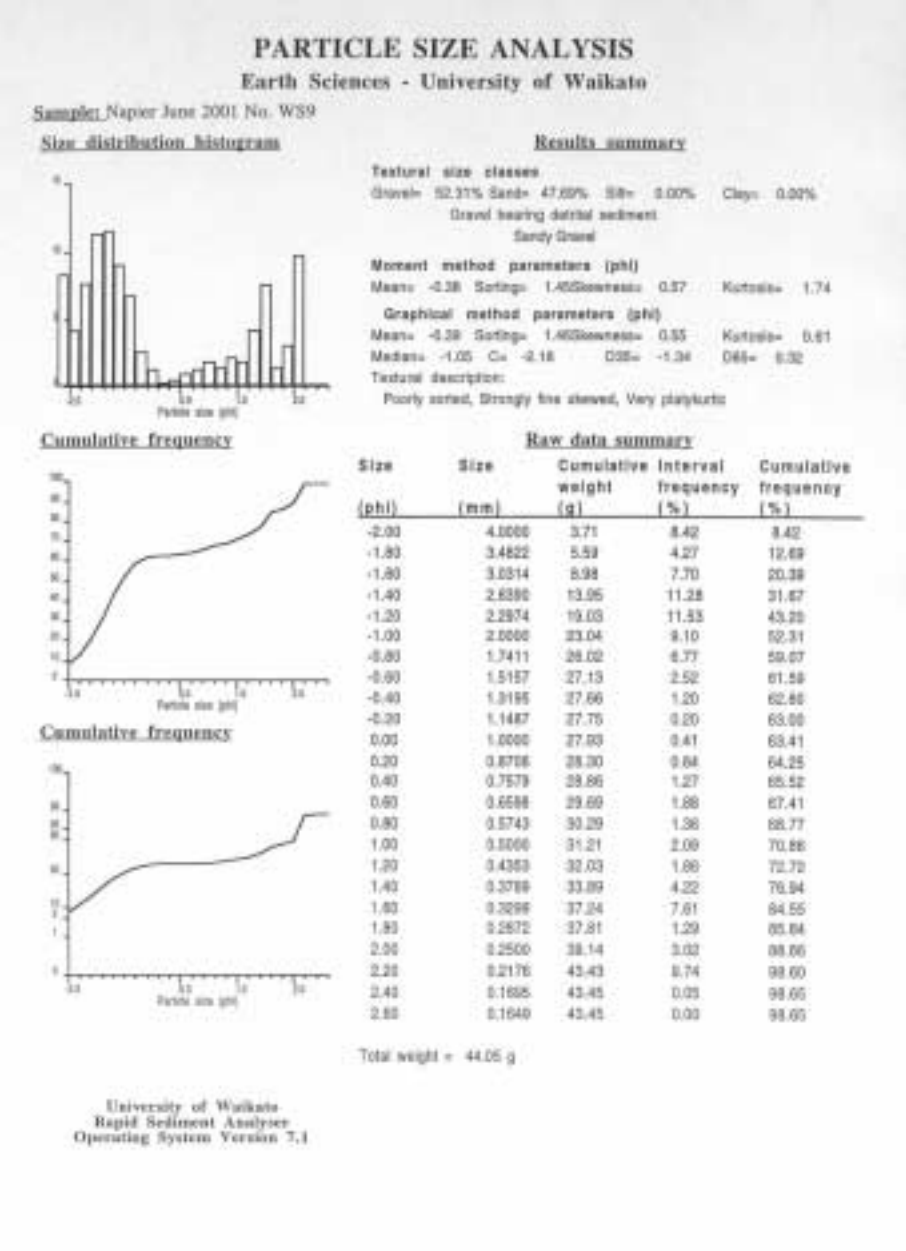

PARTICLE SIZE ANALYSIS

Earth Sciences - University of Waikato

Sample: Napier June 2001 No. WS9

Size distribution histogram

Cumulative frequency

Cumulative frequency

Results summary

Textural size classes

Gravel= 52.31% Sand= 47.69% Silt= 0.00% Clay= 0.00%

Gravel bearing detrital sediment

Sandy Gravel

Moment method parameters (phi)

Mean= -0.38 Sorting= 1.46 Skewness= 0.37 Kurtosis= 1.74

Graphical method parameters (phi)

Mean= -0.39 Sorting= 1.46 Skewness= 0.55 Kurtosis= 0.61

Median= -1.05 Cx= -2.18 D35= -1.34 D65= 0.32

Textural description:

Poorly sorted, Strongly fine skewed, Very platykurtic

Raw data summary

Size (phi)	Size (mm)	Cumulative weight (g)	Interval frequency (%)	Cumulative frequency (%)
-2.00	4.0000	3.71	8.42	8.42
-1.80	3.4822	5.59	4.27	12.69
-1.60	3.0314	8.98	7.70	20.39
-1.40	2.6390	13.95	11.28	31.67
-1.20	2.2974	19.03	11.53	43.20
-1.00	2.0000	23.04	9.10	52.31
-0.80	1.7411	26.02	6.77	59.07
-0.60	1.5157	27.13	2.52	61.59
-0.40	1.3195	27.66	1.20	62.80
-0.20	1.1487	27.75	0.20	63.00
0.00	1.0000	27.93	0.41	63.41
0.20	0.8706	28.30	0.84	64.25
0.40	0.7579	28.86	1.27	65.52
0.60	0.6598	29.69	1.88	67.41
0.80	0.5743	30.29	1.36	68.77
1.00	0.5000	31.21	2.09	70.86
1.20	0.4353	32.03	1.86	72.72
1.40	0.3789	33.89	4.22	76.94
1.60	0.3298	37.24	7.61	84.55
1.80	0.2872	37.81	1.29	85.84
2.00	0.2500	38.14	3.02	88.86
2.20	0.2176	43.43	9.74	98.60
2.40	0.1895	43.45	0.05	98.65
2.60	0.1649	43.45	0.00	98.65

Total weight = 44.05 g

University of Waikato
Rapid Sediment Analyser
Operating System Version 7.1

Figure 4.4. Example of the output of particle grain size distributions using a Malvern Laser-Sizer.

4.2.2 Time-lapse video recording

Time-lapse video recordings were made from the second story of a house on Marine Parade (No. 25). Automatic recordings were made for 5 minutes every 1.5 hrs during daylight throughout the 30-day study period. Figure 4.5 shows the position of the camera and the approximate field of view and is inset with a frame grab of a typical view. This information

provided a running record of the site conditions and checks (by scrolling through the video record) were made to verify current/wave meter records.

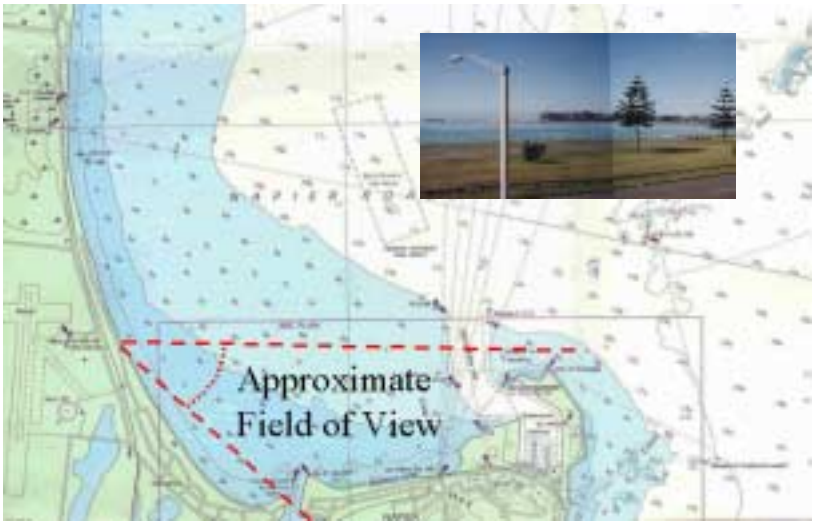

Figure 4.5. Field of view of time-lapse videoing of study area.

4.3 Waves and currents

Two Falmouth Scientific, Inc. 3D-ACM WAVE meters were used to measure directional waves and currents at sites CM1 - CM4 (Fig. 4.1). At each site, a stainless steel triangular frame was anchored to the seabed, onto which the 3D-ACM WAVE meter was attached, positioning the velocity sensors 1 m above the seabed. The instrument and frame were recovered after each deployment, the instrument downloaded, and the frame repositioned at the next site. Velocity and pressure data were recorded at 5.36 Hz in 9-minute bursts every two hours. Time-series data recovered from the meters were analysed according to the techniques summarised below. Hourly directional wave data from the Port of Napier waverider buoy was also made available for the study, and this instrument was located adjacent to site CM1 (Fig. 4.1). These data provided a cross-check with our own measurements, calibration for numerical wave refraction modelling, and a longer measure of the nearshore wave climate.

4.3.3.1 Pressure-sensor data

Non-directional wave information was derived from the pressure sensor data recorded by the FSI 3D-ACM's. Direction was obtained from the combination of pressures and horizontal orbital velocity measurements. With the pressure data, the atmospheric pressure was removed and the burst time-series of residual pressures were converted to sea surface elevations by applying linear wave theory. This conversion involves filtering to remove frequencies above a depth-dependent cut-off,

$$f_{cut} = 0.282\sqrt{g/d} \qquad \textbf{(4.1)}$$

(Hutt & Black, 1997) where f_{cut} is the frequency cut-off, g is gravitational acceleration and d is the instrument depth below the surface. Linear detrending was applied to the data, and the following statistics were computed for each burst:

- Maximum, minimum, mean and root-mean-square of the raw data;
- Standard deviation, skewness, kurtosis, top3rd (mean of the largest 1/3 of values) and top10th (mean of the largest 1/10 of values) of detrended data.

A power spectrum was computed using Welch's averaged periodogram method. From the computed spectral energy density $S(f)$, the peak frequency f_p and peak energy $S_p = S(f_p)$ of the spectrum was located. Spectral moments, given by

$$M_j = \int_0^\infty f^j S(f)\, df \qquad \textbf{(4.2)}$$

were computed, allowing further statistics to be defined:

Significant height

$$H_s = 4\sqrt{M_0} \qquad \textbf{(4.3)}$$

Mean apparent period

$$T_{mean} = \sqrt{M_0 / M_2} \qquad \textbf{(4.4)}$$

Mean frequency

$$f_{mean} = M_1 / M_0 \quad \textbf{(4.5)}$$

Mean crest period

$$T_{cr} = \sqrt{M_2 / M_4} \quad \textbf{(4.6)}$$

Spectral width

$$SW = 1 - \frac{M_2^{\,2}}{M_0 M_2} \quad \textbf{(4.7)}$$

Period ratio

$$T_2 = T_{mean} f_p \quad \textbf{(4.8)}$$

Goda's spectral peakedness parameter, given by

$$Q_p = \frac{2}{M_0^{\,2}} \int_0^{\infty} f\, S(f)^2\, df \quad \textbf{(4.9)}$$

(Goda, 1970) was also computed. The spectrum obtained from the data was fitted with a 2-parameter Weibull distribution defined by

$$S_{Weibull}(f) = M_0 \alpha \beta f^{-\beta} \exp(-\alpha f^{-\beta}) \quad \textbf{(4.10)}$$

using the method of Lee & Black (1978), to compute the fitting parameters α, β and correlation R^2.

After linear detrending, zero downcrossing analysis was applied to each burst to establish a sequence of individual wave heights and periods. From these *Hz3* (mean of the largest 1/3 of wave heights) and *Tz3* (mean period of these waves) were computed, as were *Hz10* (mean of the largest 1/10 of wave heights) and the corresponding *Tz10*.

4.3.3.2 Velocity data

Current velocity measurements were made at frequencies of 2 Hz (or greater) to allow statistics on the wave orbital velocities to be defined, as well as the mean (burst-average)

vectors. A magnetic variation of 22° east was used to rotate velocities to eastward and northward components *u* and *v* respectively, and the mean velocity and direction was taken over the length of the data burst. After subtracting the mean, the velocity was rotated into components of u_p and v_t, which are respectively parallel, and transverse to, the principal wave direction. The rotation angle was determined from the scatter of the velocity data, as the direction for which

$$\left\langle u_p v_t \right\rangle \equiv \frac{1}{N}\sum_{i=1}^{N} u_p^i v_t^i = 0 \qquad \textbf{(4.11)}$$

thereby minimising the variance $\left\langle v_t^{\,2} \right\rangle$ of the transverse velocities. This leaves a 180° ambiguity in the principal wave direction, which was resolved in favour of the shoreward direction. A rotationally invariant correlation function for this regression is defined as

$$R_{uv}^2 = \frac{\left\langle u_p^{\,2} \right\rangle - \left\langle v_t^{\,2} \right\rangle}{\left\langle u_p^{\,2} \right\rangle + \left\langle v_t^{\,2} \right\rangle} \qquad \textbf{(4.12)}$$

Wave-orbital velocities at the near-bed level were estimated from the current data. The time-series were extrapolated to bed-level using linear wave theory and a range of statistics defined. For sediment entrainment applications, Black & Rosenberg (1991) found that the third moment of the wave-orbital velocity (U_3) was the most appropriate value to represent this variance where

$$U_3 = 1.4\left[\sum_{j=1}^{N} \left|U_j\right|^3 \Big/ N\right]^{\frac{1}{3}} \qquad \textbf{(4.13)}$$

4.3.3.3 Directional waves

Directional wave information was resolved using cross-spectral analysis of wave orbital motion and sea-surface elevations (derived from the pressure data). The full methodology used for resolving directional information is described by McComb *et al.* (2001).

4.3.3.4 Suspended sediments

Suspended sediments are particles (such as sand) that have been lifted off the seabed into suspension in the water column. In nearshore coastal regions, the suspension of such particles is associated with wave-induced orbital currents (Green & Vincent, 1990; Osborne & Greenwood, 1991; Aagaard & Greenwood, 1994) and the seabed characteristics (Nielsen, 1986, 1992; Greenwood *et al*., 1990; Osborne & Vincent, 1992). Particles suspended in the water column may be transported from the entrainment site by currents, thus providing the primary mechanism of sediment transport in the littoral zone.

Time-averaged suspended sediment concentrations (SSC) were resolved using sediment traps to measure the downward flux of suspended particles. This technique has recently been validated by McComb and Black (submitted) for use in a range of coastal environments, including high-energy conditions. At Napier, sediment traps (Fig. 4.6) were positioned at two levels above the seabed (0.4 m and 0.8 m) attached to seabed frames in 8 different locations (Fig. 4.1).

Figure 4.6. Example of a sediment traps mounted on a typical seabed frame

Trapped sediment samples were wet-sieved at 45 μm, dried and weighed. Grain size and settling velocity distributions were obtained using the RSA. The masses (M) collected in the traps were converted to a downward flux (f_d) with the units $kg.m^{-2}s^{-1}$ as follows:

$$f_d = M/At \qquad \textbf{(4.14)}$$

where A is the area of the aperture of the trap and t is the time of the sampling. The downward sediment flux was converted to a time-average suspended sediment concentration (C) using the full settling velocity distribution of the trapped sediment (Armanini & Ruol, 1988; Nishi *et al.*, 1992). Concentration distributions were calculated as:

$$C = \frac{M_i}{w_i A \Delta t}, \qquad \textbf{(4.15)}$$

where M_i is the mass trapped, A is the area of the collection orifice of the trap, w_i is the settling velocity of the sediment particles of the i^{th} sediment fraction in the distribution and Δt is the deployment time. These were then summed to provide concentrations for the whole sample as:

$$C = \frac{1}{\Delta t} \sum_{i=1} \frac{M_i}{w_i A}. \qquad \textbf{(4.16)}$$

4.3.2 Wind and tide data

One-minute wind, tide and barometric pressure data were made available from sensors at the Port of Napier (courtesy of Port of Napier Ltd).

4.4 Results

4.4.1 Surficial sediments

Mean and median particle sizes for 56 seabed and intertidal samples are given in Table 4.2, and also presented on the bathymetry map in Figure 4.7. The data show the seabed sediments are typically fine sands with median (D_{50}) particle sizes of 0.1-0.16 mm. Generally, the intertidal sediments tend to be coarser, with gravels present at several sites (Tab. 4.2), and a trend of increasing grain size towards the north most likely reflecting the relative wave exposure. Notably, the bay is almost totally covered by sand with gravel contents that are

mostly less than 10%. The mean particle size of the sandy component is most commonly about 0.12-0.14 mm.

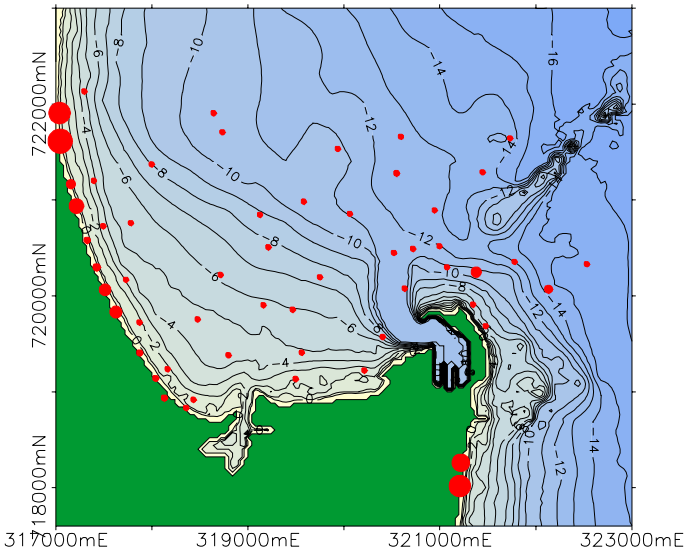

Figure 4..6. Bathymetric map of Westshore showing the median (D_{50}) particle size for surficial samples collected on 25/5/01. Data points are linearly scaled in size to represent median particle sizes from 0.107 to 4.056 mm.

Table 4.2. Median particle sizes for surficial seabed and intertidal samples.

Site	Easting	Northing	Mean size (mm)	Median size (mm)	% Gravel	% Sand	Comment
6	321220.8	718257.4		2.639			
7	321210.1	718015.1		3.458			
8	318360.1	718830.9	0.119	0.147		100	sand
9	318132.3	718933.3	0.441	0.310	7.32	92.68	s.grav sand
10	318042.5	719138.9	0.252	0.266	0.47	99.53	s.grav sand
11	317875.3	719403.9	0.297	0.308	2.71	97.29	s.grav sand
12	317628.2	719830.1	1.240	1.495	45.04	54.96	grav sand
13	317515.4	720061.6	1.110	1.414	5.5	94.5	s.grav sand
14	317427	720296.8	0.470	0.547	9.43	90.57	s.grav sand
15	317328.7	720578.3	0.457	0.342	7.71	92.29	s.grav sand
16	317216.2	720935.7	1.301	2.071	52.31	47.69	sandy grav
18	317159.3	721163.4	0.547	0.889	1.62	98.38	s.grav sand
19	317046.9	721611.4	2.085	4.056	71.79		sandy grav
20	317040.4	721905.7	1.000	3.482			
62	322135.1	720068.3	0.646	0.678		100	sand
65	321780.2	720354.3	0.081	0.115	1.4	98.6	s.grav sand
67	321381.2	720246.3	0.483	1.181	31.75	68.25	sandy gravel
68	321348.7	719907.7	0.130	0.123	0.53	99.74	s.grav sand
69	321480	719683.4	0.138	0.130		100	sand
73	320997.5	720517.4	0.135	0.120		100	sand
74	320722	720488.6	0.138	0.127		100	sand

75	320524	720446.6	0.137	0.131	0.07	99.93	s.grav sand
76	320634.9	720076.1	0.142	0.132		100	sand
77	320405.5	719569.8	0.144	0.140	0.81	99.19	s.grav sand
78	320215.3	719220.5	0.151	0.147	0.29	99.71	s.grav sand
79	319499.5	719131.7	0.162	0.160		100	sand
80	319469.8	719855.3	0.135	0.129		100	sand
81	320064.7	720854.8	0.137	0.131	1.42	98.58	s.grav sand
82	320946.9	720891.4	0.149	0.113	0.91	99.09	s.grav sand
83	321447.2	721287.8	0.129	0.122		100	sand
84	321733.6	721642.3	0.020	0.107		100	sand
85	320596.1	721658.4	0.128	0.110	0.73	99.27	s.grav sand
86	320552	721277.3	0.281	0.238	3.3	96.7	s.grav sand
87	319938.7	721532.4	0.143	0.142	0.06	99.94	s.grav sand
88	319584.4	720981.9	0.202	0.149	12.7	87.3	s.grav sand
89	319216.1	720505.4	0.127	0.126		100	sand
90	319164.4	719902.3	0.146	0.132	0.74	99.26	s.grav sand
91	318717.7	720217.9	0.167	0.140	3.2	96.8	s.grav sand
92	319128	720844.3	0.241	0.145	23.97	76.03	grav sand
93	318737	721705.6	0.173	0.122	12.9	87.1	s.grav sand
94	317998.9	721370.6	0.134	0.122	0.42	99.58	s.grav sand
95	317397.5	721199.9	0.108	0.112		100	sand
96	317495.4	720725.9	0.140	0.133		100	sand
97	317783.8	720758.6	0.124	0.119		100	sand
98	317732.2	720166.6	0.144	0.124	3	97	s.grav sand
99	317873.2	719722.2	0.150	0.136	0.06	99.94	s.grav sand
100	318166	719234.8	0.157	0.149	0.85	99.15	s.grav sand
101	318434.9	718915.9	0.132	0.116		100	sand
CM3	318478.5	719754.1	0.141	0.133		100	sand
ST3	318800.3	719379.5	0.165	0.152	0.17	99.93	s.grav sand
ST2	319751.7	720193.2	0.139	0.132		100	sand
CM4	317297.7	722130.9	0.152	0.128		100	sand
ST4	318644.3	721903.9	0.142	0.136	0.27	99.73	s.grav sand
CM1	322533.1	720329.9	0.138	0.122		100	sand
ST1	321075.8	720297	0.148	0.130		100	sand
CM2	319563.3	719407.2	0.157	0.144	1.41	98.59	s.grav sand

4.4.2 Wind, tide and barometric pressure

The time-series of wind speed and direction recorded at Port Napier over the 30-day measurement programme is given in Figure 4.8. These data show that a range of wind conditions was encountered, particularly fro the south west and north east. Wind speeds of up to 30 kts were measured. Tide levels derived from the Port sensor are presented in Figure 4.9.

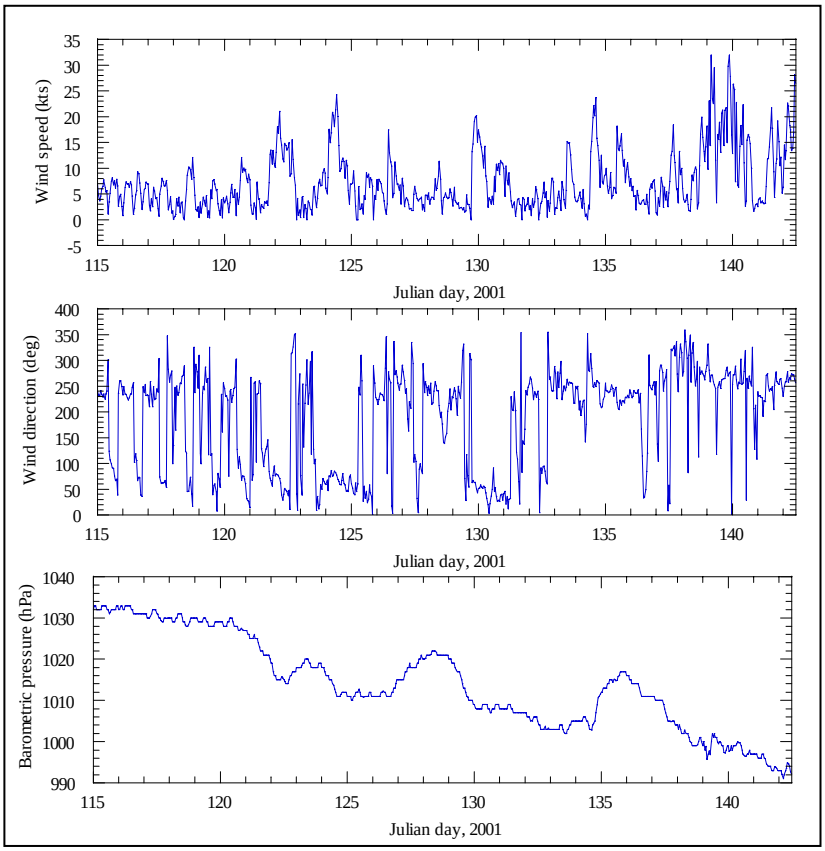

Figure 4.8. Time-series of mean wind speed (kts), wind direction (i.e. coming from), and barometric pressure (hPa) over the field measurement programme.

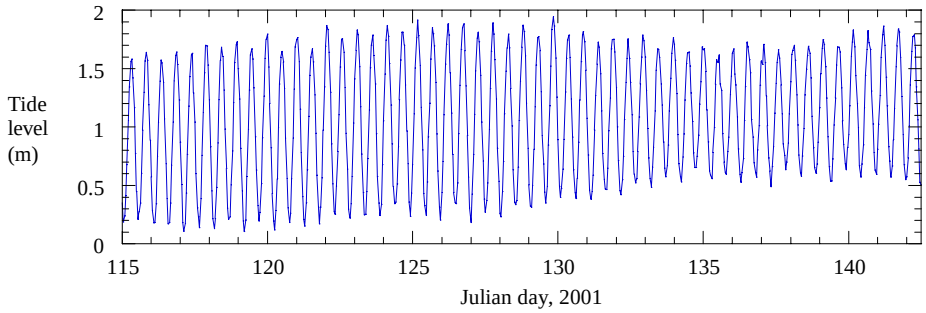

Figure 4.9. Time-series of mean water levels recorded at Port Napier. Data is referenced to Chart Datum, which is 0.043 m above the level of LAT.

4.4.3 Waves

Wave conditions are usually characterised by three main parameters; height, period and direction. The significant wave height (H_s) is the average of the highest third of waves measured, period (T_p) is the time between wave crests, and direction is the predominant direction of wave advance (these parameters are defined in section 4.2).

4.4.3.1 Offshore wave data

Waves were recorded at two offshore locations; CM1 and the adjacent Port of Napier Waverider buoy. CM1 was deployed for an initial two-week period, after which it was moved to an inshore site (CM4). A time-series plot of the incident wave conditions measured at these sites is given in Figure 4.10, showing good agreement between the two instruments, and indicating the significant wave heights reached 2.5 m over that period. The relationship between wave height and period (Figs. 4.11 & 4.12) shows that for this period the larger wave events (i.e. > 1.5 m Hs) were of relatively short period (~6 seconds). CM1 wave directions exhibited a 33-degree range, and the larger waves were associated with waves approaching from the east (80-90 degrees; Fig. 4.13).

Longer-term data from the Waverider buoy is presented in Figures 4.14-16, derived from measurements made over the period September 2000 to May 2001. These data show that the more energetic wave conditions are dominated by low-frequency swells with peak spectral wave periods of 10-15 seconds, and mean spectral periods 8-10 seconds. Directions of wave

approach are narrowly focussed about 090 degrees (i.e. from the east). A joint probability distribution for the significant wave height and mean wave direction data is given in Table 4.3. That distribution illustrates the very narrow range of incident wave directions, as some 88% of all waves measured came from ENE - ESE quarter.

4.4.3.2 Offshore wave climate

When deriving an offshore wave climate, it is desirable to have the maximum possible length of data in order to represent the seasonal and annual variations in wave conditions. Thus, to supplement the eight months of wave data from the Port of Napier Waverider Buoy, a 20-year numerical wave hindcast was obtained (from Dr R. Gorman of NIWA) for a site 7.4 km offshore (bearing 130^{o}) of the CM1 site (39^{o}30'S, 177^{o}0'E) (Fig. 4.1). This hindcast model is described by Gorman & Laing (2000), although the present application uses a higher spatial resolution of the model grid and a longer time-series.

The joint probability distribution of the significant wave heights and mean wave directions from the 20-year hindcast time-series is provided in Table 4.4. This distribution is very similar to that derived from the Port Waverider buoy (Table 4.3) and further illustrates that the most energetic waves events are dominated by waves approaching from the NNE-E quarter. The percentage exceedence statistics for these data indicate a 5% exceedence at the 2 m level, 50% exceedence at the 0.9 m level, and a 95% exceedence at the 0.3 m level. This means that the offshore significant wave height is greater than 2 m for 5% of the time, and greater than 0.9 m for 50% of the time. The largest significant wave height in the hindcast was 6.2 m.

The seasonal variation in the offshore wave climate is summarised in Table 4.5, with monthly mean values for the significant wave height, mean wave direction, peak wave direction, mean wave period and peak wave period. December and January are shown to be the least energetic months, while June and July have the largest mean wave heights (approximately 1.6 times that of the summer months). The average wave periods are greater in the winter months, and wave directions are slightly more southerly.

Studies of waves in Hawke Bay by Smith (1968 and 1984 – cited Hume *et al.*, 1989), that are based on long-term observations records, describe a high energy wave climate with waves over 0.5 m in height occurring for 42 % of the time, which is significantly less than both the measured and hindcast wave climate (Tabs. 4.3 and 4.4, respectively). Smith (1984 – cited Hume *et al.*, 1989) found that some 55% of all waves approach from the E-SE, while 42% approach from the E-NE, and the dominant wave periods are from 8-10 seconds (E-ENE) and 11-13 seconds (E-SE). These observed directions also differ from the measured and hindcast wave climate (Tables 4.3 and 4.4, respectively), which suggest a large component of NE directed waves. However, the waverider data (the longest record of measured data) suggests that the most energetic waves approach from a narrow band focussed on 90° (East), although some sheltering of waves from north of NE would result from the presence of Pania Reef (Fig. 3.1). Hume *et al.*, (1989) suggested that the bulge in the isobaths in the lee of Pania Reef shows that SE swells predominate. This deflection of isobaths is discernable in both the 1954 and 1981 nautical charts and on closer inspection suggests the local wave climate is dominated by waves focussed on 90° as the waverider data suggests. While the present data gives a fairly good description of the Napier wave climate, in the coming decade, the Port of Napier waverider buoy will allow for a more precise definition.

4.4.3.3 Nearshore wave data

Wave data measured at the nearshore sites (CM2, CM3, CM4) is presented in time-series in Figures 4.17-4.20, along with the coincident wave data measured at the offshore site (CM1).

Two events with significant offshore wave heights above 1.5 m were recorded in each deployment period (Fig. 4.17). The wave height records three nearshore current meters show the sheltering effect of the headland, with CM 2 showing the biggest difference from the offshore wave record. The wave heights at the nearshore sites may be considered as a function of the offshore conditions. This reduces the nearshore values to a wave height ratio, which can be very informative of the site-specific wave transformation processes that are occurring as waves proceed shoreward. Wave height ratios are given in Table 4.6, and

indicate that the northern end of Westshore (i.e. site CM4) receives considerably more wave energy than the southern corner near the Port (sites CM2 and CM3).

The wave directions measured at the different sites also displays the effect of the headland, in this case the rotation of waves due to refraction into Westshore Bay. CM2, the site furthest inside the headland shows the biggest rotation of wave directions (Fig. 4.20) and the amount of direction change (from the predominant easterly direction of 270°) decreases the further north the site is, away from the effect of the headland (Fig. 4.1).

Peak period mostly ranged between 5-16 s during the deployments. The peak period decreased significantly during each of the events over the deployment, which indicates that these were local storms.

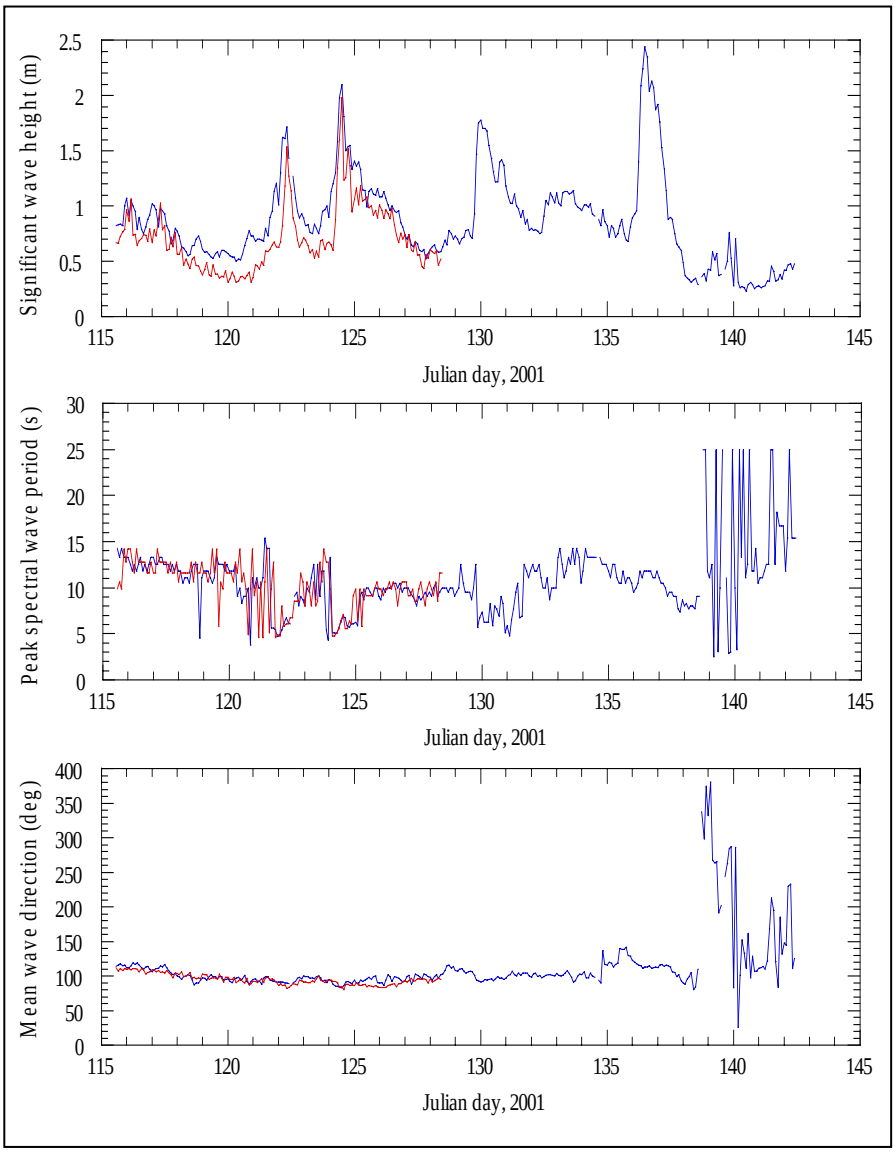

Figure 4.10. Time-series of significant wave height, peak spectral wave period, and mean wave direction (i.e. coming from) for the offshore measurement sites CM1 (red) and the Port of Napier Waverider buoy (blue). Note that over the last four days the Waverider period and direction data appears to be erroneous, which may be due to the instrument resolution in very small waves (i.e. < 0.4 m).

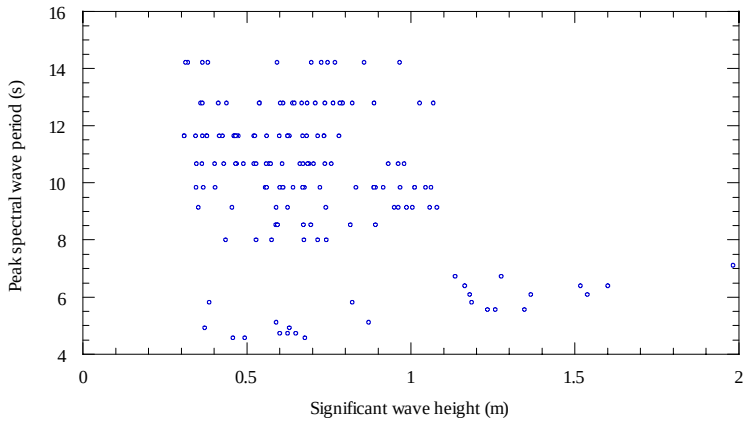

Figure 4.11. Scatter plot of significant wave height vs the peak spectral wave period for site CM1 over the 14-day data collection period.

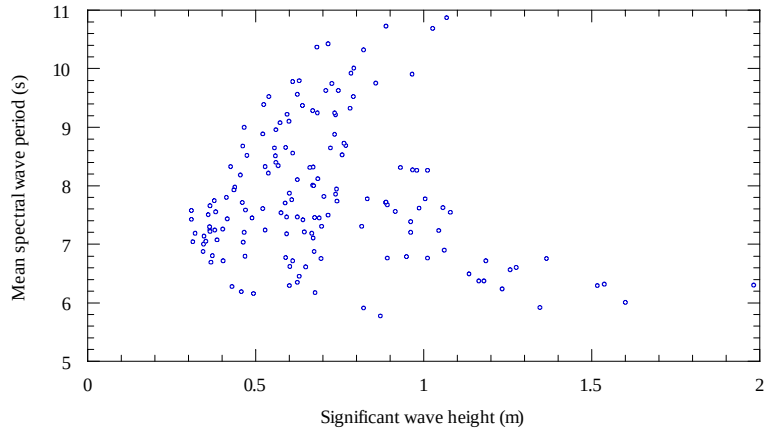

Figure 4.12. Scatter plot of significant wave height vs the mean wave period for site CM1 over the 14-day data collection period.

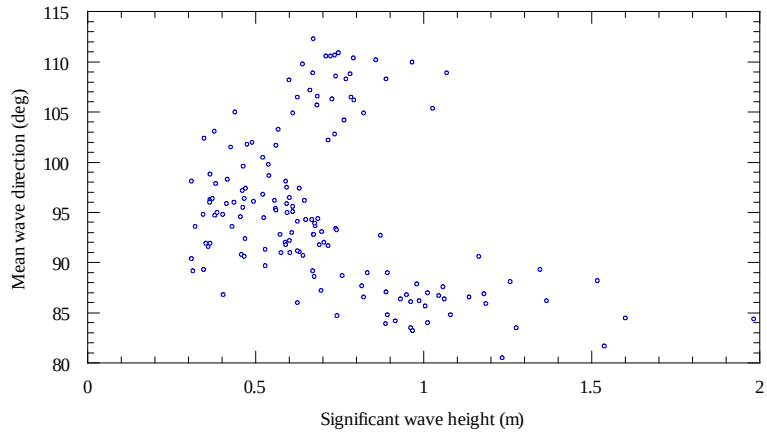

Figure 4.13. Scatter plot of significant wave height vs the wave direction for site CM1 over the 14-day data collection period.

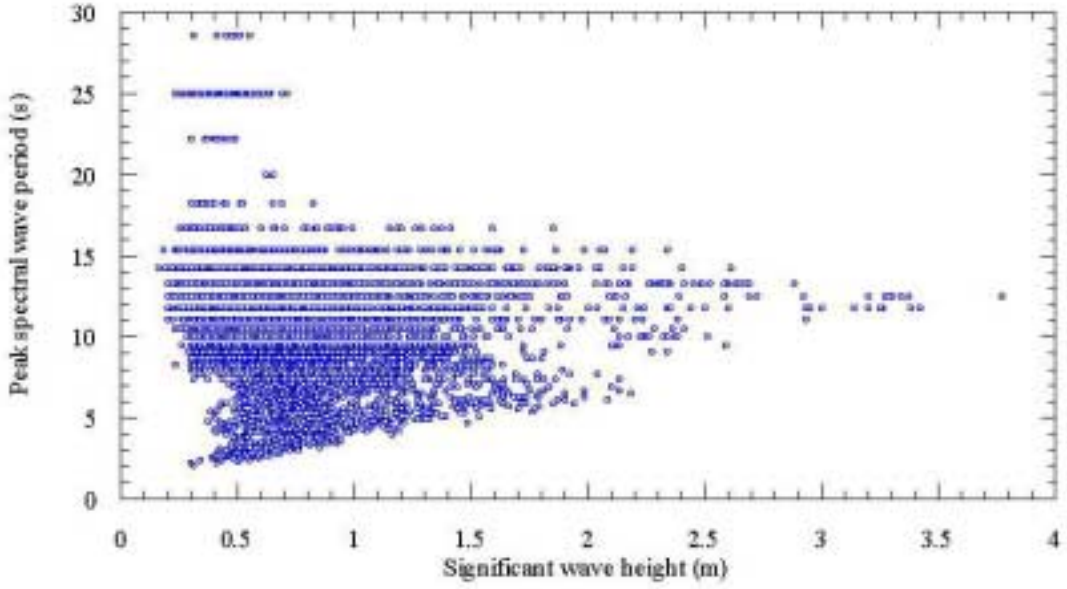

Figure 4.14. Scatter plot of significant wave height vs the peak spectral period for port Waverider buoy over the period September 2000 - May 2001 (6372 data).

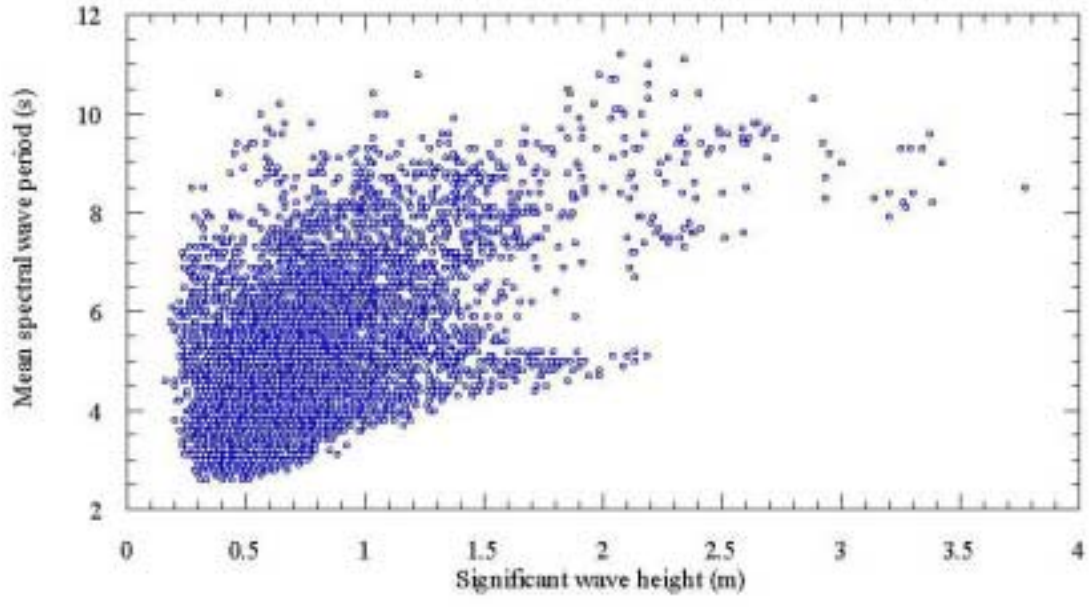

Figure 4.15. Scatter plot of significant wave height vs the mean wave period for port Waverider buoy over the period September 2000 - May 2001 (6372 data).

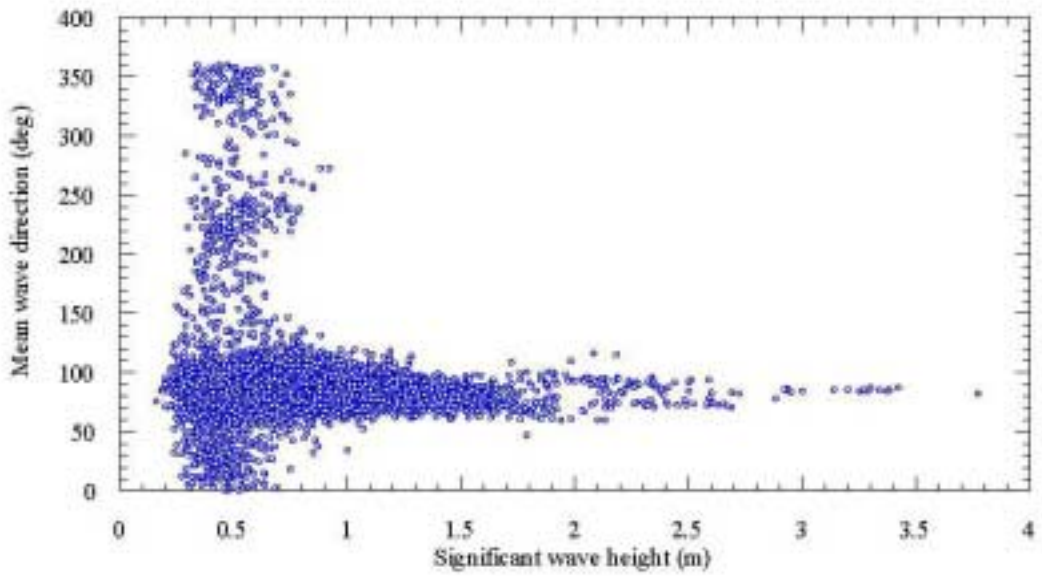

Figure 4.16. Scatter plot of significant wave height vs the mean wave direction for port Waverider buoy over the period September 2000 - May 2001 (6372 data).

Table 4.3. Joint probaility distribution for significant wave height (m) and mean wave direction for data collected by the Port of Napier Waverider buoy over the period September 2000 - May 2001.

	< 0.2	**< 0.5**	**< 1.0**	**< 1.5**	**< 2.0**	**< 2.5**	**< 3.0**	**< 3.5**	**< 4.0**	**< 5.0**	**TOTAL**
NNE	0	1.21	0.58	0	0	0	0	0	0	0	1.79
NE	0	1.48	0.99	0.03	0.02	0	0	0	0	0	2.51
ENE	0.02	5.19	15.8	5.41	1.88	0.41	0.17	0	0	0	28.89
E	0.03	9.79	28.97	9.29	1.63	0.72	0.17	0.2	0.02	0	50.83
ESE	0	1.96	5.48	0.69	0.03	0.03	0	0	0	0	8.19
SE	0	0.46	0.53	0	0	0	0	0	0	0	0.99
SSE	0	0.28	0.19	0	0	0	0	0	0	0	0.47
S	0	0.35	0.17	0	0	0	0	0	0	0	0.52
SSW	0	0.41	0.16	0	0	0	0	0	0	0	0.56
SW	0	0.66	0.47	0	0	0	0	0	0	0	1.13
WSW	0	0.28	0.52	0	0	0	0	0	0	0	0.8
W	0	0.19	0.24	0	0	0	0	0	0	0	0.42
WNW	0	0.08	0.14	0	0	0	0	0	0	0	0.22
NW	0	0.13	0.35	0	0	0	0	0	0	0	0.47
NNW	0	0.5	0.52	0	0	0	0	0	0	0	1.02
N	0	0.71	0.47	0	0	0	0	0	0	0	1.18
SUM	0.05	23.67	55.57	15.43	3.56	1.16	0.35	0.2	0.02	0	100

Table 4.4. Joint probaility distribution for significant wave height (m) and mean wave direction for numerical hindcast data (1979 - 1998) derived for position 39°30'S, 177°0'E (7.4 km offshore of the Port Napier waverider bouy location).

	0.25	**0.5**	**0.75**	**1**	**1.25**	**1.5**	**1.75**	**2**	**2.25**	**2.5**	**2.75**	**3**	**3.25**	**3.5**	**3.75**	**4**	**4.25**	**4.5**	**4.75**	**5**	**5.25**	**SUM**
NNE	0.068	1.624	3.164	2.969	2.657	1.583	0.772	0.481	0.217	0.161	0.087	0.068	0.036	0.033	0.003	0.003	0.003	0.005	0.005	0	0	13.941
NE	0.24	3.313	7.305	7.011	4.68	3.001	1.728	0.97	0.637	0.423	0.248	0.123	0.068	0.026	0.012	0.01	0.007	0.009	0.005	0.014	0.003	29.832
ENE	0.207	2.748	5.525	5.246	3.489	2.426	1.494	0.864	0.513	0.371	0.175	0.096	0.067	0.055	0.019	0.024	0.017	0.009	0	0	0.003	23.349
E	0.209	2.871	6.176	4.988	3.07	1.761	1.016	0.647	0.402	0.301	0.166	0.123	0.096	0.065	0.044	0.043	0.036	0.01	0	0.002	0	22.026
ESE	0.091	1.653	2.248	1.275	0.611	0.252	0.043	0.021	0.015	0.024	0.005	0	0	0	0	0	0	0	0	0	0	6.237
SE	0.053	0.712	0.614	0.197	0.072	0.031	0.01	0.005	0.002	0	0	0	0	0	0	0	0	0	0	0	0	1.696
SSE	0.044	0.428	0.32	0.11	0.031	0.002	0	0	0	0	0	0	0	0	0	0	0	0	0	0	0	0.934
S	0.022	0.334	0.21	0.067	0.015	0.002	0	0.002	0	0	0	0	0	0	0	0	0	0	0	0	0	0.652
SSW	0.009	0.255	0.159	0.024	0.003	0.002	0	0	0	0	0	0	0	0	0	0	0	0	0	0	0	0.452
SW	0.01	0.147	0.096	0.01	0	0	0	0	0	0	0	0	0	0	0	0	0	0	0	0	0	0.264
WSW	0.003	0.08	0.038	0.003	0	0	0	0	0	0	0	0	0	0	0	0	0	0	0	0	0	0.125
W	0.002	0.048	0.017	0.009	0	0	0	0	0	0	0	0	0	0	0	0	0	0	0	0	0	0.075
WNW	0	0.029	0.036	0.003	0	0	0	0	0	0	0	0	0	0	0	0	0	0	0	0	0	0.068
NW	0.005	0.029	0.036	0.002	0	0	0	0	0	0	0	0	0	0	0	0	0	0	0	0	0	0.072
NNW	0.002	0.034	0.029	0.003	0	0	0	0	0	0	0	0	0	0	0	0	0	0	0	0	0	0.068
N	0.003	0.091	0.082	0.027	0.005	0	0	0	0	0	0	0	0	0	0	0	0	0	0	0	0	0.209
SUM	0.969	14.396	26.056	21.944	14.634	9.059	5.063	2.989	1.786	1.28	0.681	0.411	0.267	0.178	0.079	0.08	0.063	0.033	0.01	0.015	0.007	100

Table 4.5. Monthly wave statistics from numerical hindcast data (1979 - 1998) derived for position 39°30'S, 177°0'E (7.4 km offshore of the Port Napier waverider bouy location).

Month	Significant wave height (m)	Mean wave direction (deg)	Peak wave direction (deg)	Peak wave period (s)	Mean wave period (s)
Jan	0.75	110	116	8.07	6.06
Feb	0.88	109	110	8.38	6.42
Mar	1.03	114	116	8.80	6.70
Apr	1.03	118	123	9.01	6.82
May	1.05	125	133	9.16	6.84
Jun	1.20	124	133	9.69	7.17
Jul	1.20	121	126	9.60	7.10
Aug	1.07	119	124	9.35	6.94
Sep	0.99	117	124	8.96	6.67
Oct	0.81	114	120	8.30	6.14
Nov	0.80	112	119	7.89	5.98
Dec	0.72	107	113	7.70	5.89

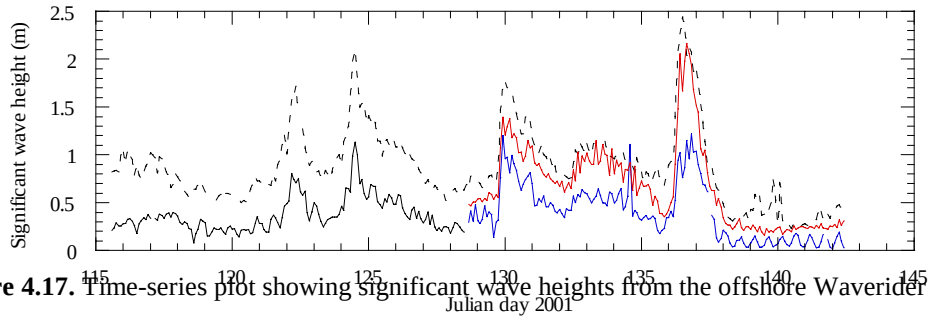

Figure 4.17. Time-series plot showing significant wave heights from the offshore Waverider buoy (dashed line) and the nearshore sites CM2 (black line), CM3 (blue line) and CM4 (red line).

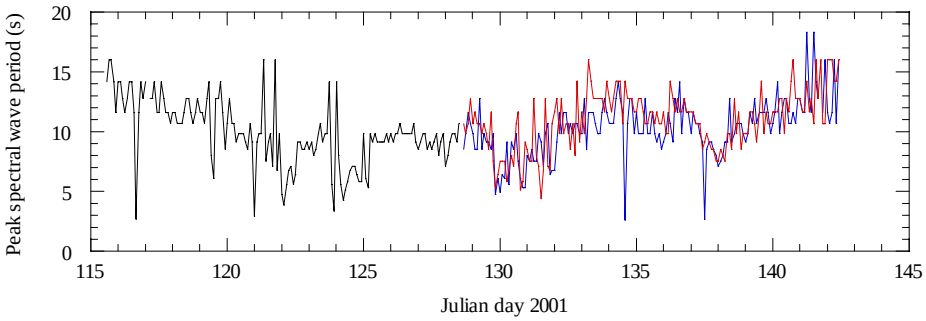

Figure 4.18. Time-series plot showing peak spectral wave periods at the nearshore sites CM2 (black line), CM3 (blue line) and CM4 (red line).

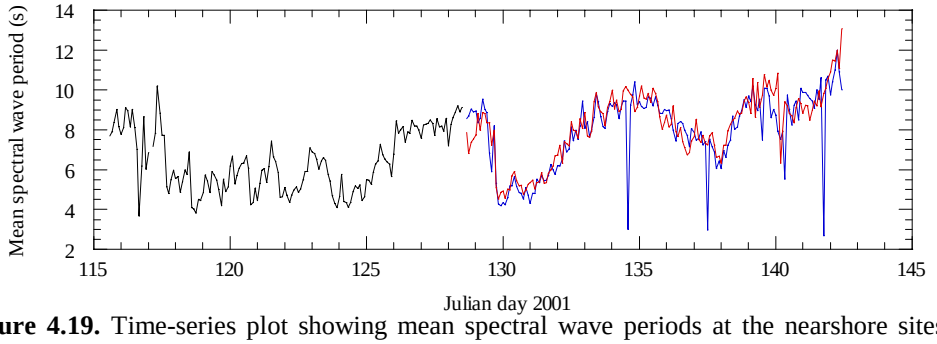

Figure 4.19. Time-series plot showing mean spectral wave periods at the nearshore sites CM2 (black line), CM3 (blue line) and CM4 (red line).

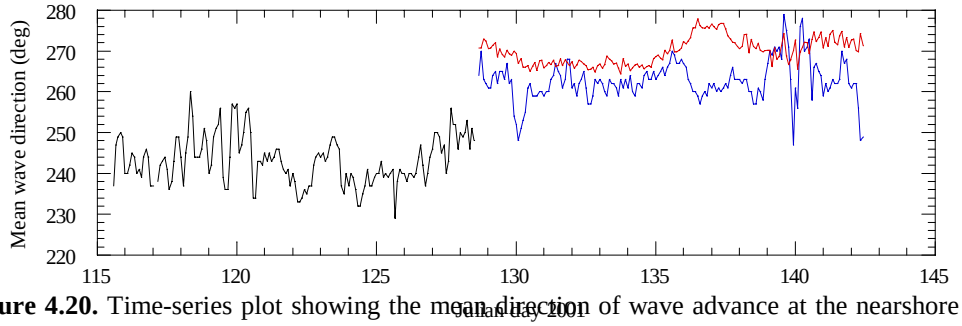

Figure 4.20. Time-series plot showing the mean direction of wave advance at the nearshore sites CM2 (black line), CM3 (blue line) and CM4 (red line).

Table 4.6. Average wave height ratios for the nearshore sites. This ratio is calculated as the nearshore Hs / offshore Hs.

Site	Ratio (nearshore / offshore)
CM2	0.40
CM3	0.41
CM4	0.76

4.4.4 Currents

Coastal circulation patterns are often the net result of several forcing functions (e.g. tidal, wind-driven, or wave-driven parameters) interacting with the coastal morphology. This may lead to complex or reversing flows. The net currents measured at 1 m above the seabed at the four sites (e.g. Fig. 4.1) are presented in the following figures as a times-series of speed and direction, and as scatter plots.

At the offshore site (CM1), measured currents over 14 days were typically < 10 cms^{-1}, although speeds of up to 14-16 cms^{-1} were measured. The scatter plot (Fig. 4.21) indicates the higher velocities are associated with ESE and NNW currents, which is approximately congruous with the isobaths at this location and is indicative of a tidal oscillation.

Similar current velocities were also measured at the nearshore sites, although the spread of direction varied at each site. At CM2 in the sheltered zone between the port headland and Westshore Beach (Fig. 4.1), the current directions were primarily directed to the NE, with very few data measurements having a westerly vector (Fig. 4.22). The coast at this location is approximately aligned east-west, and the currents are directed toward the dredged channel and port entrance.

At site CM3 (~1125 m west of CM2, just north of the surf lifesaving club at Westshore beach), the current directions have a very different distribution, and generally run along the isobaths with a SE-NW trend (Fig. 4.23). Further north at site CM4, the currents have a very strong bimodal trend, exhibiting approximately equivalent up-and down-coast flows (i.e. N-S directed) (Fig. 4.24), which is partly related to the general wind direction (Fig. 4.8) during periods of low wave height and generally N directed during larger wave events (Fig. 4.10).

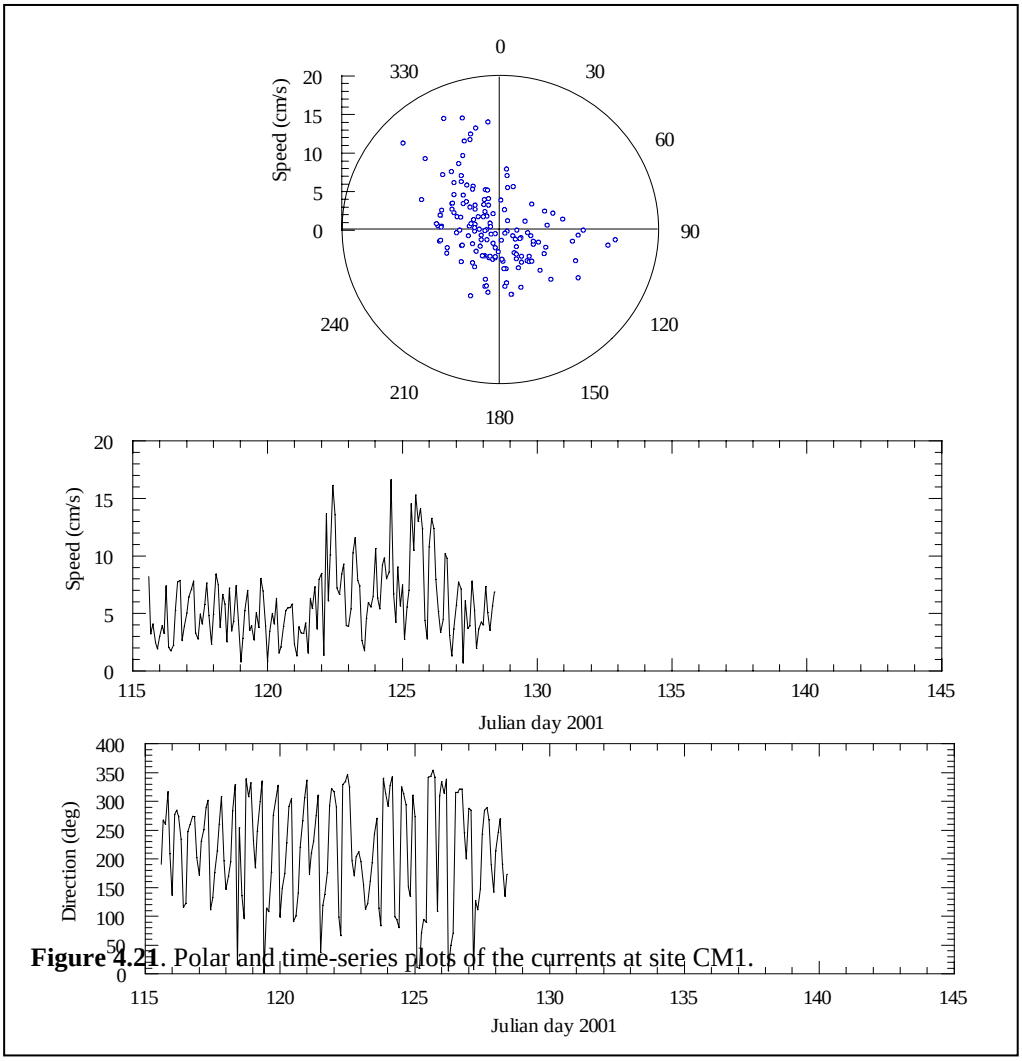

Figure 4.21. Polar and time-series plots of the currents at site CM1.

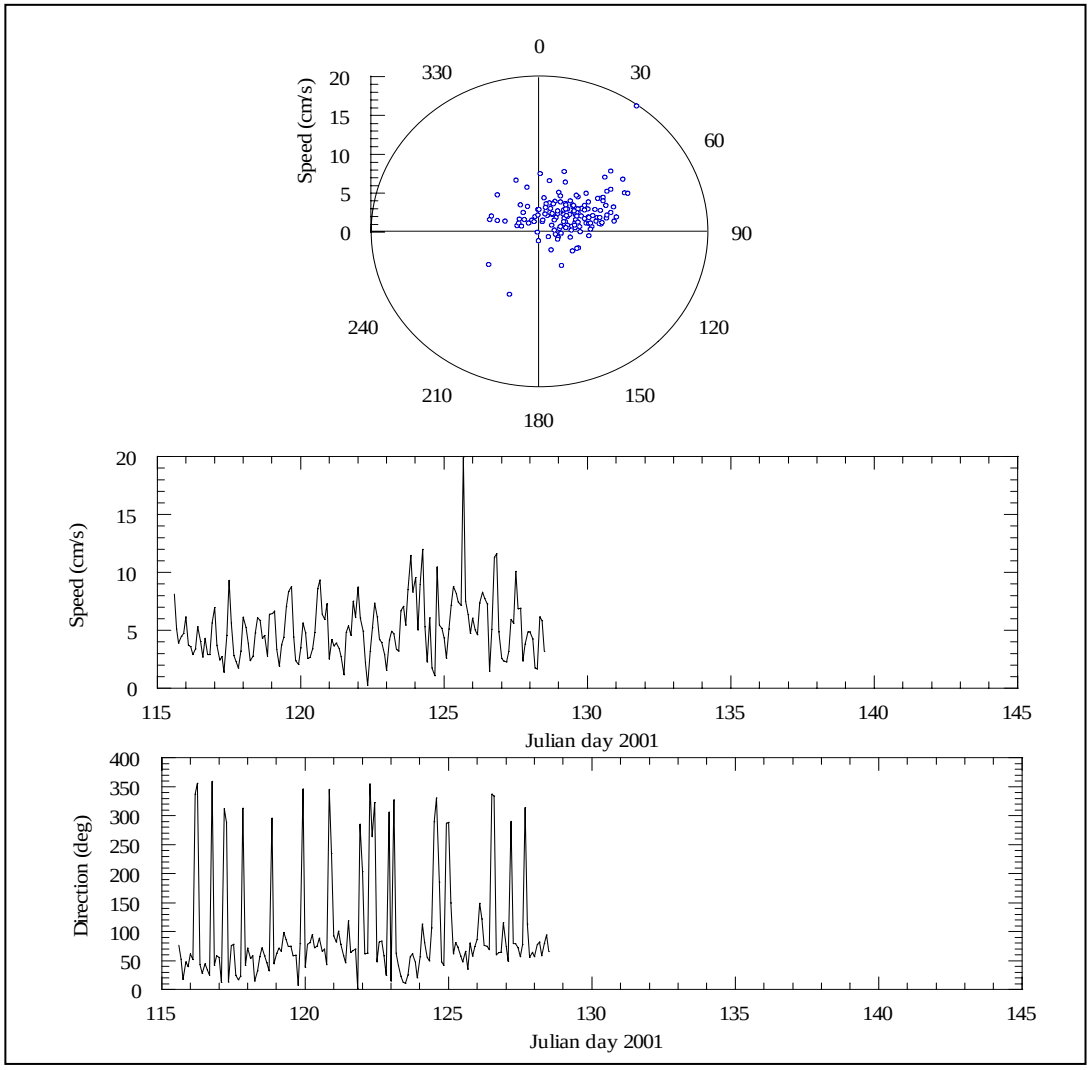

Figure 4.22. Polar and time-series plots of the currents at site CM2.

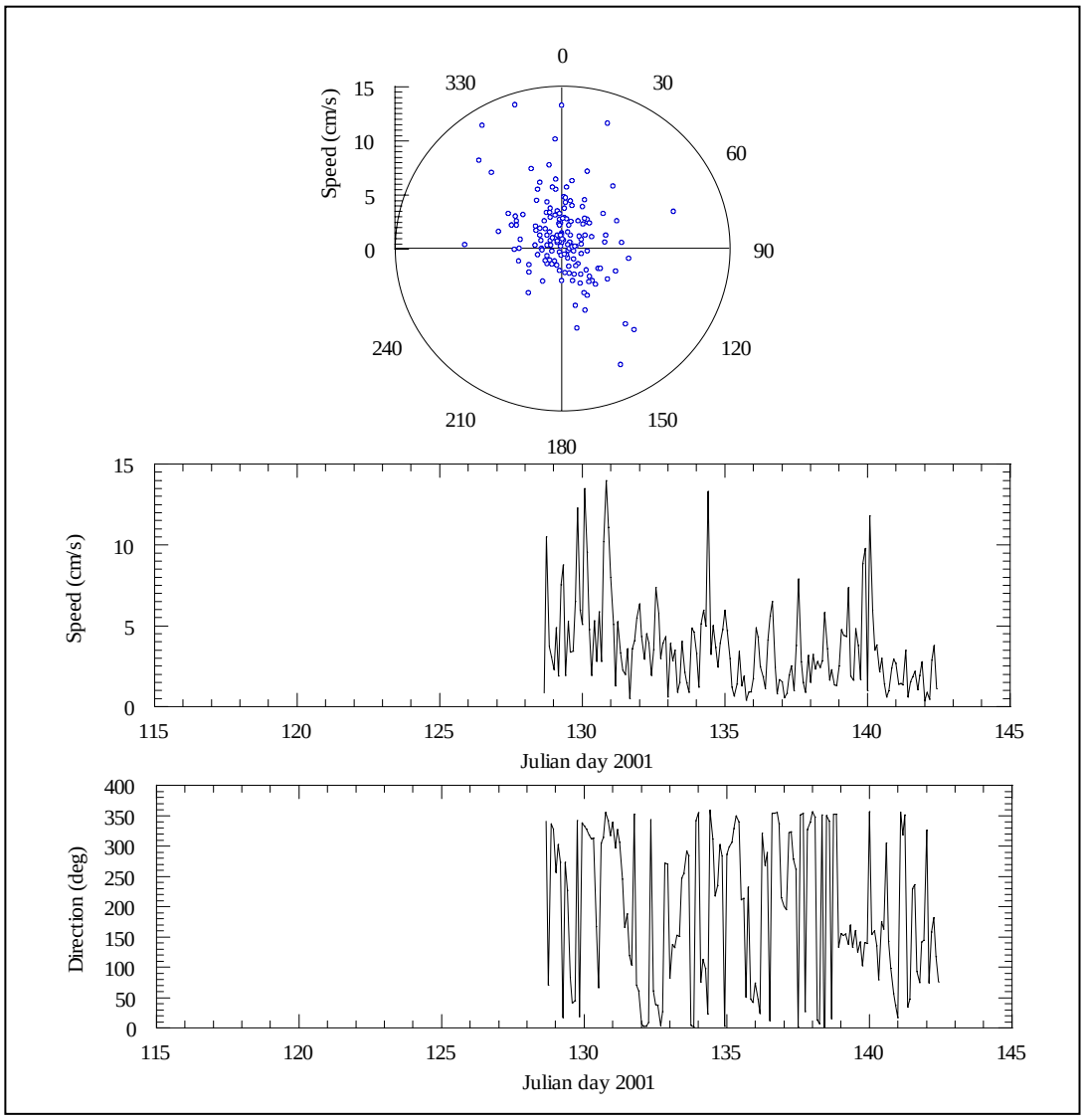

Figure 4.23. Polar and time-series plots of the currents at site CM3.

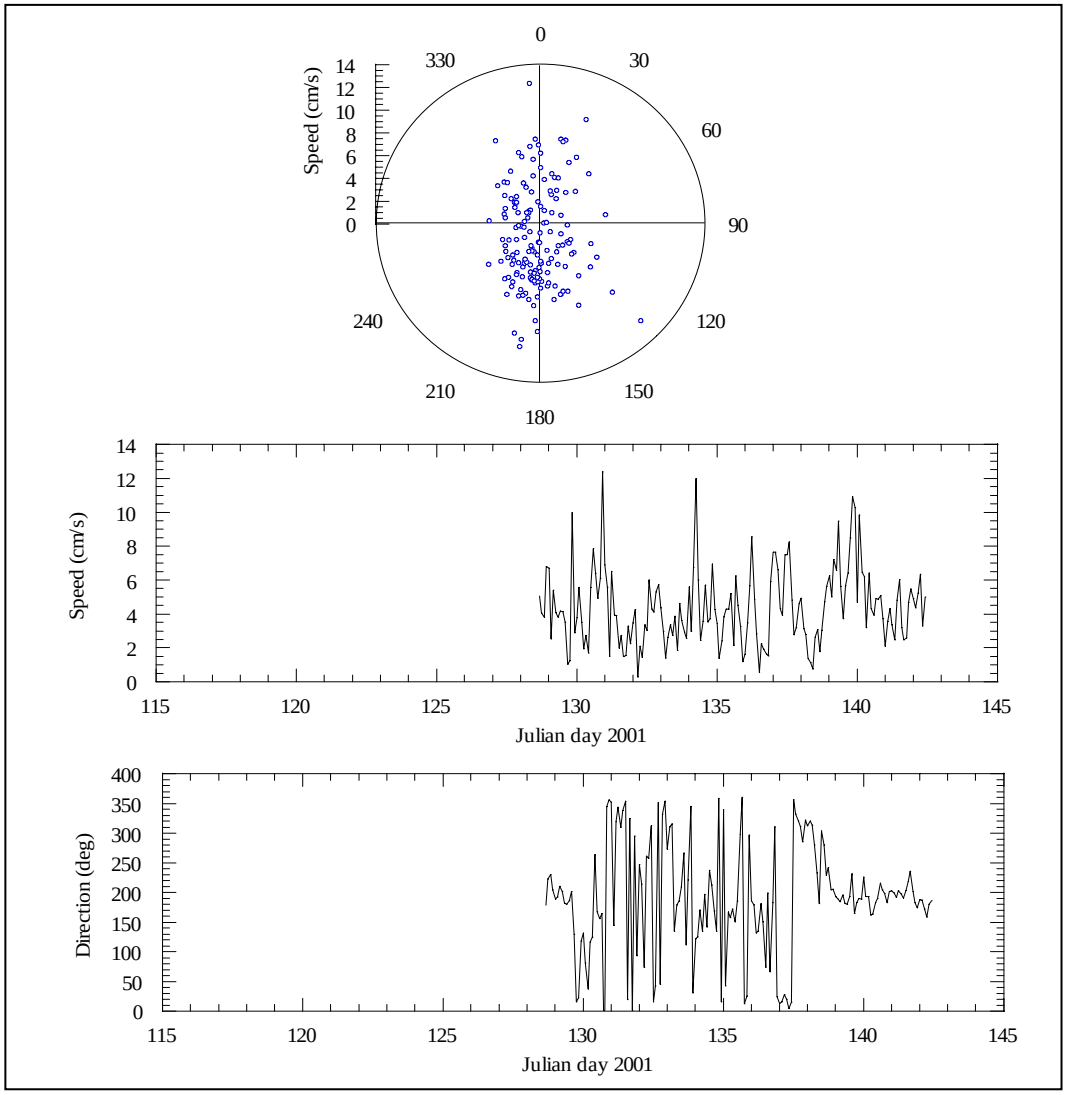

Figure 4.24. Polar and time-series plots of the currents at site CM4.

The vector-averaged currents for each current meter during its 15-day deployment are presented in Table 4.7 and Figure 4.25. The pattern of vector-averaged currents suggests a predominantly northerly current flow on the open coast with a reversal of current direction in the lee of the Port and headland. Some caution must be exercised when interpreting these data, as they represent an average of the currents recorded over a short period of time, which is biased towards the wave and wind conditions that were present during this time. While these data are useful for interpreting current circulation within the study region, their application to model calibration is far more valuable in understanding the processes operating within Westshore Bay (Chapter 5).

Table 4.7. Vector averaged currents measured at sites CM1 to CM4. Velocities in cm s^{-1} and directions in °T.

	CM1	CM2	CM3	CM4
u	-1.1221	1.557291	-0.02588	-0.27094
v	0.462151	1.741932	1.225628	-1.22247
Velocity	1.213542	2.336553	1.225901	1.252137
Direction	292.385	48.20321	358.7902	192.4967
Mean Vel.	5.92385	4.37352	3.651043	4.381784

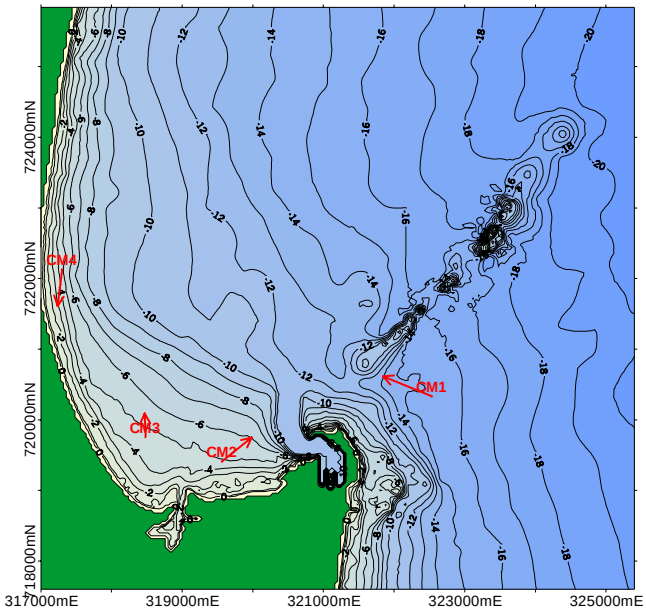

Figure 4.25. Vector average currents at the four current meter sites (CM1 and CM2 from 25/4/01 to 10/5/01; CM3 and CM4 from 10/5/01 to 24/5/01).

4.4.5 Suspended sediment concentrations

The amount of sediment suspended in the water is directly related to the grain size of the sediment, and the wave-orbital induced stress on the seabed. Consequently, higher concentrations of suspended sediments are expected during the larger wave events, and also in regions that experience higher wave energy or shallower water depths. The suspended sediment concentrations (SSC) measured with traps are given in Table 4.8. The data range from 0.0002 - 0.0313 kgm^{-3}, which is approximately 15% of the values observed in high-energy environments (such as the Taranaki coast). The lowest values were recorded offshore in the deep water (site CM1), while the highest values were observed at the shallow nearshore site CM4.

The data from 0.4 m elevation above seabed is presented in Figure 4.26

Table 4.8. Results from sediment trapping measurements. Trap set A and B refer to the first and second two-week deployments, z is the elevation of the trap aperture above seabed, time is the duration of the trap deployment, *W* is the mean settling velocity as measured by the RSA fall tube, and C(z) is the time-averaged suspended sediment concentration at level z.

Site	Trap set	z (m)	Time (s)	Mass (kg)	*W* mean (m/s)	C(z) (kg/m^3)
CM1	A	0.4	597600	0.00544	0.155	0.00022
	A	0.8	597600	0.00054		
CM2	A	0.4	1202400	0.01895	0.034	0.0017
	A	0.8	1202400	0.00251		
ST1	A	0.4	1202400	0.08408	0.021	0.0126
	A	0.8	1202400	0.0298	0.019	0.0050
ST2	A	0.4	1202400	0.02374	0.054	0.0014
	A	0.8	1202400	0.0033		
ST3	A	0.4	1202400	0.03343	0.018	0.0057
	A	0.8	1202400	0.0031		
ST4	A	0.4	1202400	0.00456	0.027	0.0005
	A	0.8	1202400	0.00069		
CM1	B	0.4	594000	0.02189	0.027	0.0052
	B	0.8	594000	0.00896		
CM3	B	0.4	1195200	0.14036	0.058	0.0077
	B	0.8	1195200	0.01489	0.031	0.0015
CM4	B	0.4	1195200	0.31027	0.031	0.0313
	B	0.8	1195200	0.01946	0.031	0.0020
	B	0.8	1274400	0.00351		
ST2	B	0.4	1274400	0.05595	0.034	0.0049
	B	0.8	1274400	0.00203		
ST3	B	0.4	1274400	0.0681	0.021	0.0094
	B	0.8	1274400	0.01126	0.018	0.0018
ST4	B	0.4	1274400	0.12362	0.027	0.0134
	B	0.8	1274400	0.0171	0.040	0.0013

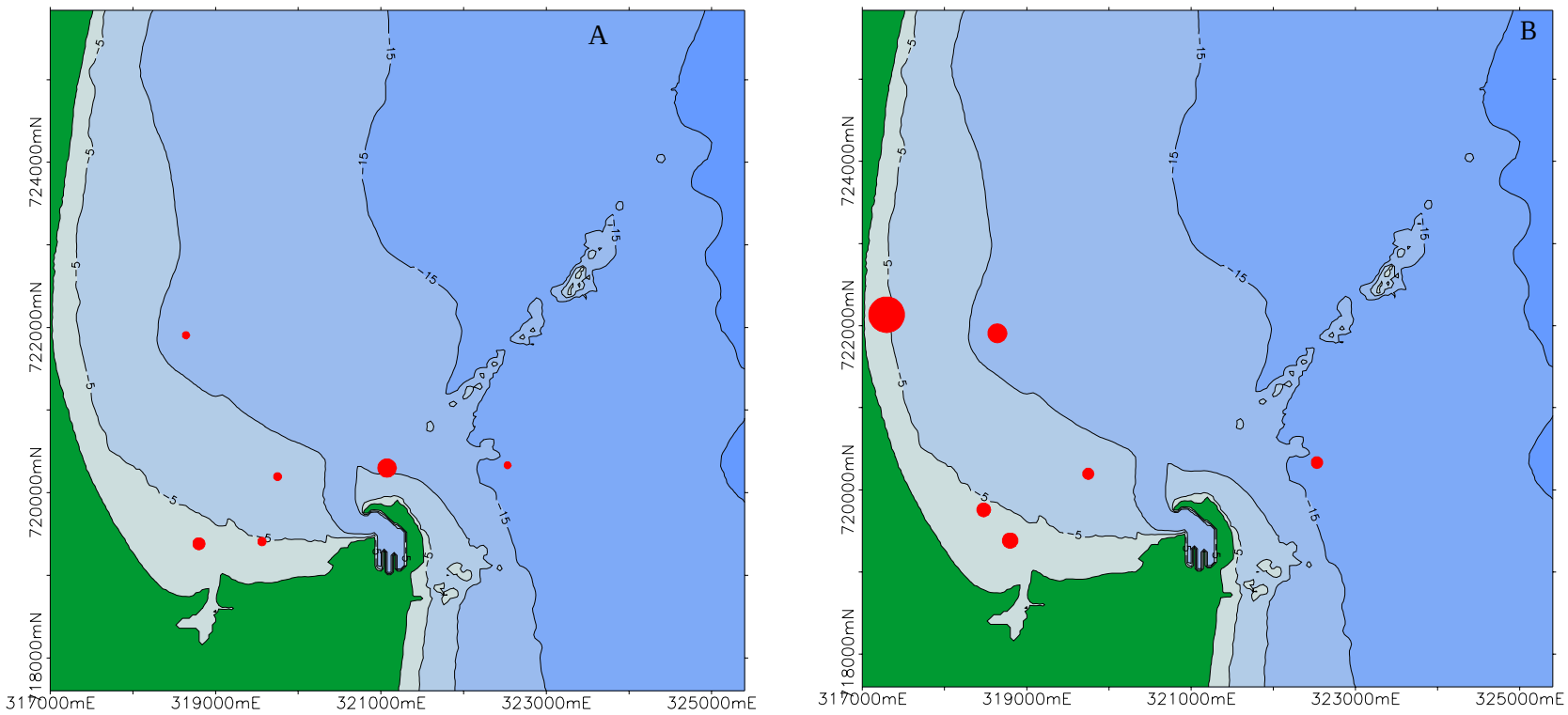

Figure 4.26. Bathymetric map showing the time-average suspended sediment concentration measured by traps from the 0.4 m level above bed. Data presented are from deployments A and B (Table 4.7) and the SSC is given as dots linearly scaled in size from 0.0002 kg.m^{-3}to 0.032 kg.m^{-3}.

4.4.6 Tides

While waves are often the dominant process controlling sediment movement and beach morphology, the tidal range and tidal currents can also influence the beach and nearshore system. Over the measurement period, a tidal range of 1.83 m was observed (Fig. 4.8) and the published values for Port Napier indicate a mean spring range of 1.8 m (Table 4.8). This relatively low range means there is only moderate translation of surf and breaker zones across the beach face

Table 4.8. Tidal water levels about Chart Datum at Port Napier

TIDE LEVELS	ELEVATION (m)
HAT	1.8
MHWS	1.6
MHWN	1.5
MSL	0.9
MLWN	0.3
MLWS	0.2
LAT	0

4.4.7 Seabed Description

Diver inspection of the seabed during deployment and servicing at the wave/current meter and sediment trap sites (Fig. 4.1) indicated that the seabed consists of a fine sand in the deeper regions to the south and east of the study site and was covered by a muddy ooze in shallow areas and even in depths of 10 m in the northern region. Very small sand ripples, measuring less than 20 cm peak to peak with a trough to peak heights of less than 2 cm were observed at some sandy sites; others were featureless. Sand dollars (*Fellaster zelandiae*) were common at the shallower sandy sites and hermit crabs and signs of bristle worms were evident at deeper sites.

4.4.8 Beach Profiles

The results of the beach profile surveys from each site (Fig. 4.27) are presented in Figures 4.28 to 4.40, described below and summarised in Table 4.9.

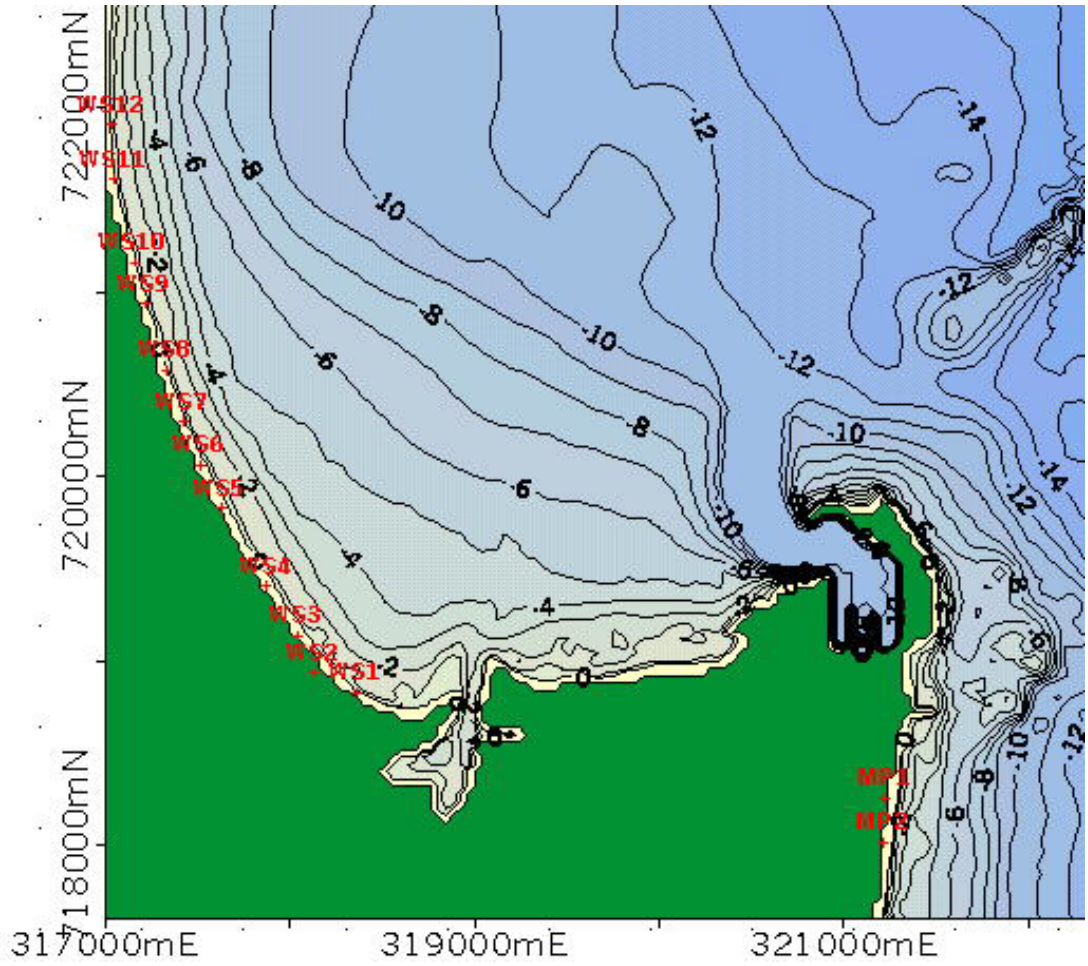

Figure 4.27. Location map of beach surveys.

WS 1:

- Slight erosion of upper berm by second survey
- Accretion along the entire berm profile by third survey

WS 2:

- Erosion and steepening of berm after each survey
- Largest erosion after completion of second survey

WS 3:

- Small net change in profile between first and second surveys with steepening of berm due to storm event
- Complete erosion of berm by third survey

WS 4:

- Significant cut away of berm by second survey
- Accretion over entire cross-section with profile returning to original state by final survey

WS 5:

- First survey showed stepped berm
- Accretion by second survey and berm smoothed out
- Frontal dune slumped to build up upper berm while lower berm eroded

WS 6:

- Berm profile data only for last two surveys
- Profile shows well defined steps in berm

- The third survey shows erosion along entire frontal dune and berm, whole profile transposed landward approximately 2m

WS 7:

- Berm cut away by second survey
- Significant accretion by third survey that is not sourced from the frontal dune

WS 8:

- Lower berm accretes by second survey
- Erosion over entire berm profile by third survey with step in berm

WS 9:

- Original profile has a significant step in the berm
- By the second survey the berm has accreted and smoothed out and retains the same profile for the third survey

WS 10:

- Not much change between first two surveys
- Erosion by third survey

WS 11:

- Berm evolves slowly from smooth profile to a profile with more of a step
- Most erosion occurs between first and second surveys

WS 12:

- Accretion and flattening of berm profile between surveys one and two
- Erosion and steeping of berm profile between surveys two and three

MP 1:

- Not much change between first two surveys
- Smooth profile for fist two surveys
- Step and slight accretion by third survey

MP 2:

- Toe of berm erodes and middle of berm accretes by second survey
- Lower and middle berm retain profile after the third survey but upper berm accretes significantly

Many stages of berm and frontal dune evolution can be seen in the 28 profiles. Smooth berm and dune profiles are eroded after storm events, of which there were two in each two-week period (e.g. Fig. 4.17), to form a stepped berm in profiles WS1, WS8 and WS11. The opposite can be seen with profiles WS3 and WS10 where the berm has a well-formed step after survey one but smoothes out to a more regular profile by survey three.

Slumping of the upper berm causing accretion of sediment on the lower berm can be seen in profiles WS1, WS3, WS8, WS10, WS11 and MP1.

The most significant change in beach profiles between the surveys is seen in WS3, WS5 and WS6 where the frontal dune is eroded. This dune erosion presents a more critical coastal management problem than the more sustainable onshore-offshore exchanges of sediment over the berm. Depending on the supply of sediment and wave conditions the dune may take a long time to recover from a significant storm – at Westshore annual renourishment in required. The dune sediment from WS3 has been transported either offshore or longshore, through general diabathic processes. The dune sediment from WS5 and WS6 seems to be retained in the berm during the time of the surveys. Subsequent wave events may have transported the sediment away similar to WS3.

Table 4.9. Summary table of beach profile trends during the field study. E = Erosion A = Accretion

SURVEY	WS1	WS2	WS 3	WS 4	WS 5	WS 6	WS 7	WS 8	WS9	WS10	WS11	WS12	MP1	M P2
1-2	E	E	E	E	A	-	E	A	A	-	E	A	-	E
2-3	A	E	E	A	E	E	A	E	-	E	-	E	A	A

Table 4.91 shows whether erosion or accretion has occurred between the three surveys for each profile. There is no consistent trend of either erosion or accretion along the Westshore profiles indicating that the beach has three dimensional sediment transport pathways. The general trend is that the profiles eroded, evolving into their winter states with some localised areas of accretion. 66% of the profiles eroded between surveys one and two with a slight increase to 75% between surveys two and three. It is difficult to quantify exactly what accretion and erosion processes are happening from beach profiles when the beach has cuspate formations. Between surveys if cusps develop then the profile may be shown to erode or accrete depending on the location of the cusp relative to the survey line. However realistically the trend for the profile may be the opposite.

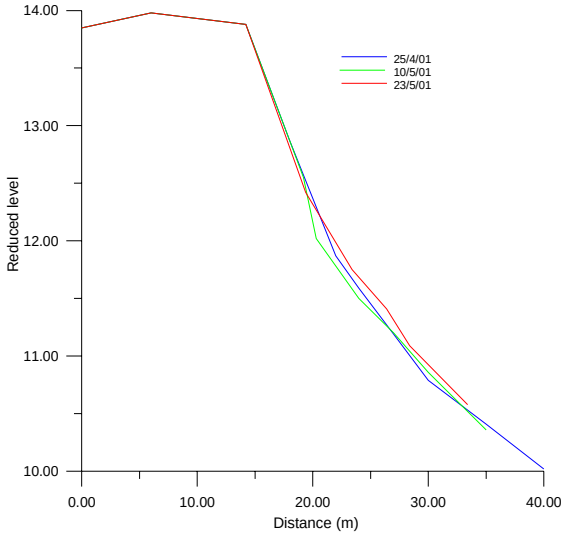

Figure 4.28 Westshore 1

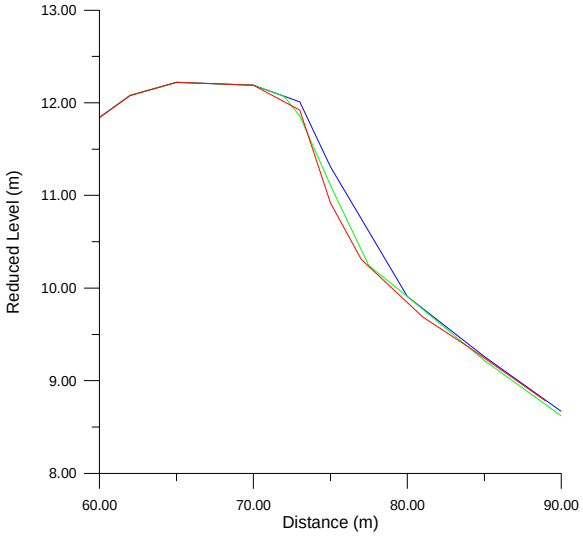

Figure 4.29 Westshore 2

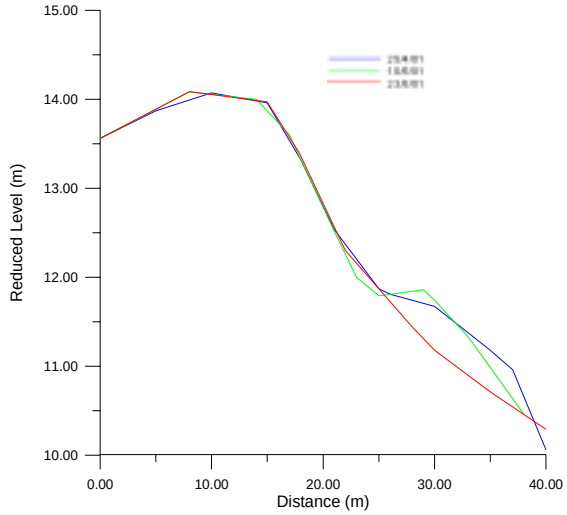

Figure 4.29 Westshore 3

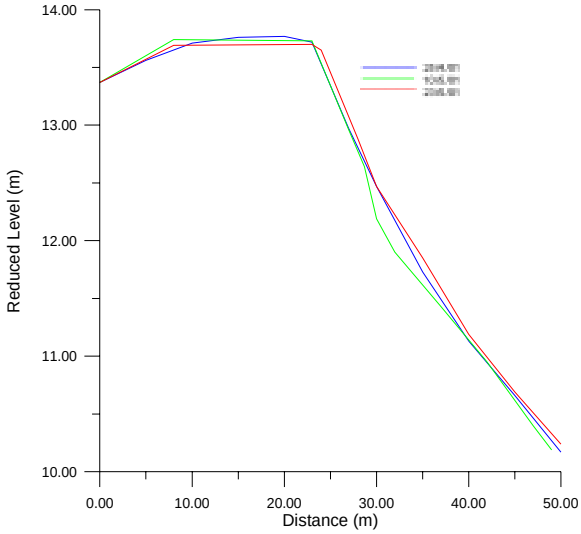

Figure 4.30 Westshore 4

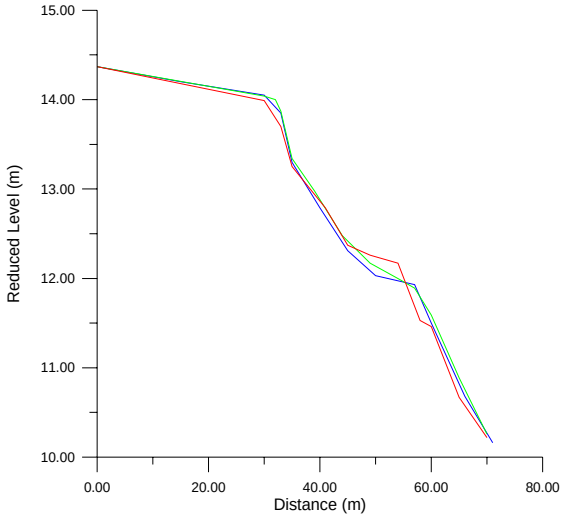

Figure 4.31 Westshore 5

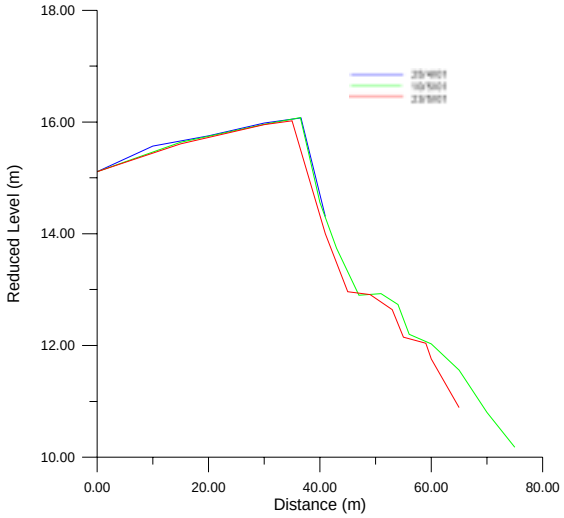

Figure 4.32 Westshore 6

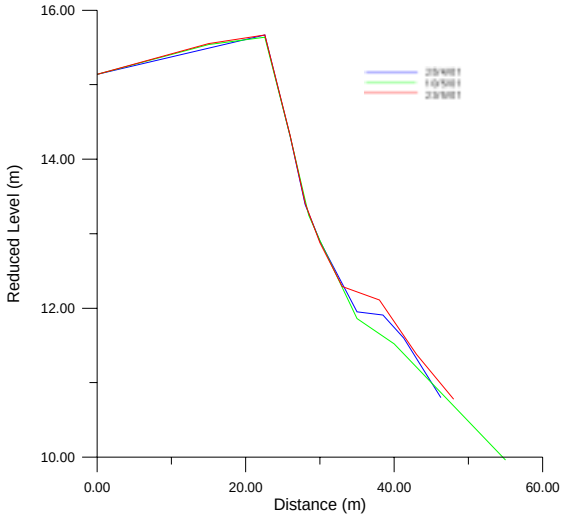

Figure 4.33 Westshore 7

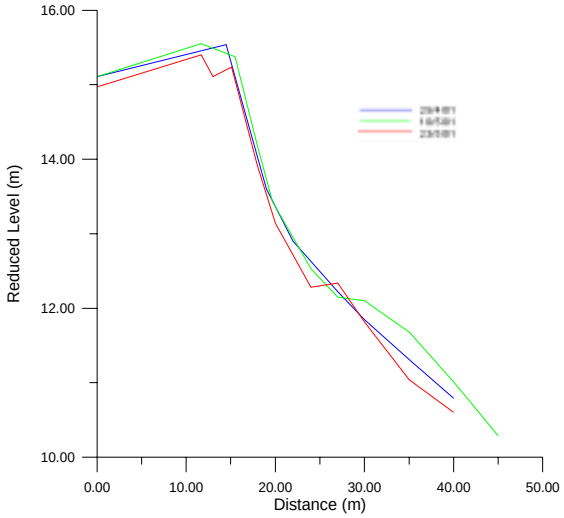

Figure 4.34 Westshore 8

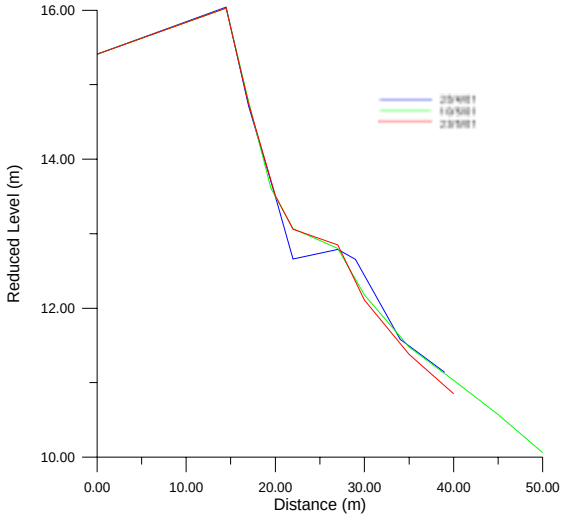

Figure 4.35 Westshore 10

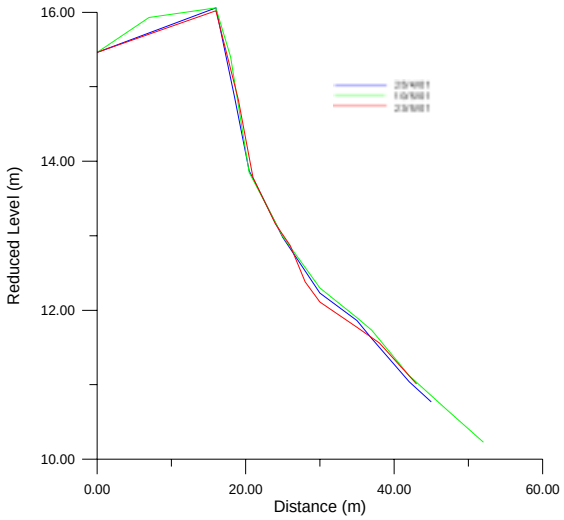

Figure 4.36 Westshore 10

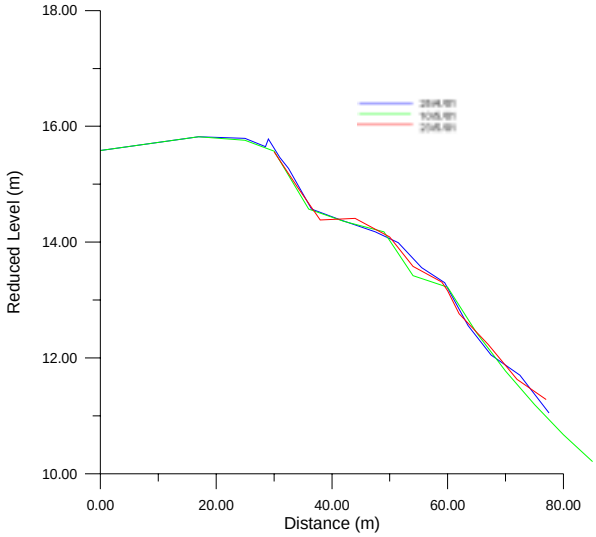

Figure 4.37 Westshore 11

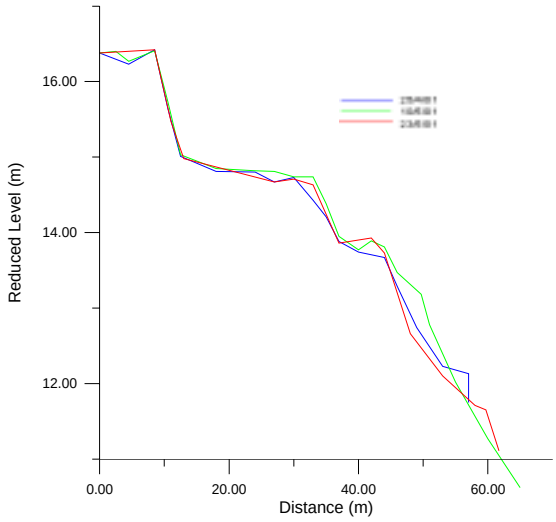

Figure 4.38 Westshore 12

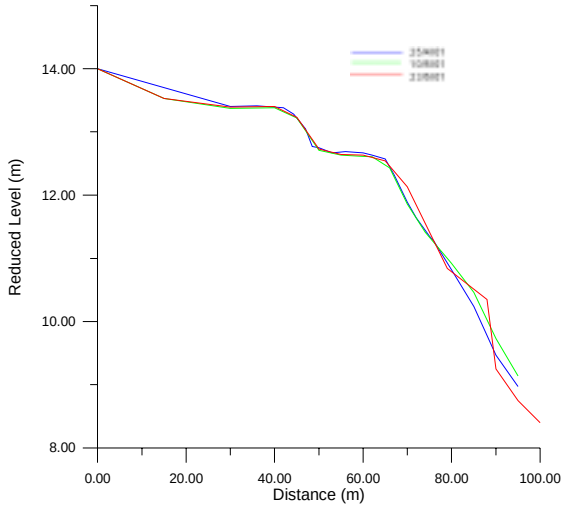

Figure 4.39 Marine Parade 1 (False Datum)

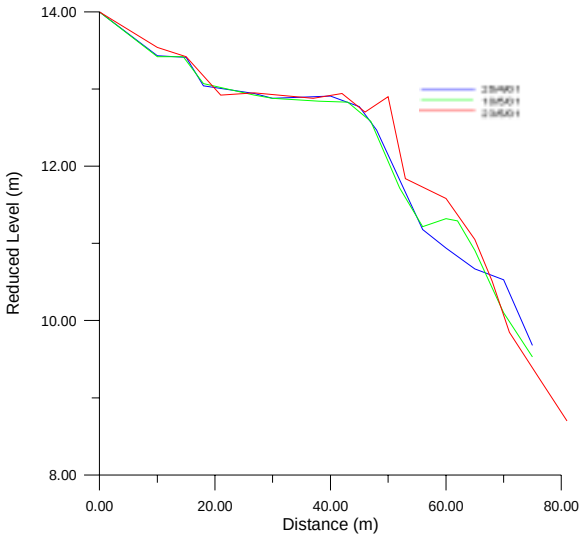

Figure 4.40 Marine Parade 2 (False Datum)

5 NUMERICAL MODEL CALIBRATION

5.1 Introduction

Numerical modelling is a powerful tool in physical systems. The models are able to examine systems to unravel the complexity of the multiple processes that may occur simultaneously. Also, the models can be used in forecast mode to predict future outcomes. In the present study, we are using models for both of these options.

The models take point-data to provide detailed spatial information on waves, currents and sediment movement, but only after the suite of models is calibrated against the measurements can there be confidence in these predictions. The models are then used to simulate a much broader range of cases and to assimilate the full dataset into an overall prediction of the sediment fluxes. The models supported by field measurements are being used in this project to provide an understanding of circulation and wave dynamics at Westshore.

To underpin the modeling by understanding and quantifying the physical processes at the study site, the previous chapters have presented summaries of historical measurements and the field program of the present study. Many insights have been gained including observations of wave distributions, current patterns and current strengths. The models need to assimilate this knowledge, and shown to be predicting the essential character of the system before we can have confidence in their capability. This stage of the modeling process is called model calibration.

Specifically, the goals of the modeling are to:

- transfer waves measured at the wave buoy and our own offshore site into Westshore Bay.
- Simulate the measured currents in the bay to examine overall circulation patterns, residual flows and the likely net movement of sediment.

5.2 The process of model calibration

Calibration of computer models is the most important (and sometimes the most time-consuming) aspect of any numerical model study. Calibration achieves two main outcomes:

- the level of confidence in the model predictions is established; and
- the best possible accuracy is obtained after the calibration is carefully done and the model is properly optimised.

However, the process of calibration requires a detailed assessment of the local data and of the field site characteristics to fully realise the potential of the models.

Every site has special characteristics such as the presence of a headland, rocky patches, unusual wave climate, strong seasonality, sand inputs from various sources or man-made structures. This means that errors can develop in a model simulation if these special features are not properly accounted for. Consequently, computer models need to be able to be refined to match the site, and the decision-making leading to any modifications occurs during the calibration phase.

The process of calibration also involves adjustment of empirical coefficients in the models. While some mathematically rigorous equations of a model cannot be adjusted, some of the terms in these equations are empirical (i.e. derived from data analysis). As such, the coefficients may vary from site to site and therefore need calibration so that predictions best match the data (at which time the model is said to be “calibrated”). To be certain that these adjustments are not simply correct for the one dataset, the model is subsequently “verified” against a different dataset from the site, without changing any of the empirical coefficients in the model.

On the open coast, recent studies for the design of a beach protection unit at Noosa, southern Queensland, Australia, involved coupled modelling of multiple processes (Black *et al.*, 2001). As at Westshore, the main beach is situated adjacent to a headland where waves have to refract through large angles to reach the site. These waves are responsible for suspending

sediment and for the formation of strong longshore (wave-driven) currents, which lead to changes in the seabed and beach erosion. As such, it was necessary to use independent, but coupled, models to predict wave transformation and circulation.

In the next section, the process of model calibration at Westshore is described. The data available for calibration remains relatively limited in this phase of the study, as currents could only be recorded for 4 weeks in total. However, the capacity of the model to reproduce these data can be confirmed and the calibrated model can then be used for data interpretation. We use 3 models and treat several categories of modelling:

- Wave transformation – with Model WBEND
- Surfzone longshore transport - with Model GENIUS
- Coastal circulation - with Model 3DD

The models are described in Appendices 1 to 3. Because of the various spatial scales involved in the study, we have developed a series of model grids that deal with the different relevant processes at different scales. These are described in Chapter 2. We separately consider the calibration of the wave model WBEND and then the hydrodynamic model 3DD. The hydrodynamic model 3DD is used in Boussinesq mode for short-wave simulations and 2-dimensional depth-averaged mode for simulations of wind-driven, tidal and shelf currents. In all cases, the models are validated against the measurements made at the 4 sites during the field program.

5.3 Wave Height and Direction

The directional wave data recorded in the first deployment period (Section 4.4.3) were used to calibrate Model WBEND. Wave height, angle (rotated to model orientation and converted to Cartesian angles) and period measurements recorded at CM1 (Fig. 4.1) were applied to the model as the boundary conditions. A series of model simulations with a combination of model calibration parameters (wave angle eddy viscosity, wave height eddy

viscosity, seabed friction) (Appendix 1) were undertaken and each output was then compared back to the recorded data (at CM1 and CM2).

Figures 5.1 to 5.4 present the results of the calibration parameters with model outputs that closely reproduced those recorded by the wave/current meters.

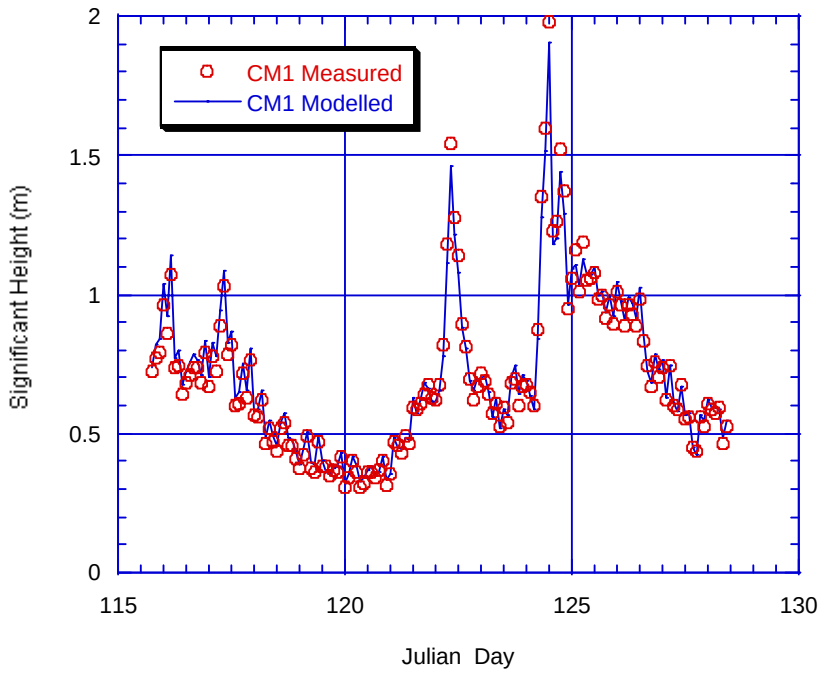

Figure 5.1. CM1 wave height calibration for model WBEND

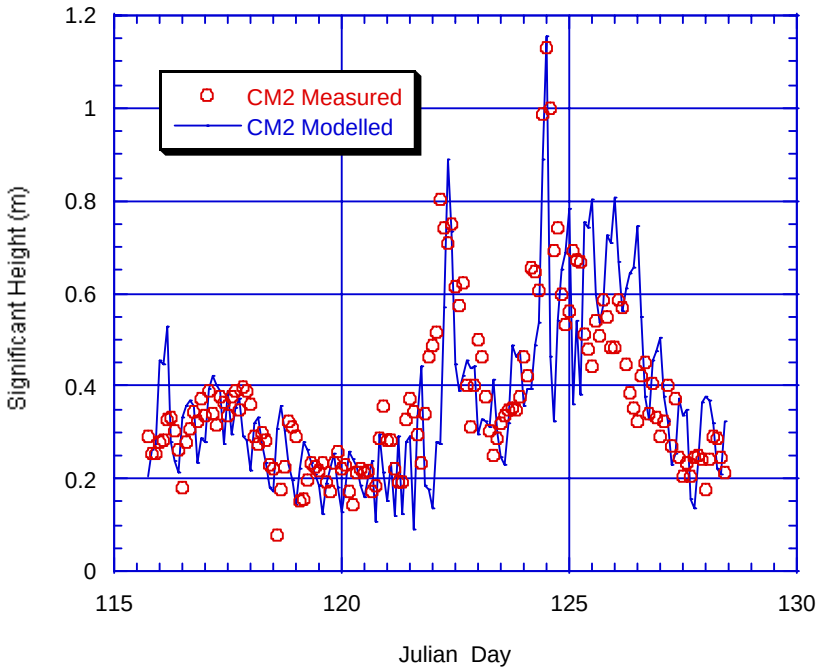

Figure 5.2. CM2 wave height calibration for model WBEND

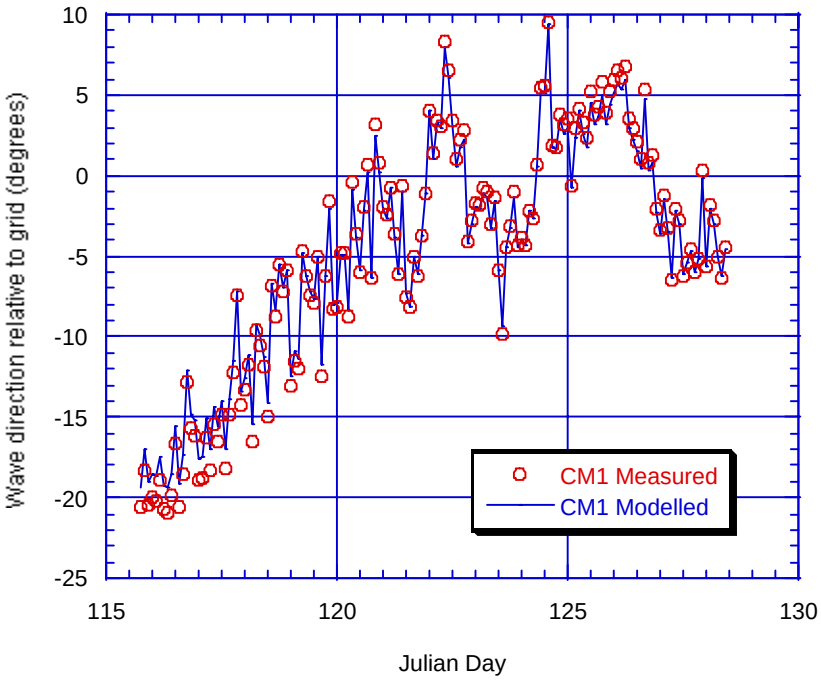

Figure 5.3. CM1 wave direction calibration for model WBEND

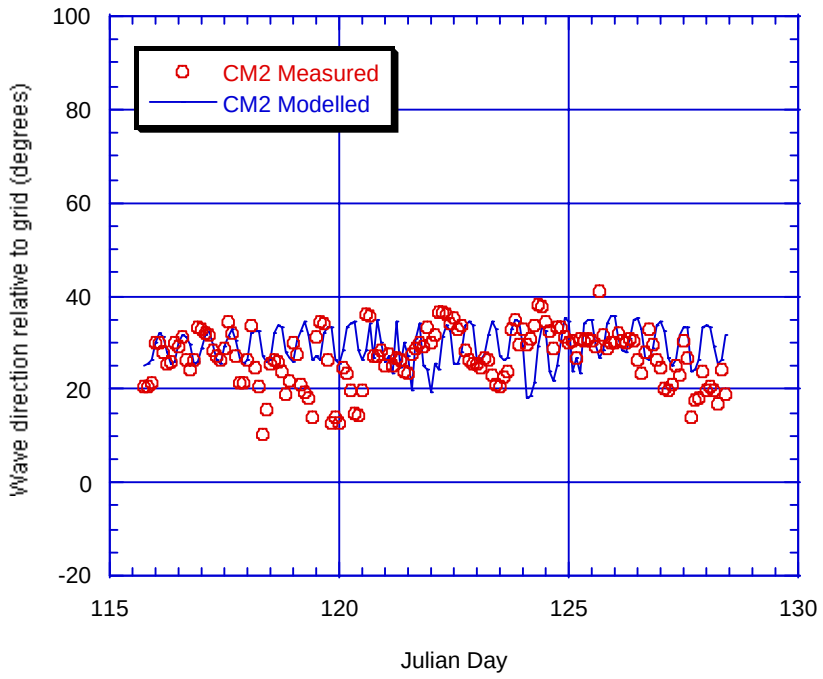

Figure 5.4. CM2 wave direction calibration for model WBEND

5.4 Boussinesq modelling

With Model 3DD in Boussinesq mode, the model can be used to simulate short-waves, i.e. the 10-14 s waves that are observed on beaches. We have modelled a typical case of waves from the east in Figure 5.5 and have compared the model output to a series of aerial photographs (Fig. 5.6), which clearly show the rotation and propagation of the waves into the bay. While this is only a qualitative comparison, the model appears to be reproducing the features of the aerial photographs with the same rotation (refraction) patterns and wave height transformations. Further comparisons are made to our field data. Both the rotation of wave direction and the reduction in wave height due to refraction into the Westshore Bay are clearly evident in the wave/current meter records (Figs. 4.17 and 4.20), and can be seen in both the model simulation (Fig. 5.5) and the aerial photographs Fig. 5.6).

There many relevant features of the model run, including the two bands of higher wave energy stretching from the offshore reefs and the tip of the port, the strong refraction in the

lee of the port along the coast, the small wave heights which diffract into the port and the shoaling over the sand spit at the tip of the port entrance. Also relevant is the refraction of energy into the Ahuriri Entrance along the headland. Similar, reinforcement of wave energy and higher breaking waves is observed in the aerial photograph.

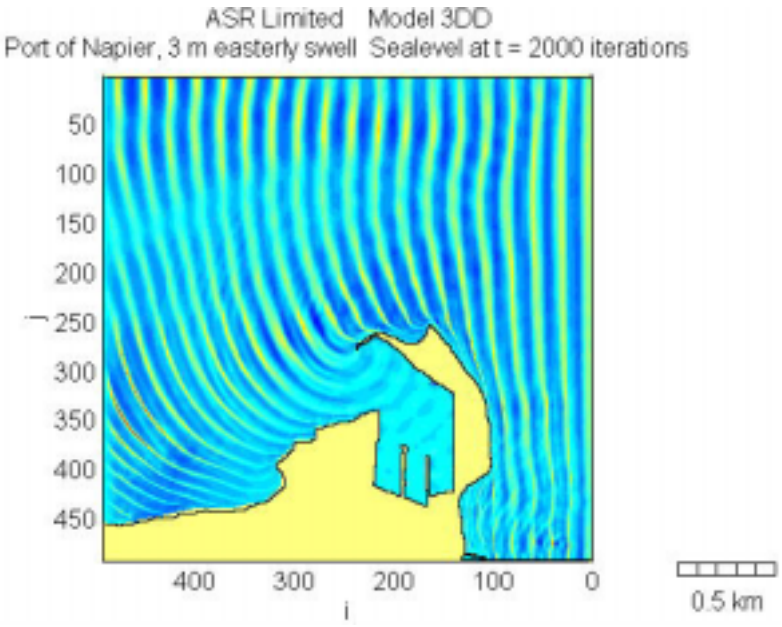

Figure 5.5. Numerical model output of a 2 m swell from the dominant, easterly, direction.

Figure 5.6. Aerial photo mosaic of the Port and Ahuriri Entrance showing wave refraction.

5.5 Calibration of the 3DD Depth-Averaged Circulation Modeling

5.5.1 Hydrodynamics

Model 3DD solves the momentum and mass conservation equations given by:

$$\frac{\partial u}{\partial t}+\frac{u\partial u}{\partial x}+\frac{v\partial u}{\partial y}+\frac{w\partial u}{\partial z}-fv=-\frac{g\partial \zeta}{\partial x}-\frac{1\partial P}{\rho\partial x}+A_H\left(\frac{\partial^2 u}{\partial x^2}+\frac{\partial^2 u}{\partial y^2}\right)+\frac{\partial}{\partial z}\left(N_z\frac{\partial u}{\partial z}\right)+S_b \qquad \textbf{(5.1)}$$

$$\frac{\partial v}{\partial t}+\frac{u\partial v}{\partial x}+\frac{v\partial v}{\partial y}+\frac{w\partial v}{\partial z}+fu=-\frac{g\partial \zeta}{\partial y}-\frac{1\partial P}{\rho\partial y}+A_H\left(\frac{\partial^2 v}{\partial x^2}+\frac{\partial^2 v}{\partial y^2}\right)+\frac{\partial}{\partial z}\left(N_z\frac{\partial v}{\partial z}\right)+S_b \qquad \textbf{(5.2)}$$

$$w=-\frac{\partial}{\partial x}\int_{-h}^{z}u\,dz-\frac{\partial}{\partial y}\int_{-h}^{z}v\,dz \qquad \textbf{(5.3)}$$

t is the time, u, v are velocities in the x, y directions respectively, w the vertical velocity in the z direction (positive upward) at the top of each layer, h the depth, g the gravitational acceleration, ζ the sea level above a horizontal datum, f the Coriolis parameter, P the pressure, ρ the density of water, A_H the horizontal eddy viscosity coefficient, and N_Z the vertical eddy viscosity coefficient. S_b represents Boussinesq terms, and other forcing terms including body forces or radiation stress calculated from the wave height spatial gradients. To validate the model, the horizontal eddy viscosity, bed friction coefficients and boundary conditions have to be established or calibrated.

The model uses a complex set of inputs. First, a “body force” was applied to simulate the large-scale, pressure gradient-driven flows. The analysis of data showed that currents, at the offshore Site CM1 in particular, were responding to regional scale dynamics. That is, the flows were not just driven by local wind and tides but were responding to the passage of continental shelf waves which may be generated outside of the Napier region. It is not possible to model these directly because no sea level gradients were recorded over the required space scales. Instead, in the design of the field programme, allowance was made for the use of a body force. The same body force technique was successfully applied at New Plymouth to model the hot water discharges from the New Plymouth Power Station by Black & Sokolov (1993) and by Black and McComb (2001) in studies for the port of New Plymouth.

In essence, the body force is a surrogate pressure gradient calculated from the measured currents. By using a reduced version of the momentum balance of forces, the pressure gradient is obtained by calculating the bed friction, local acceleration, wind stress and Coriolis force terms in the momentum balance and summing these to obtain the pressure gradient. In the simplest terms, we are finding the unmeasured pressure gradient force that must have been present in the ocean that was responsible for creating the observed oscillations in the measured currents.

The body force is applied as a boundary condition via an extra term in the momentum equation. A constant roughness length of z_o=0.001 m was applied and checked by calibration. Local winds and water levels were measured at the Port. The body force was calculated at each current meter site and then the time series of body forces is time interpolated and then spatially interpolated onto the model grid using an inverse distance weighting. A calibration scale factor is applied to the body force time series and determined by trial and error adjustments during model calibration.

We compare the model to the first deployment of wave/current meters, as no offshore current meter was deployed during the second period.

5.6 Calibration results

During the measurement period, current meters were located offshore of the port and reefs (Site CM1) and in the lee of the port (Site CM2) (Fig. 4.1). The sites have individual character and it is the challenge of the model to reproduce this character and the magnitudes of the measured speeds and directions. The offshore site is situated in the inner shelf band, but is affected by the presence of the port and downstream reefs. The inner site is very sheltered and was placed to determine if an eddy exists in the lee of the headland.

The calibrated model results are shown in Figure 5.7a-d. The body force scale factors applied were 1.0 at the offshore site (CM1) and 0.05 in the eddy (CM2). The offshore factor of 1 is expected because the offshore site is in relatively open water, which means that it reflects the regional sea gradients, mostly unaffected by land forms. However at site CM2, much of the circulation and pressure gradients are local, i.e. associated with an eddy in the

headland and so the apparent pressure gradients associated with the local eddy cannot be applied throughout the model grid. Consequently, a small factor of 0.05 was adopted. Further trials with these factors could have slightly improved the results.

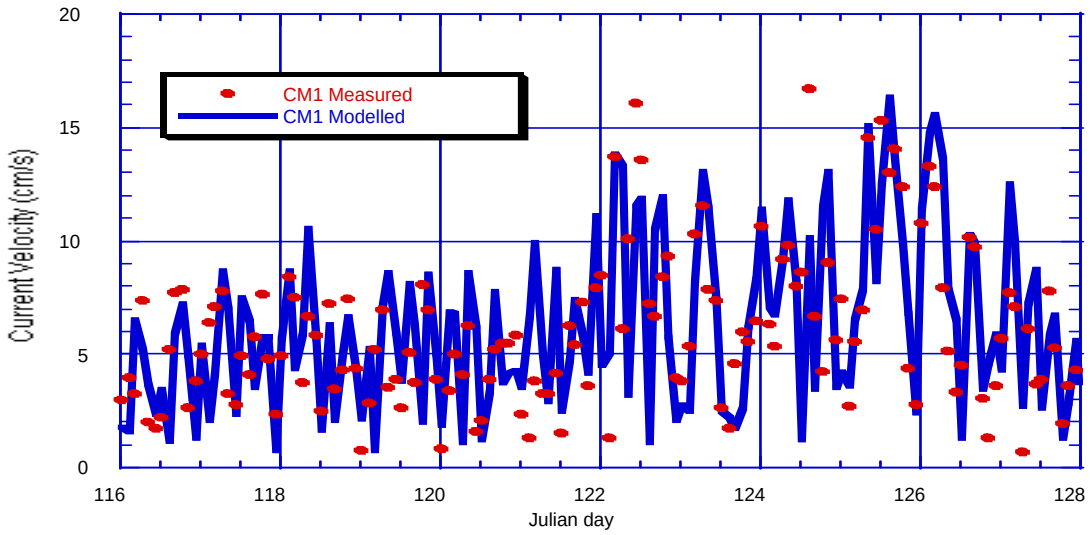

Fig. 5.7a. Modelled versus measured current velocities at CM1.

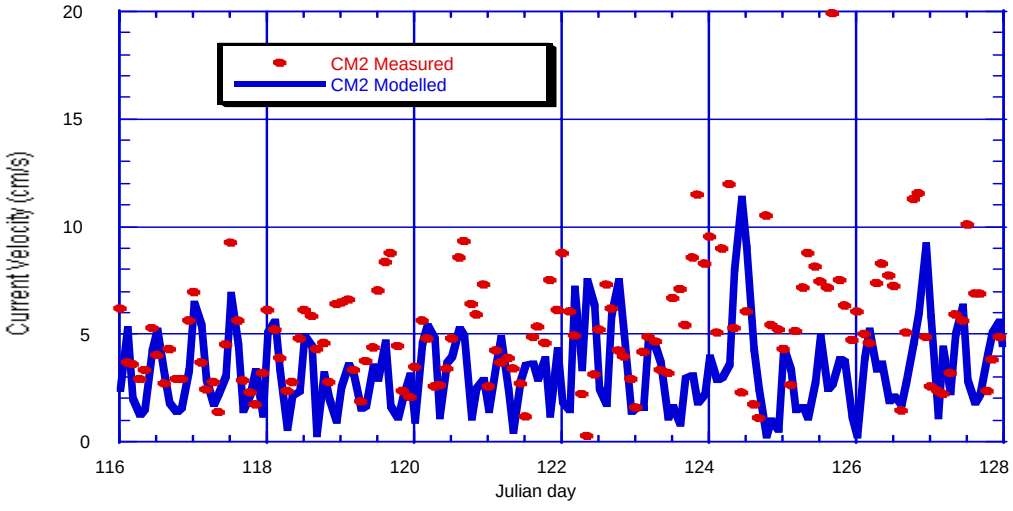

Fig. 5.7b. Modelled versus measured current velocities at CM2.

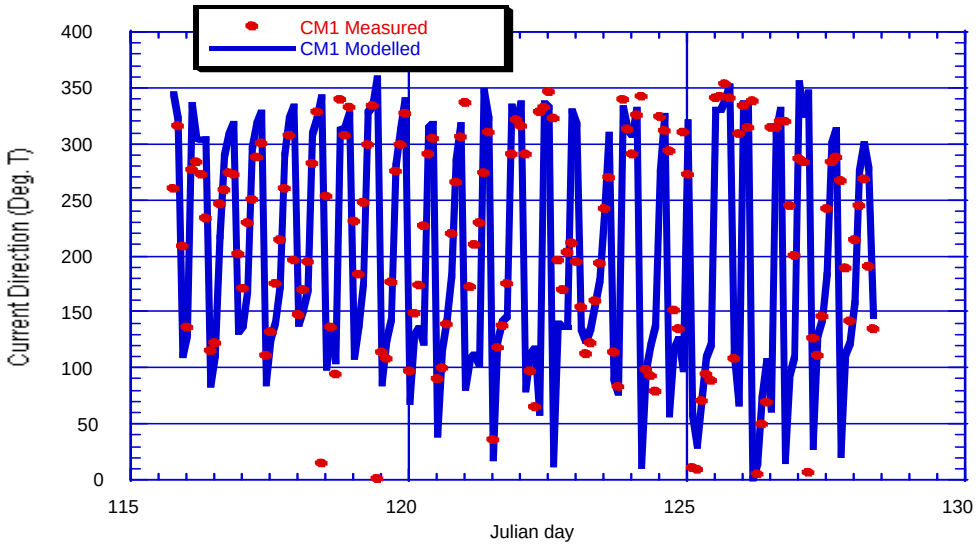

Fig. 5.7c. Modelled versus measured current directions at CM1.

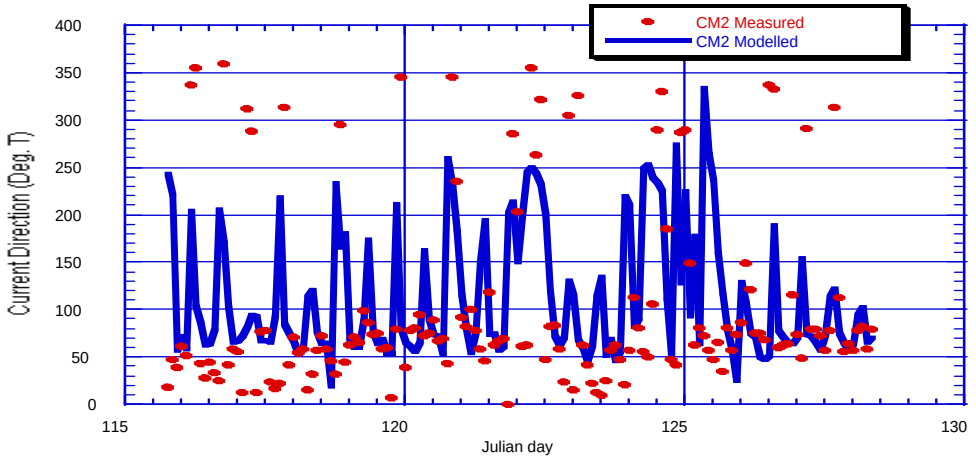

Fig. 5.7. Modelled versus measured current directions at CM2.

The calibration agreement is very satisfying given the limited amount of information available for model boundary conditions. The model is reproducing the measured currents and directions, particularly at Site CM1 where the directions are very close to the measurements. At Site CM2, the model is showing the presence of the eddy (indicated by dominant east to north-east current directions) at the site.

Notably, no sea level gradients were recorded, for cost saving reasons, and this would normally be done for a similar model study. It is also noteworthy that we are modeling modern currents on bathymetry that was recorded some 20 years ago. Our analysis of bathymetry indicates that the depths may have changed by up to1 m over the 20-year period. When computer modeling of hydrodynamics, the most important rule to apply is simply "bathymetry, bathymetry, bathymetry"! Undoubtedly, better results could be obtained if the bathymetry was more accurate and one of our important recommendations is that a full bathymetry survey should be undertaken. It may also be necessary to consider 3-dimensional dynamics in future. However, the model remains highly useful for understanding the bay dynamics, even given these calibration restraints.

6 MECHANISMS IN OF THE BAY NORTH OF NAPIER

6.1 Introduction and methodology

Understanding the mechanisms and processes within Westshore Bay in relation to beach erosion is the primary aim of this report. In this chapter, we bring together the field data and use the numerical models to identify the key relevant factors. We present these as "mechanisms" and consider three major factors, in relation to the modern day conditions in the bay. Factors like the earthquake uplift of the seabed and changes to the estuary have undoubtedly altered the sediment dynamics and would certainly have affected the bay's sediment budget. However, modern erosion is still continuing, suggesting that there are modern processes that are responsible for the bay's erosion problems.

Solutions to a coastal erosion problem need to consider the community's capacity to implement them, and social and environmental impacts of the "solution". This chapter deals with the causes of the erosion, while recommendations for remedial works that are designed to address the modern processes are suggested in Chapter 7. A short discussion on the effect of the estuary and the earthquake is given, but this is historical only. The issue at hand is to deal with the modern situation that currently prevails.

6.2 The Estuary and the Earthquake

Around the mid-1800's, the Ahuriri estuary was not producing significant amounts of beach sand (mostly muds were discharged), but the ebb jetting tidal flow led to the development of an ebb-tidal delta. In the presence of the delta, the beach orientation was rotated relative to today's condition, and it is likely that the old orientation was more stable in relation to the wave climate (see Section 6.3).

The effect of the earthquake was to raise bed levels, and move the beach face offshore. It is likely that this offshore movement of the beach would expose the beach to marginally more direct wave attack with less protection from the headland. In addition, as noted by Smith

(1986), the uplifting of the bed was followed by beach accretion, possibly associated with shallower depths offshore, which led to more shoreward transport of bed sediments. However, the beach is presently landward of its position prior to the earthquake and so the offshore movement has now been totally negated.

While the estuary and earthquake have undoubtedly changed the sediment dynamics of the Bay, their effect is now historical and cannot be seen as being responsible for the modern day erosion patterns, with the beach in its present position.

6.3 Mechanism #1 - Equilibrium Beach Alignment

Although erosion and accretion occurs on beaches, many beaches in New Zealand have now achieved an equilibrium alignment, as they were mostly formed about 6000-7000 years ago (including the Western Spit – Gibb, 1996), which is ample time for them to reach an equilibrium state. The orientation of equilibrium beaches (e.g. Black and Rosenberg, 1992) is governed by three main factors:

1. the wave climate that drives the longshore drift in both directions along the beach;
2. sheltering by headlands; and
3. the available supply of sediment.

If there is no supply of sediment, an equilibrium beach will orient itself so that the sediment transport in both directions along the beach is equal. That is, while large amounts of sand may be moving in total, the net movement back and forth is close to zero.

In the presence of a headland, the local wave climate is modified, because the headland eliminates or greatly reduces the wave energy from the direction sheltered by the headland. This means that a segment of the directional wave climate is eliminated and the average direction of waves reaching the beach in the headland lee is rotated.

With the introduction of an upstream sediment supply, an equilibrium beach will be oriented so that the transport along the beach from the source, is equal to the available supply.

These three factors are discussed in more detail, by example, at Napier in the following sections.

6.3.1 Hawke Bay shoreline shape

Inspection of the map of Hawke Bay shows a sweeping, arcuate shape, with Mahia Peninsula to the north and Cape Kidnappers to the south (Figure 6.1). The orientations of the beach are indicative of equilibrium conditions but no previous work has been done to examine this possibility in any detail. Here, we use the longshore sediment transport model GENIUS (Appendix 3) to determine the net movement of sediment along the coast and consider the long-term dynamics.

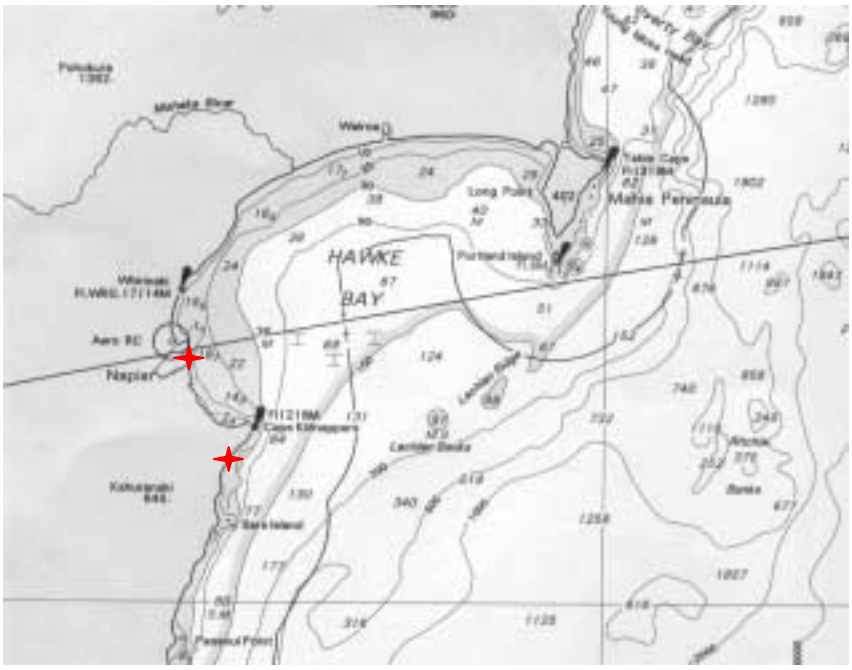

Figure 6.1. Map of Hawke Bay showing the two sites used for sediment transport calculation (Nautical Chart NZ 23)

6.3.2 Model GENIUS

The measured sediment losses are predicted using a commonly-adopted sediment transport equation in Model GENIUS (Appendix 3), which is the CERC formula for longshore sand transport rate given by,

(6.1)

where,

H = wave height

C_g = wave group speed given by linear wave theory

b = subscript denoting wave breaking condition

θ_{bs} = angle of breaking waves to the local shoreline

the non-dimensional parameter a_1 is given by

$$a_1 = \frac{K_1}{16(\rho_s / \rho - 1)(1 - P)} \qquad (6.2)$$

where,

K_1 = empirical coefficient, treated as a calibration parameter (typically 0.58)

ρ_s = density of sand (taken as 2650 kg.m^{-3} for quartz sand)

ρ_w = density of water (taken as 1025 kg.m^{-3} for seawater)

P = porosity of sand on the bed (taken to be 0.7)

Knowing the wave height, the equation for depth-limited breaking,

(6.3)

(where γ = breaker index often taken as 0.78) is adopted to obtain the wave group speed. Finding d_b from equation (6.3), the wave group speed is obtained from the shallow water approximation given by,

$$C_g = (g\, d_b)^{1/2} \qquad (6.4)$$

Equation (6.1) is solved at successive time increments using the 15-year hindcast of wave heights, angles and directions described in Chapter 4. The sediment flux is obtained by summing the fluxes for each case and converting to an annual longshore transport rate.

For the purpose of the study, we examine two open-coast sites that are relevant to our study. The first is at the northern end of Marine Parade (Fig. 6.1). This site is highly relevant as it determines the longshore fluxes of sand being carried to the north (if any), around the port and into Westshore Bay. For comparison, we examine the Ocean Beach to the south of Cape Kidnappers (Fig. 6.1). Notably, while these two beaches are relatively close, they have very different orientations. The Napier Beach has a shore normal orientation of about 100° (i.e. 10° south of east) while the exposed Cape Kidnappers Beach is oriented at about 125° (i.e. 35° south of east).

The two beaches are sufficiently close to experience very similar offshore wave climates. Thus, the 15-year hindcast is applied to both, although there is likely to be a small sheltering effect at Napier from the south, which is not experienced at the Ocean Beach.

The predicted transport rates are summarized in Table 6.1.

Table 6.1. Predicted longshore transport rates at Marine Parade near the port (Site 1) and the Ocean Beach south of Cape Kidnappers (Site 2).

Site	Flux to the north ($m^3.yr^{-1}$)	Flux to the south ($m^3.yr^{-1}$)	Net flux ($m^3.yr^{-1}$)
1. Marine Parade near the Port	232,500	-108,200	124,300 (north)
2. Ocean beach south of Cape Kidnappers	216,300	-207,600	8,700 (neutral)

The results of the modelling show that the Ocean Beach at Cape Kidnappers is approximately neutral, i.e. the fluxes of transport to the north and south are essentially equal, within the accuracy of the wave information that we have applied. This means that the beach is in equilibrium with an orientation that is in balance with the wave climate. This may be expected because there is no river supply of sand and yet the beach remains sandy, even in

such an exposed location. The coast, however, would have the potential to supply sand from the south, and so there can still be northward transport, with a stable beach. Because we have used the Napier wave climate, any effect of sheltering to the south in these data, would cause the northward flux to be under-estimated.

At Napier on Marine Parade, the modelling shows a net transport to the north of 124,300 $m^3.yr^{-1}$, suggesting that the sediment inputs are substantial and maintaining the beach at an orientation that leads to net movement to the north. There is a river supplying sediment to the south, but the volumes of sandy sediments being discharged from the river in modern times is not known and beyond the scope of the present study. The modelling, however, suggests that about 120,000 $m^3.yr^{-1}$ passes the port, to be dredged or carried into and across Westshore Bay each year.

In the light of these results, the first mechanism that leads to beach adjustment in the bay can be described. We have shown that the beaches appear to be in balance with the wave climate, headland sheltering and sediment supply. The effect of the port's extensions in this context are to increase the headland sheltering effect, i.e. to provide more shelter along Westshore Beach from the south. Given that this would rotate the mean wave climate direction to be more northward, the effect of the sheltering would be to cause the beach to accrete, by this mechanism alone. The mechanism is idealised in Figure 6.2.

While sheltering should lead to beach accretion, other factors that are expected to lead to erosion are discussed next.

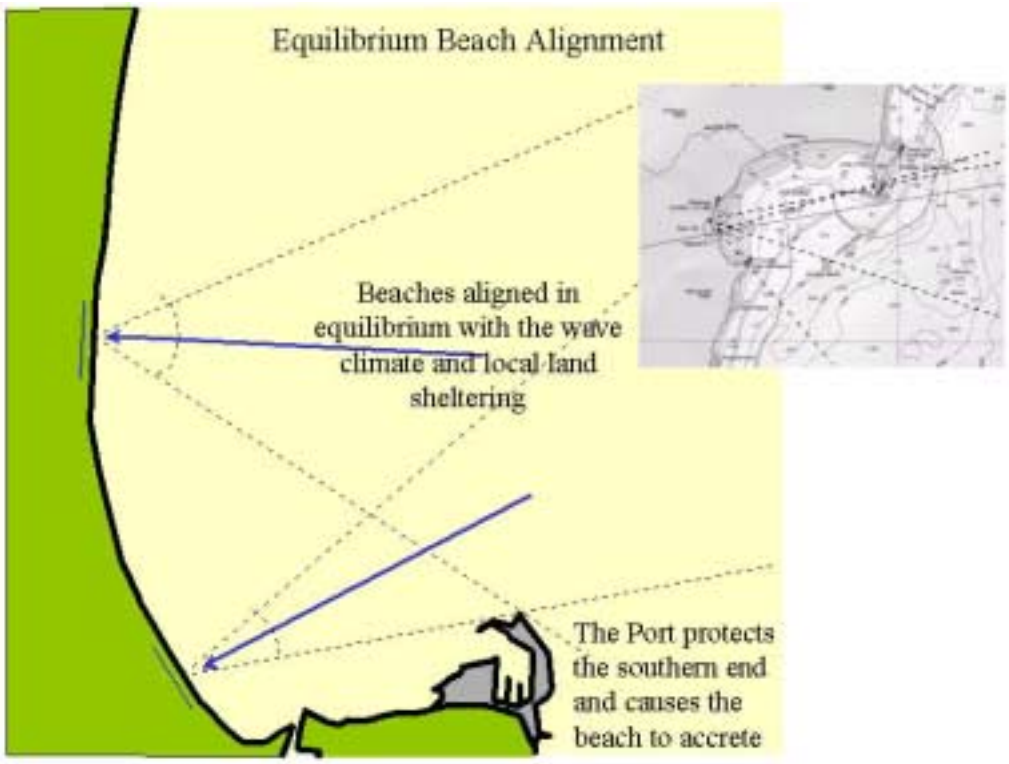

Figure 6.2. Idealised diagram of equilibrium beach alignment – Mechanism #1.

6.4 Mechanism #2 – Sediment Transport Compartments

There is a perception that beaches lose or gain sand alongshore, not cross-shore, and that the beach is a unit that is independent of the offshore inner shelf. This arises partly because the beach is above water and visible, while the offshore segments are underwater and forgotten. However, a beach is actually only the last part of a sand system that extends out to 10-12 m depth and sometimes much deeper. Thus, the beach is dependent on the sedimentary "health" of the inner shelf offshore. This means that if sand is lost from the full sedimentary system, then the beach will be impacted more severely.

In essence, the aim of this section is to define the relevant size of the sedimentary system that affects the beach. Once the system scale is defined, then the effect of gains or losses of sediment from the system can be inferred.

We do this by inference and using the numerical model techniques that have been developed during the study.

6.4.1 Bathymetry

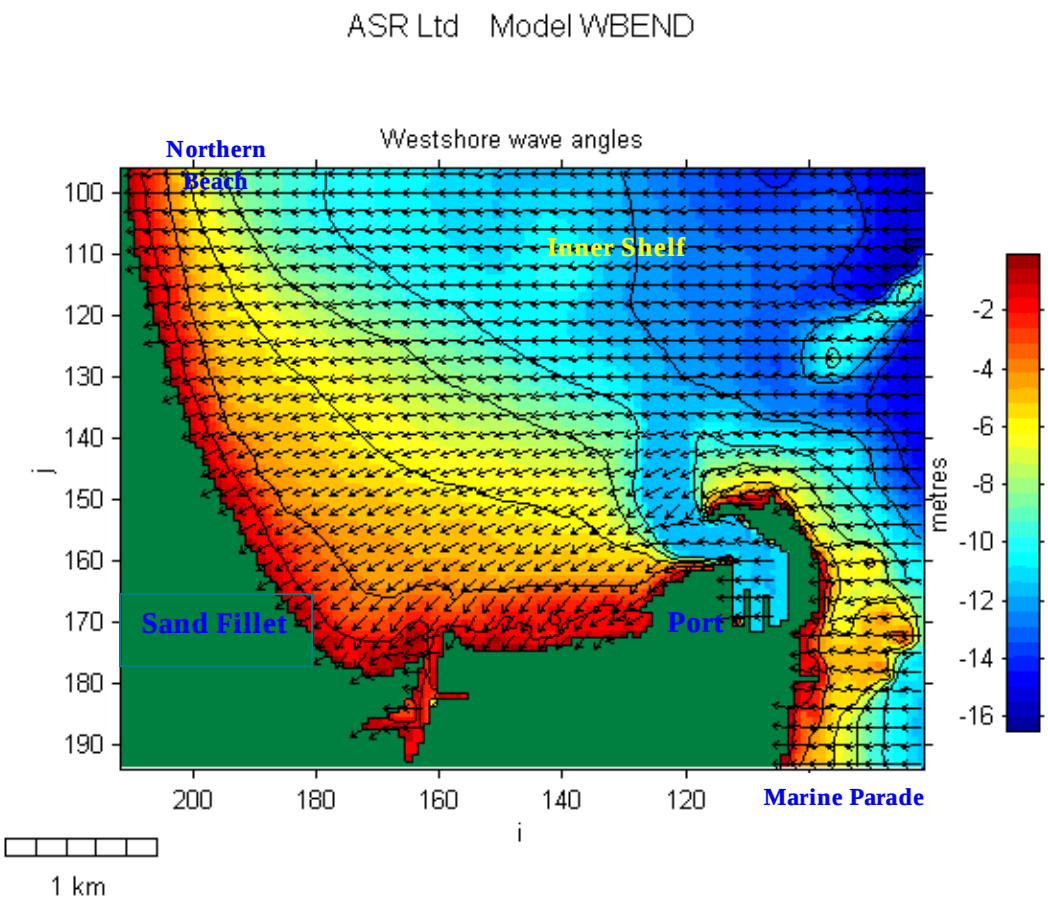

Figure 6.3. Bathymetry and wave angles at Westshore, showing the northern beach, Westshore sand fillet, port and dredged channel and Marine Parade beach.

The bathymetry at the site (Fig. 6.3) shows 4 distinct compartments:

- Northern beach
- Westshore sand fillet, which is a triangular wedge of sand in Westshore Bay

- Port and dredged channel
- Marine Parade Beach

As can be seen from Figure 6.3, the port and dredged channel is located at the eastern end, within the Westshore sand fillet. From the bathymetry, we can infer that the sand fillet is a distinctive zone and that the beach is simply the upper level of this fillet. As such, the beach can be seen as residing within the sand fillet compartment. Notably, the port and dredge channel are clearly also in this same compartment.

Examples of the circulation in the region from the model calibration period are shown in Figures 6.4 a-f.

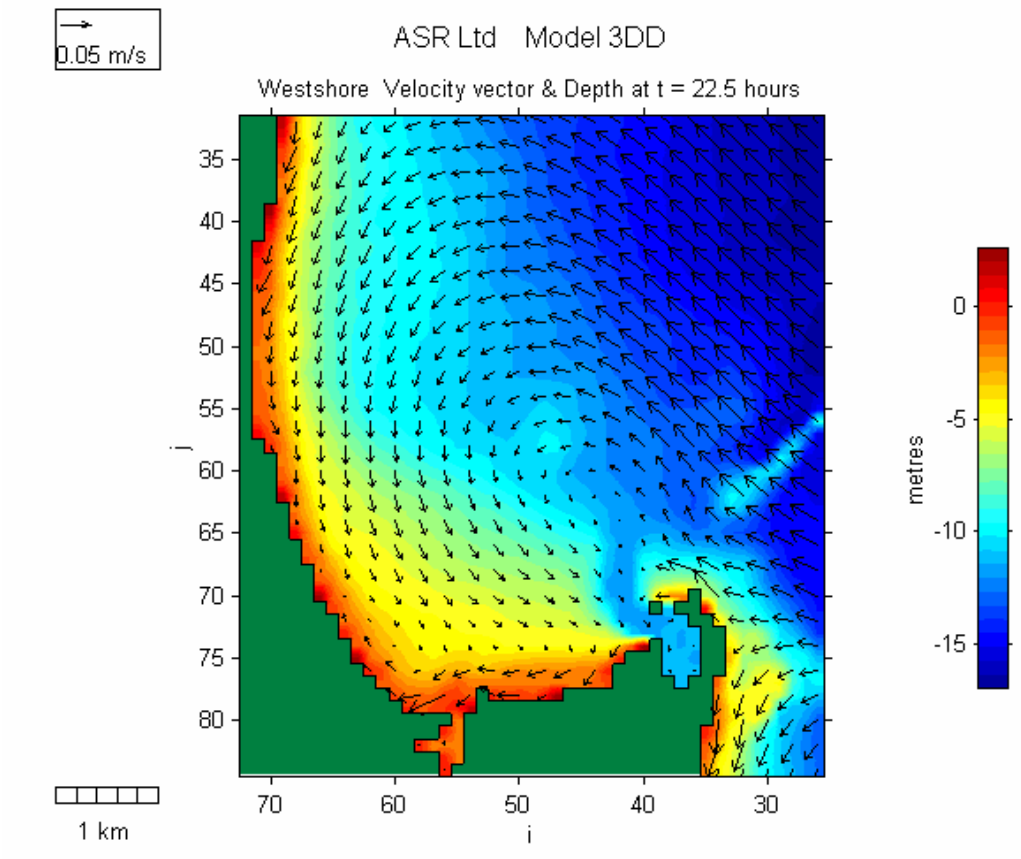

Figure 6.4a. Current pattern on Julian day 115 (day 1 of field study).

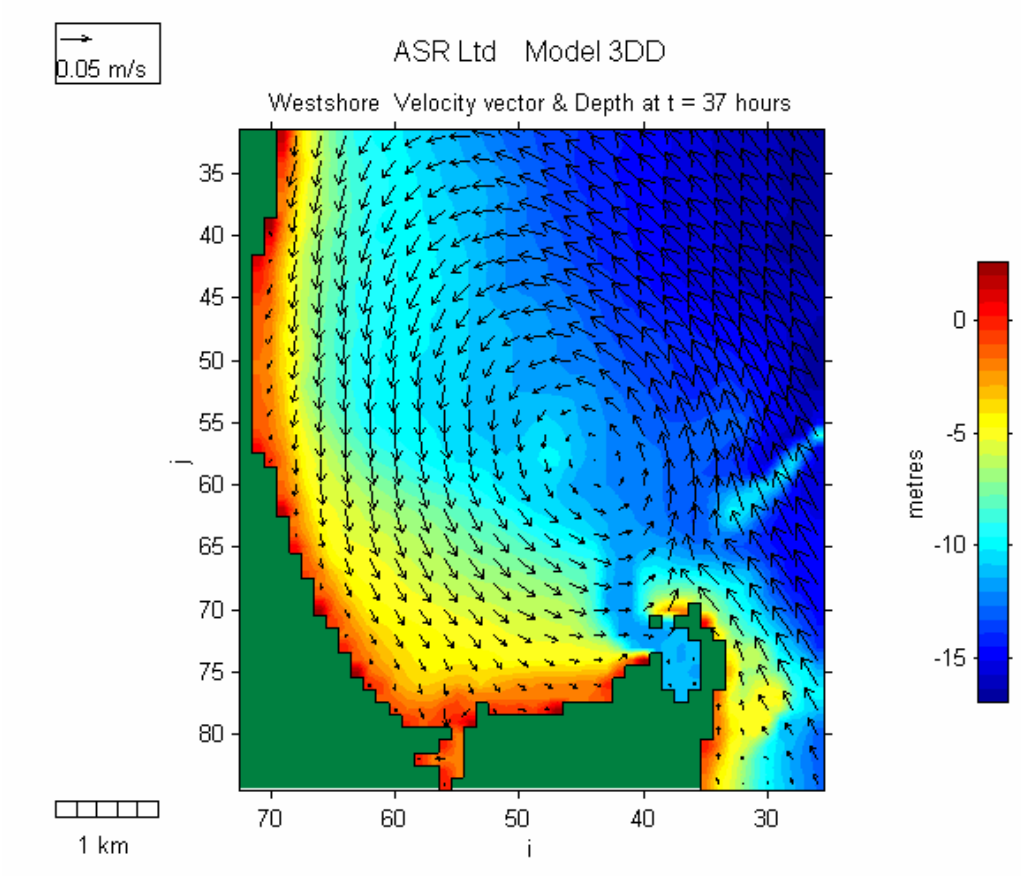

Figure 6.4b. Current pattern on Julian day 116 (day 2 of field study).

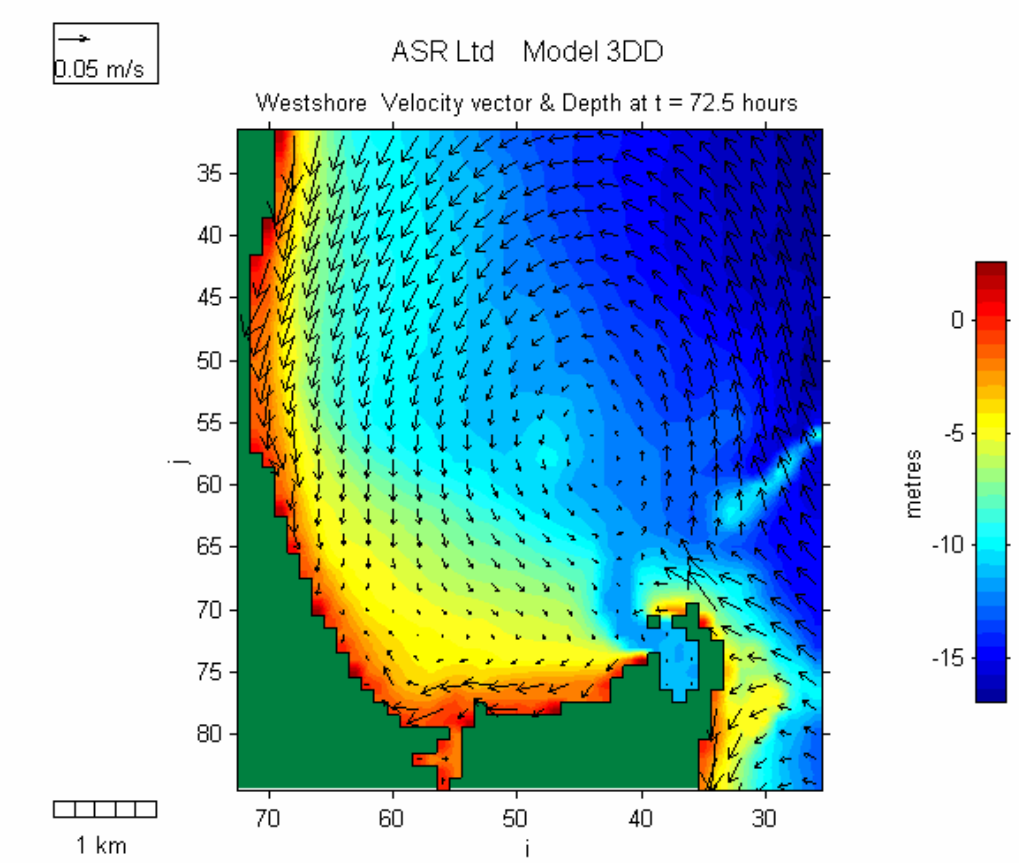

Figure 6.4c. Current pattern on Julian day 117 (day 3 of field study).

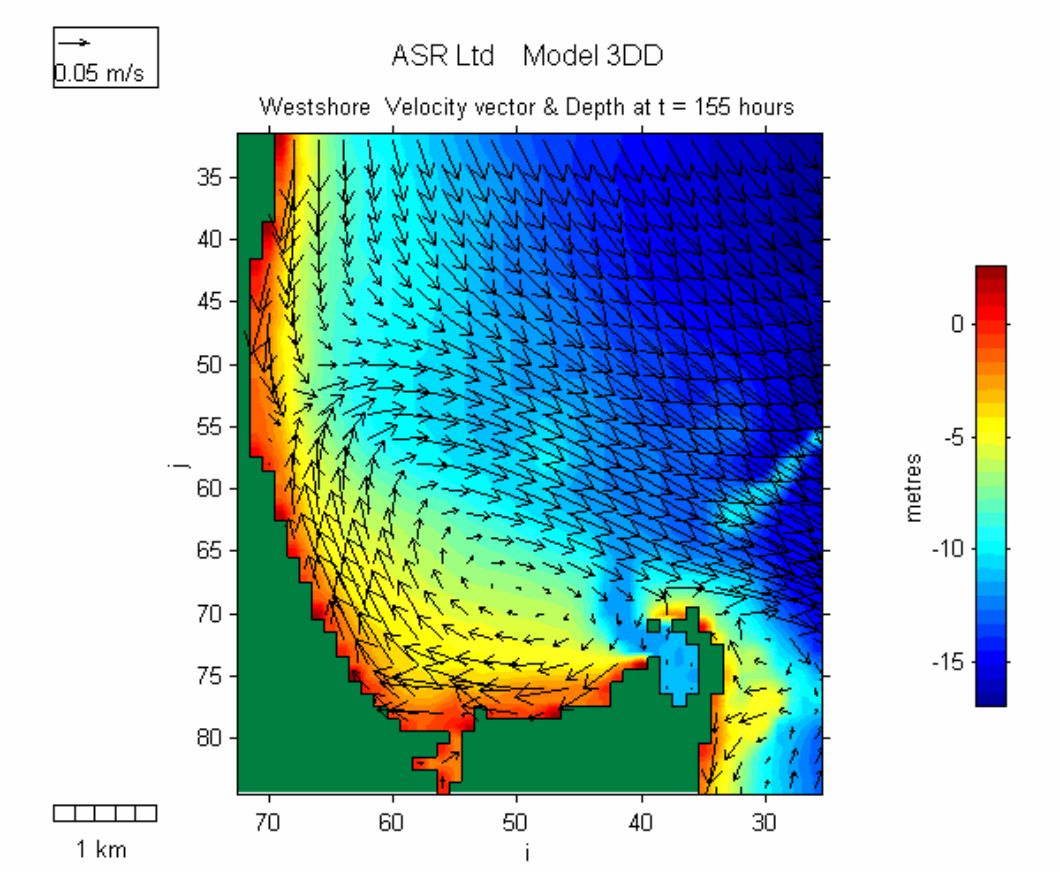

Figure 6.4d. Current pattern on Julian day 122 (day 7 of field study).

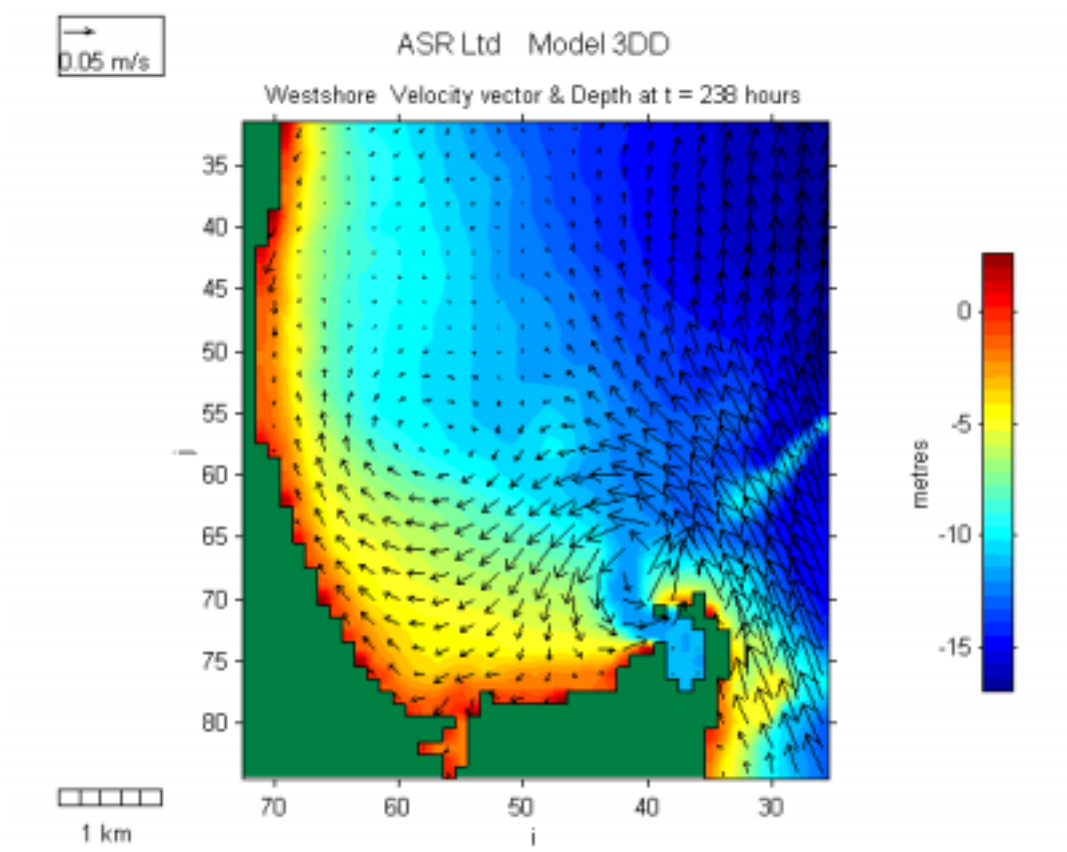

Figure 6.4e. Current pattern on Julian day 125 (day 10 of field study).

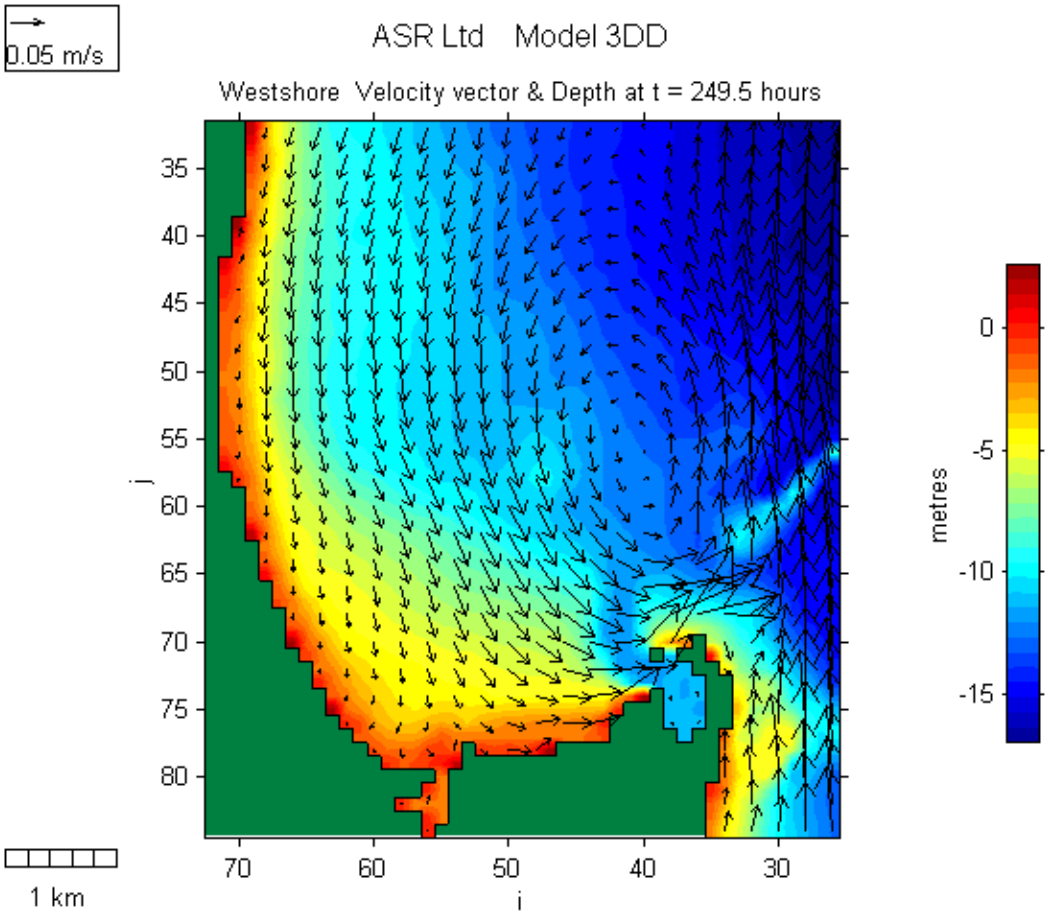

Figure 6.4f. Current pattern on Julian day 126 (day 11 of field study).

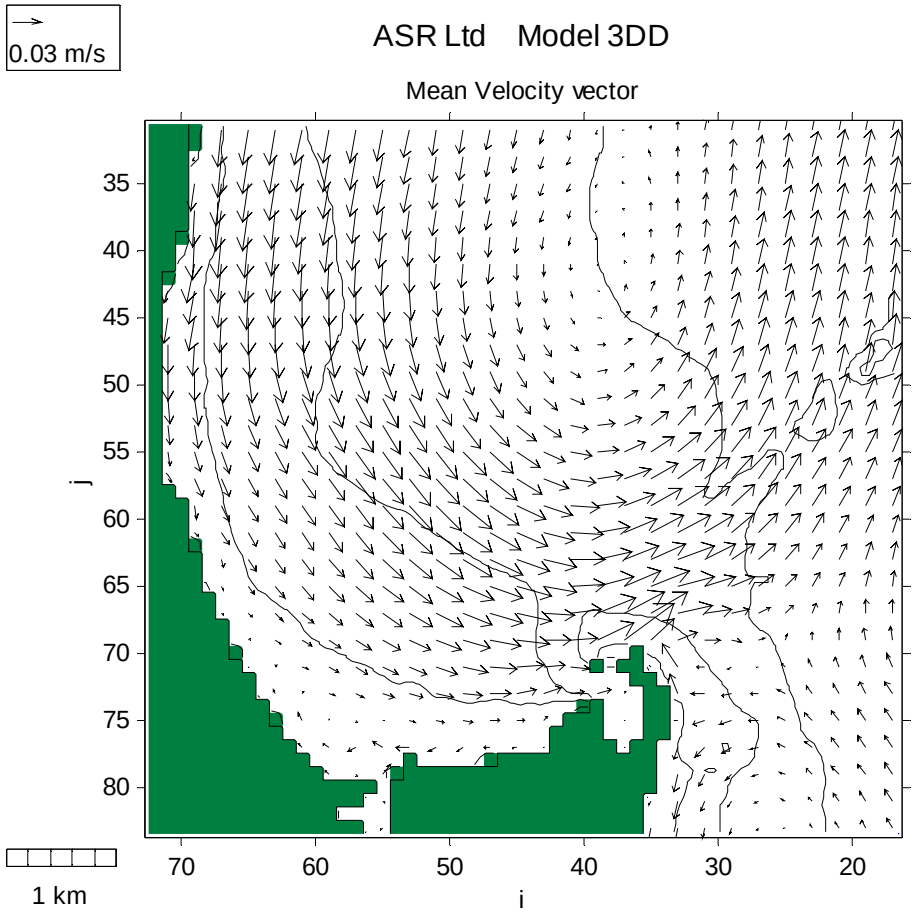

Figure 6.5. Mean velocity vector over the model simulation, showing the direction of net currents during the field study.

The mean velocity vector showing the direction and magnitude of net currents is presented in Figure 6.5. Although only a 2-week period is being considered and the model calibration relies on 2 sites only, the general trends are in good agreement with the residuals from the 4 current meters in Figure 4.25. For example, the currents flow south from the northern beach, there is a strong anti-clockwise rotation over the deeper parts of the sand fillet and a clockwise rotation inshore. These are reflected by the measured currents at CM2, CM3 and CM4. The inshore clockwise-rotating cell is evidenced by a net northward residual at site CM3 in Figure 4.25. Offshore, the measured currents are directed shorewards through the gap between the reef and port. The model is showing the same trends, but at a position a little further offshore.

The important implications of the model results and data analysis are discernible as flow patterns, as follows.

Although the flow oscillates in Westshore Bay, the currents can be directed offshore, along the headland and across the port's dredged channel. We must conclude from this that sediment can be carried from the Westshore sand fillet into the channel and that this material is being lost due to dredging. The dredging records show that about 11,000 m^3/yr (Hume *et* al., 1989) is dredged from the western side of the channel, and this has presumably come from the Westshore sand fillet.

There are also times when the currents are strong and directed north along the offshore side of the main port breakwater. These flows are clearly able to transport sand into the channel, with the assistance of wave action to suspend the sands. The port's maintenance dredging of 25,000 m^3/yr (Hume *et al.*, 1989) from the eastern side of the channel is evidence of this process.

Finally, the current vectors show that sand transported along the main port breakwater can bypass the channel on the north-eastern side. Similar results have been obtained using tracers and numerical model studies at Port Taranaki (McComb and Black, 1999; Black and McComb, 1999). It was shown that while about 120,000 m^3/yr collected in the tip shoal around the port breakwater, an equally large amount was not trapped and continued to go past the port.

These results provide the basis for an important mechanism that can result in shoreline erosion at Westshore. The port is within the Westshore sand fillet compartment and so the Port's dredging, by removing sand and placing it offshore, will be degrading the volume in the fillet and thereby causing erosion of the beach. In other words,

- **the port dredging operation is acting as a sediment sink in a recirculating sediment loop.**

Thus, it is essential that all sand dredgings from the port are placed inshore, as recently agreed to by the Port and Regional Council.

The idealized drawing of this mechanism is presented in Figure 6.6.

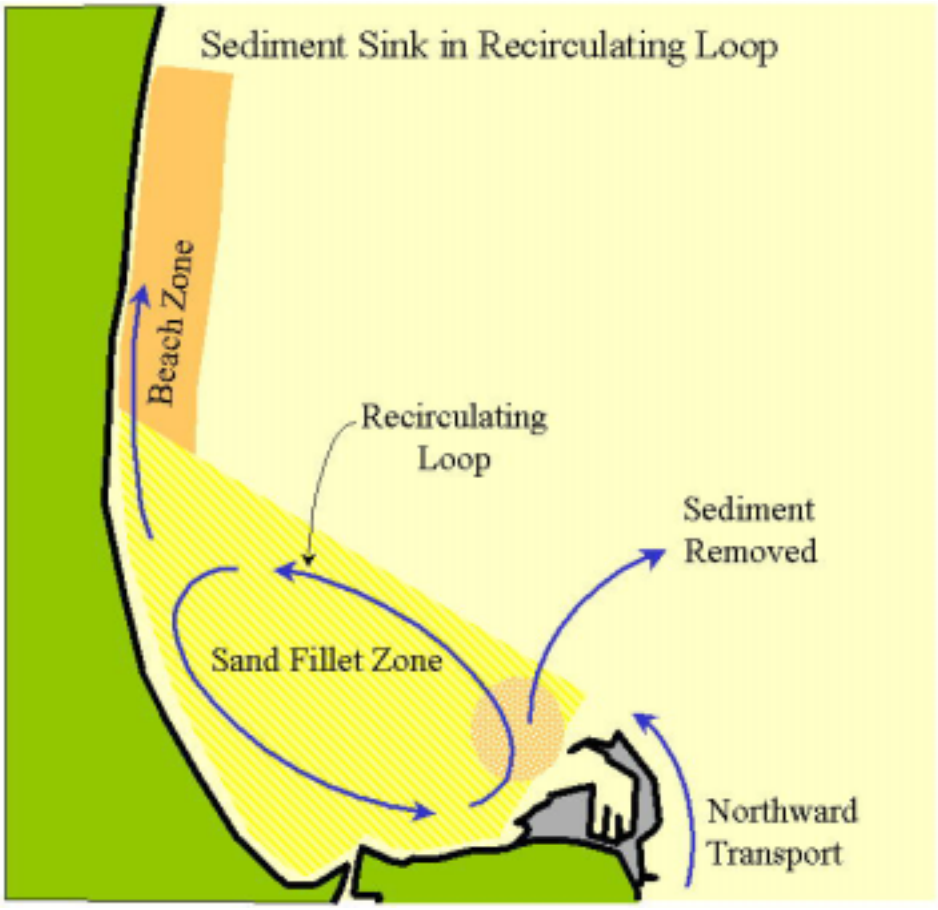

Figure 6.6. Idealised diagram of the sediment sink in the recirculating loop on the Westshore sand fillet – Mechanism #2.

6.5 Mechanism #3 - Headland extension

Sediment dynamics along a headland are very complex, but there are some features that recur. Our studies of Raglan headland, for example (Phillips and Black, 1999), have shown that the strong wave-driven currents occur near the headland in the shoreward direction. This is due to the presence of breaking waves that induce a shoreward flow along the headland.

Similar currents were observed and shown to occur in numerical models during our studies to develop a coastal protection reef for Noosa in Queensland, Australia (2001). The currents along Noosa headland were as fast as 0.5-1.0 $m.s^{-1}$ in moderate to large swells.

These shoreward currents play a critical role in bringing sand from the headland tip to the beach. The sand is carried near the coast, in shallow water where the breaking wave action is strongest, and as a consequence so are the currents.

An extension of the headland when the offshore tip is moved from shallow to deeper water, has a profound effect on this phenomenon. This has occurred with the construction of the port. Sand that formerly followed the shallow depth contours to the beach is now forced to travel around the port and into water of 9-10 m depth. The breaking wave processes are no longer present and so the sand is deposited, to create a tip shoal and sedimentation along the wall (Figure 6.7). In essence, nature is attempting to recreate the headland condition with shallow water around the tip, but the port is built well offshore of the natural contours, much of the sand is trapped in the shoal and much of it is dredged and taken offshore. The remainder which by-passes the dredged channel is left in deeper water and cannot easily find its way back to the coast, because the currents in the eddy in the lee of the headland tend to push the sand offshore or along the offshore side of the Westshore sand fillet.

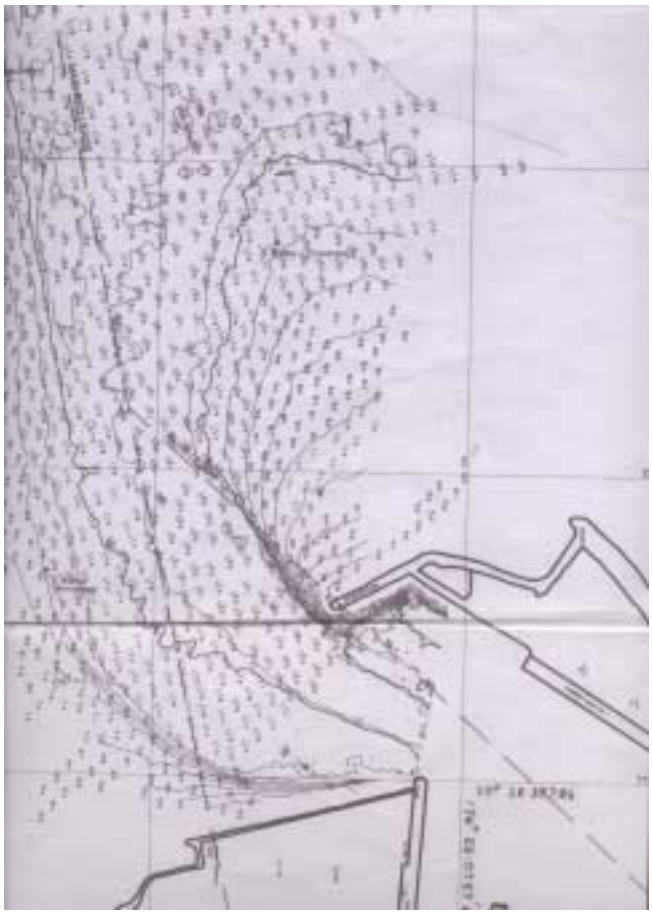

Figure 6.7. Bathymetry survey of the fairway (2000) showing the tip shoal of accumulated sand.

To confirm that the headland dynamics are altered by the port, we have modelled the same period on the same bathymetry, but with the port removed. This grid replicates the grid used for the previous model simulations with the exception of the Port and Fairway area, which was replaced by bathymetry digitised from the 1855 chart (Section 2.4) (Fig. 6.8).

The results of the model simulations are shown in Figures 6.9a-f, for the same times that were extracted in Figure 6.4a-f with the port present. In addition, the residual vector, i.e. the mean currents over the period are shown in Figure 6.10.

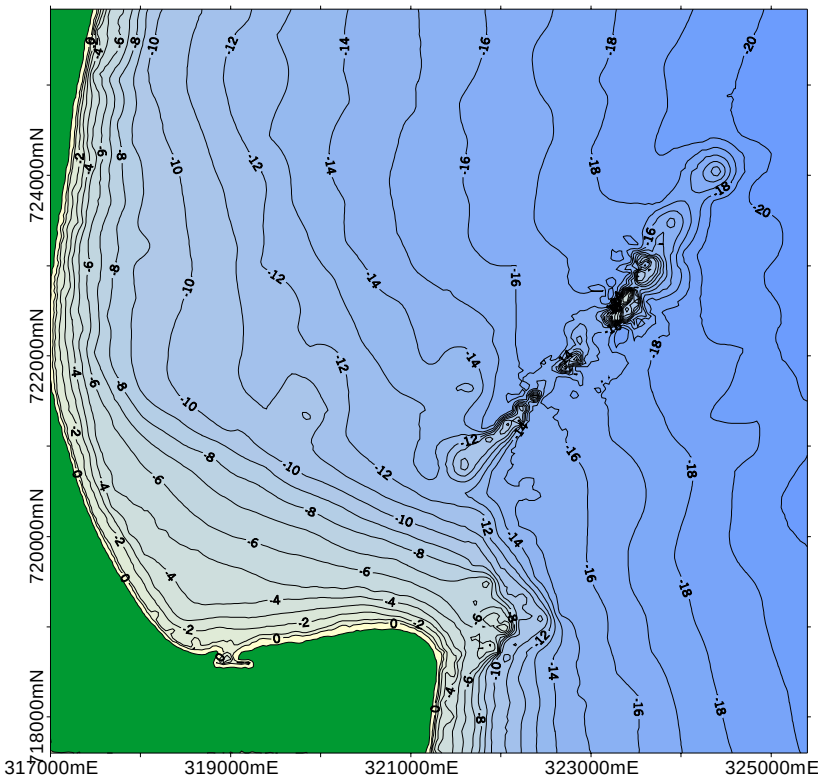

Figure 6.8. Model bathymetry grid of Westshore Bay with the Port of Napier and Fairway area replaced by the 1855 nautical chart of Ahuriri Road and Port Napier.

The most revealing comparison is at 155 hours (Figs. 6.4d and 6.9d). With the port removed, the currents in the Bay are rotating clockwise, with a strong current sweeping down the headland and along the beach. Such a flow would be bringing sand down the headland in shallow water. The neutral core of the eddy is still on the sand fillet and the return current runs along the 7-8 m isobath of the fillet.

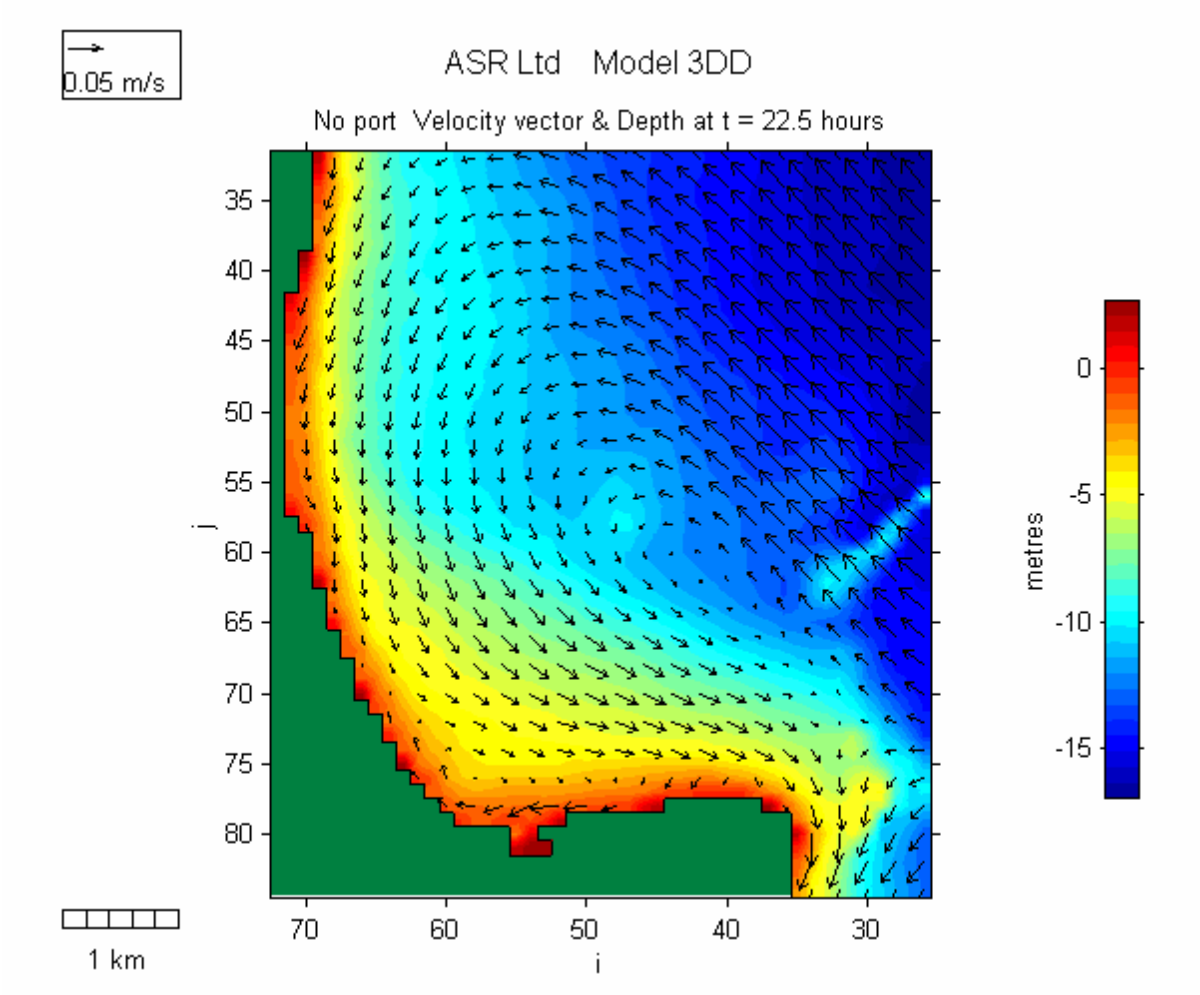

Figure 6.9a. Current pattern on Julian day 115 (day 1 of field study data).

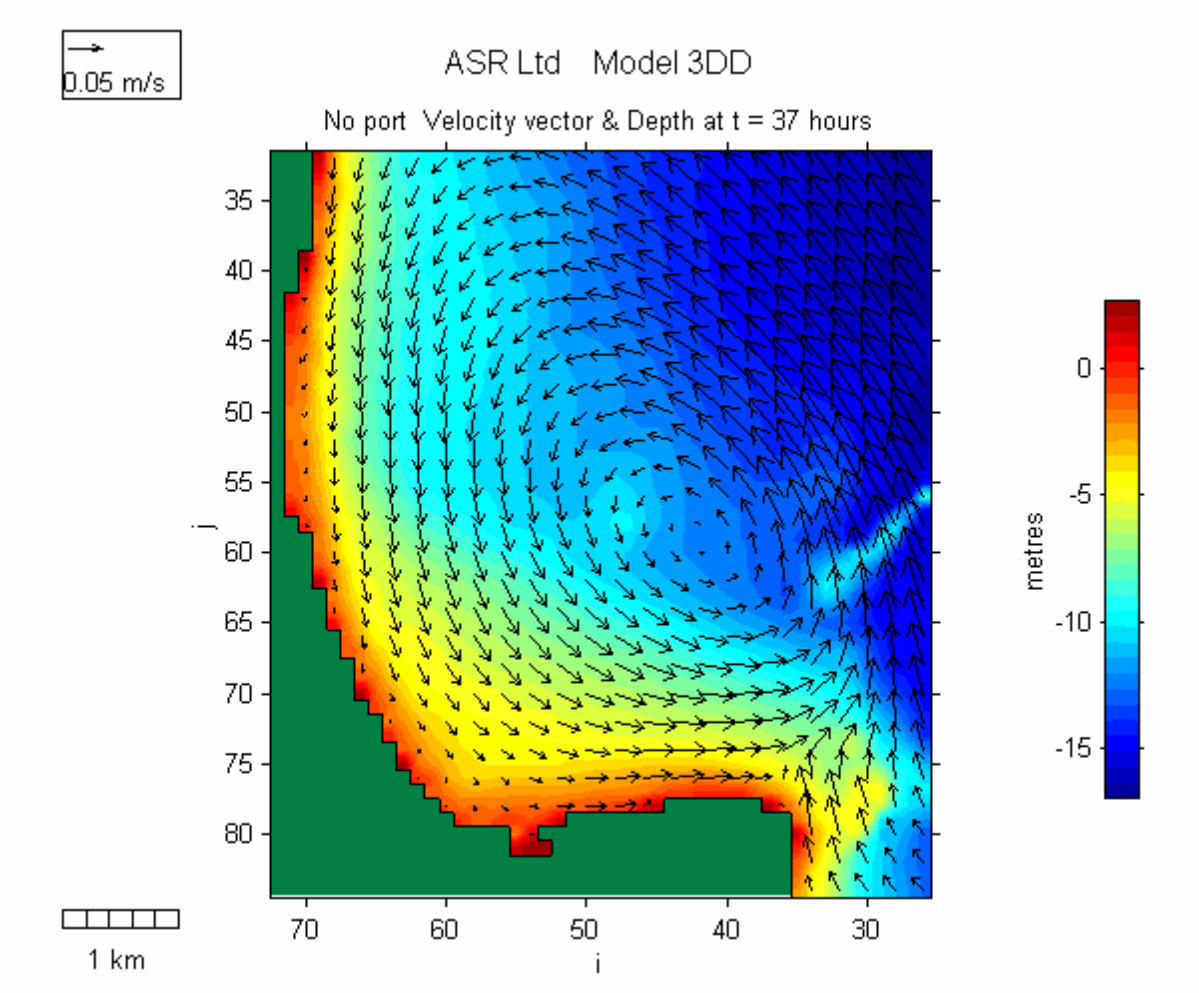

Figure 6.9b. Current pattern on Julian day 116 (day 2 of field study data).

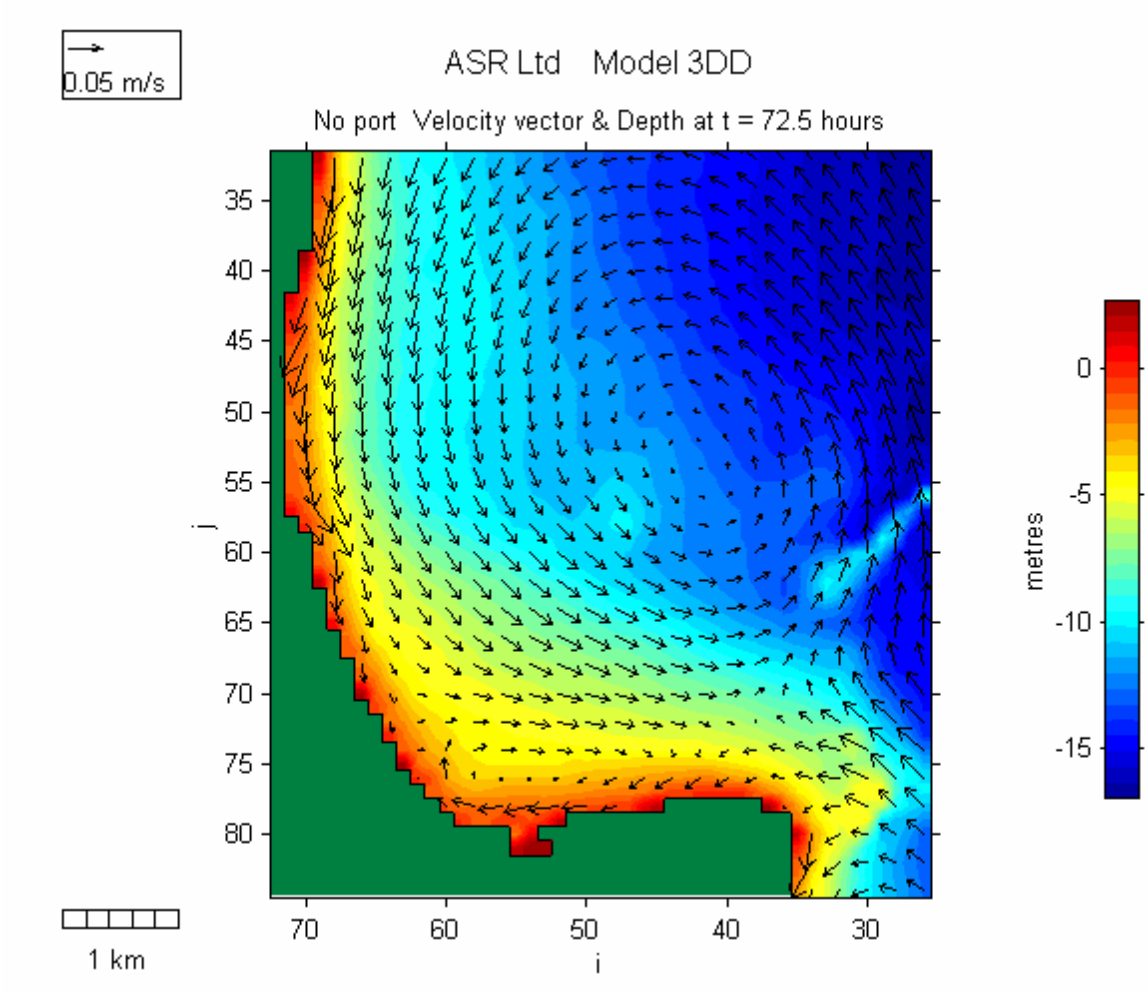

Figure 6.9c. Current pattern on Julian day 118 (day 4 of field study data).

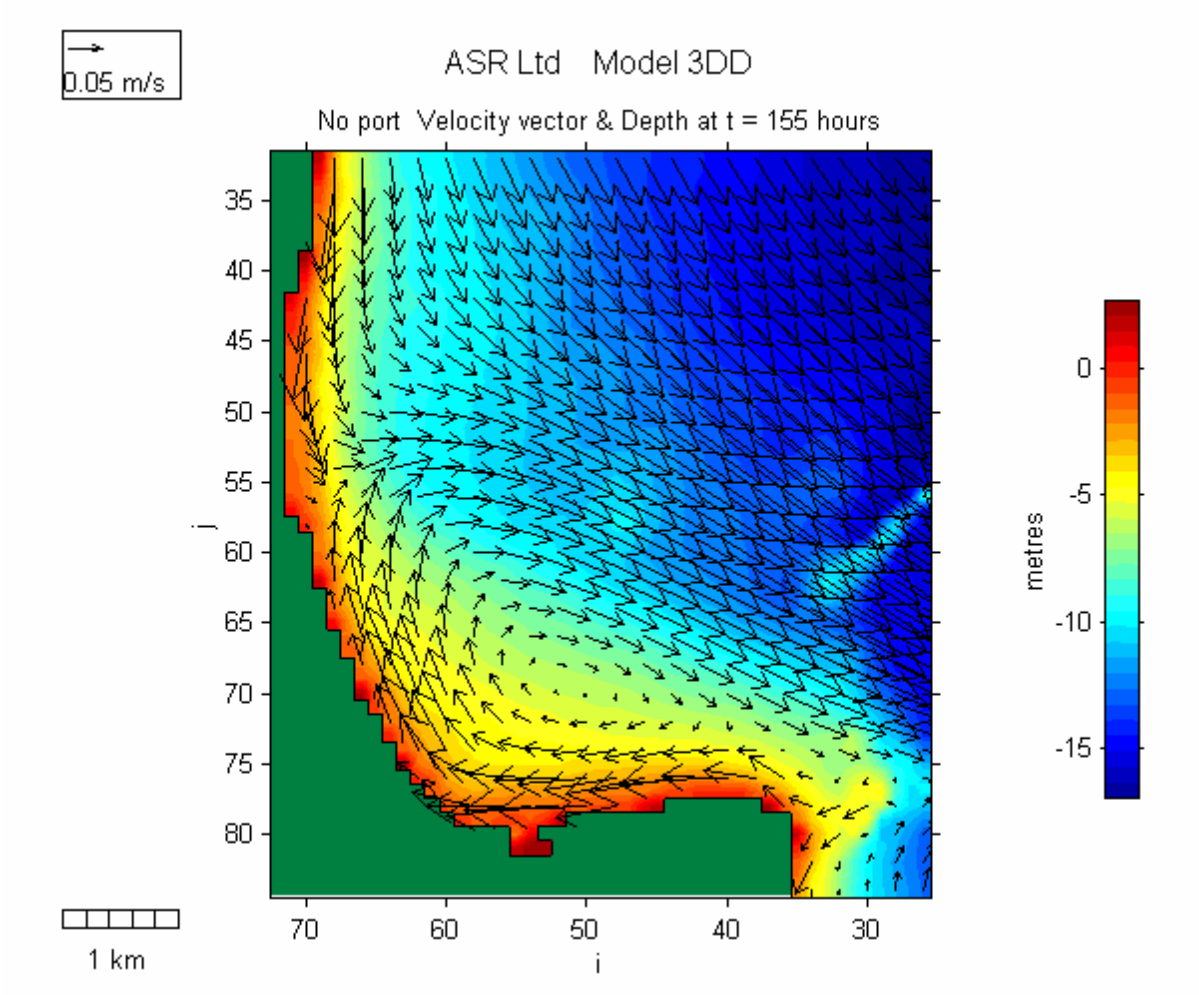

Figure 6.9d. Current pattern on Julian day 122 (day 7 of field study data).

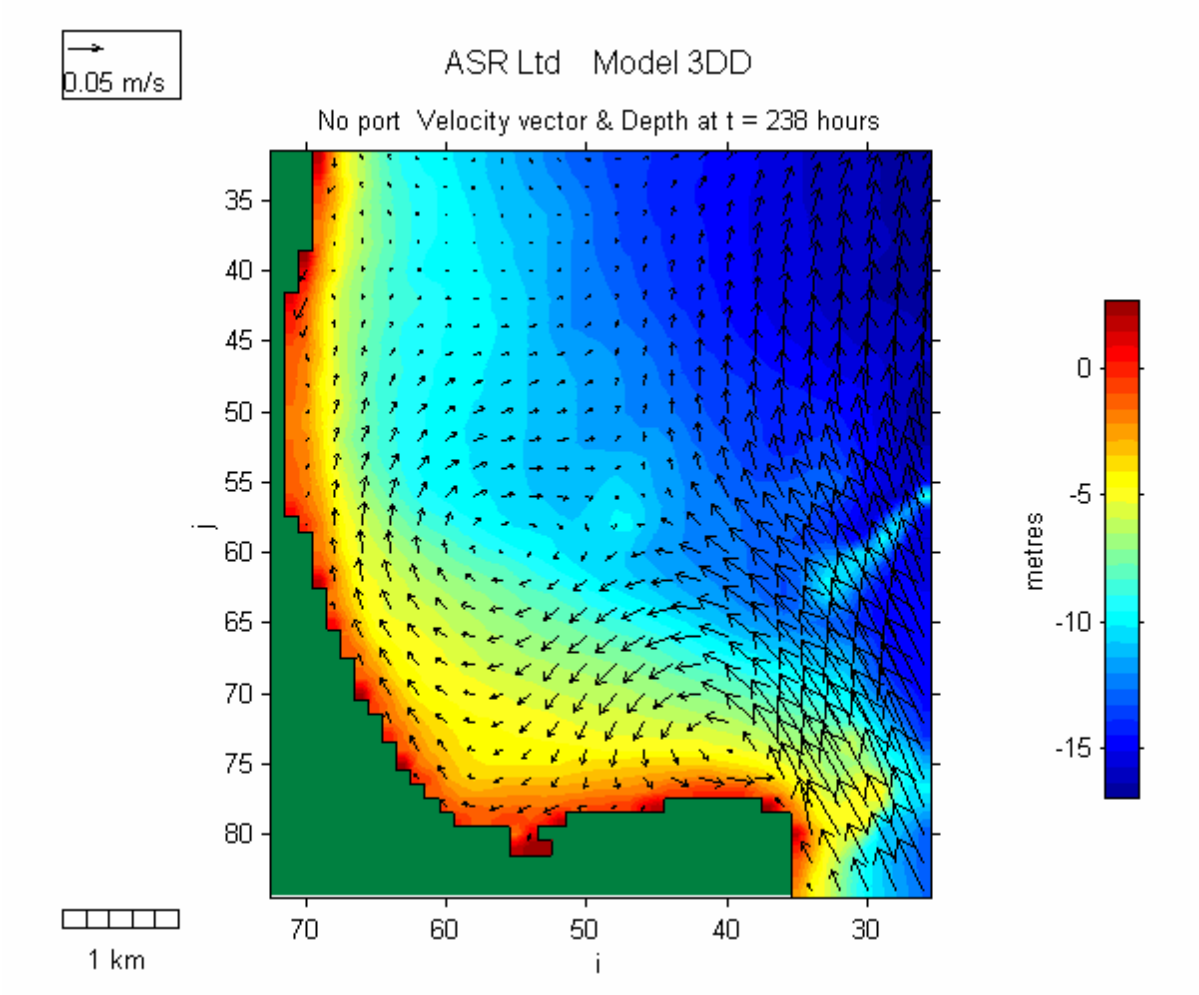

Figure 6.9e. Current pattern on Julian day 125 (day 10 of field study data).

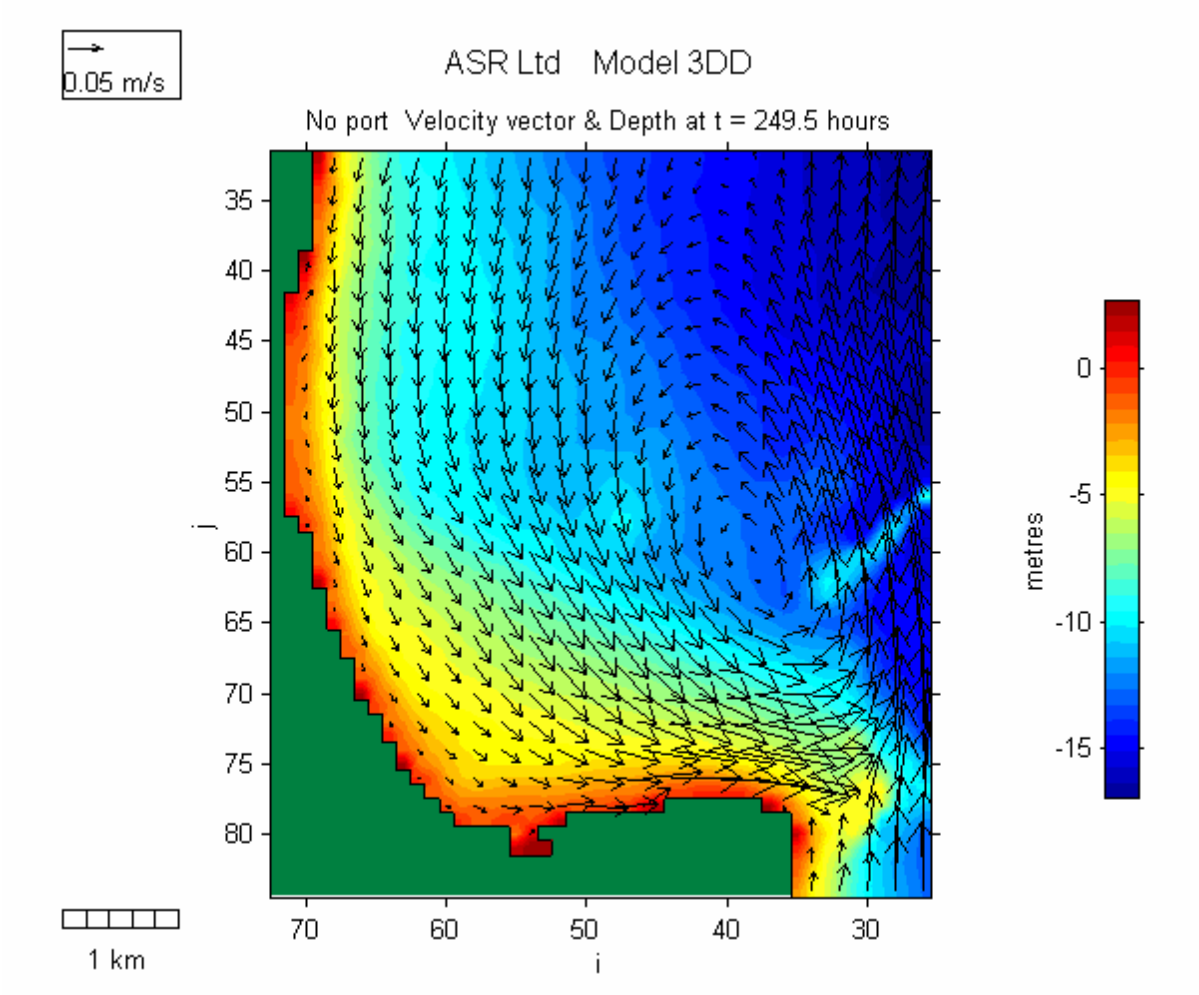

Figure 6.9f. Current pattern on Julian day 126 (day 11 of field study data).

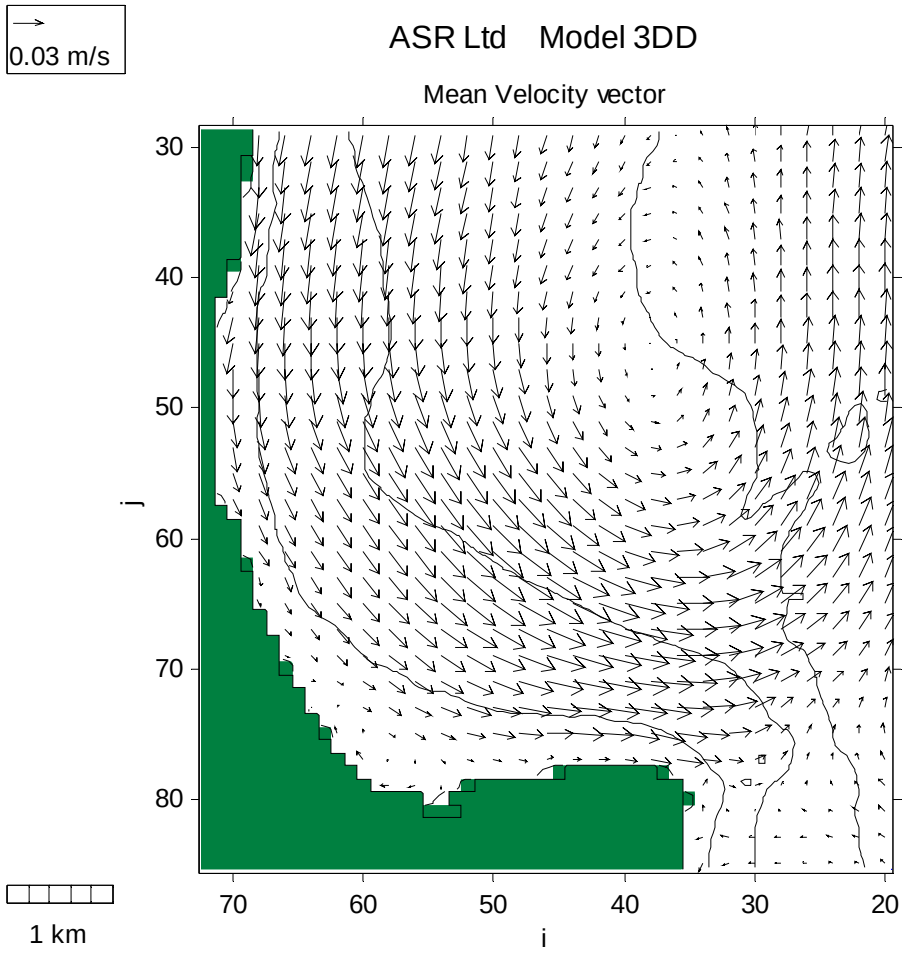

Figure 6.10. Mean velocity vector over the model simulation, on the 1981 bathymetry with the Port removed, showing the direction of net currents during the field study.

With the port in place, the pattern is profoundly different. Most importantly, the current in shallow water around the headland is not present. Around the tip of the port, which is further offshore, the currents are now directed offshore, rather than inshore. In addition, unlike the previous case with continuously strong flows around and along the headland, there is no similar flow pathway across the dredged channel. The core of the eddy has moved. Also, the general trend on the offshore side of the fillet is for sand to be carried offshore, rather than being carried back to the headland in a closed recirculating loop. The loop with the port present is open, and therefore likely to be losing sediment.

There are similar differences in the plots at other times. It should also be remembered that wave-driven currents along the headland would be directed shorewards in the original condition, while this process is not able to develop now with the port in place.

6.5.1 Wind-Driven Circulation Patterns

Further expanding on this mechanism of flow diversion into deep water, Figures 6.12-6.16 show model simulations of wind-driven currents in Westshore Bay. In all cases, currents in the sand fillet region show different characteristics to those in the rest of the study area. In most cases, the wind driven currents produce a gyre in the lee of the headland and/or Port although the size and direction of rotation varies, depending on wind direction. It is also evident that while current velocities off the end of the Port breakwater are usually relatively high, in all cases there is a reduction of current velocity in the lee of the breakwater, which corresponds to the general area of the Fairway. This enhances the Fairway's capacity to trap sediment, as the lower current velocities would result in local deposition.

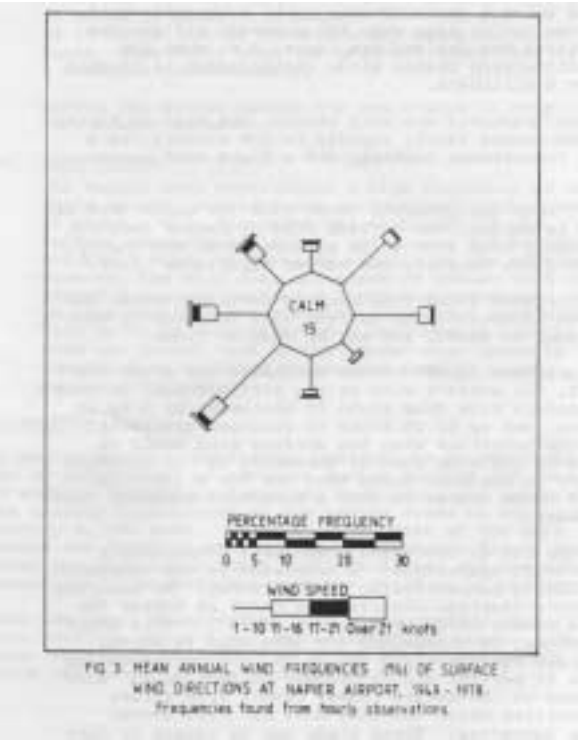

Figure 6.11. Wind climate of Napier Airport (19149-1978) (NZ MetService 1982).

Currents resulting from the prevailing SW wind (Fig. 6.11) show a reversal of current direction in the form of an anti-clockwise gyre in the lee of the breakwater, and highlight the division between the Westshore sand fillet and the other compartments (the inner shelf, Marine Parade, the Port and the Beach – Fig. 6.3). Indeed, the current measurements in a period of low wave energy (<0.4 m Hs) and strong SW winds (20-30 kts on Julian Days 139 and 140) agree with the model output, with flows towards the south-east and the south for CM 3 and CM 4, respectively (Figs. 4.23 and 4.24). As the wind backs around to the west (Fig. 6.13) the currents increase and centre of the gyre moves offshore.

As found above, the presence of the port is very pronounced, with currents being diverted offshore, accelerating around the tip of the port, reducing in the lee of the port and dredged channel and affecting the location of the centre of the gyre. The results also show that sediment is able to bypass the port, but that the patterns of the sediment pathways are altered detrimentally.

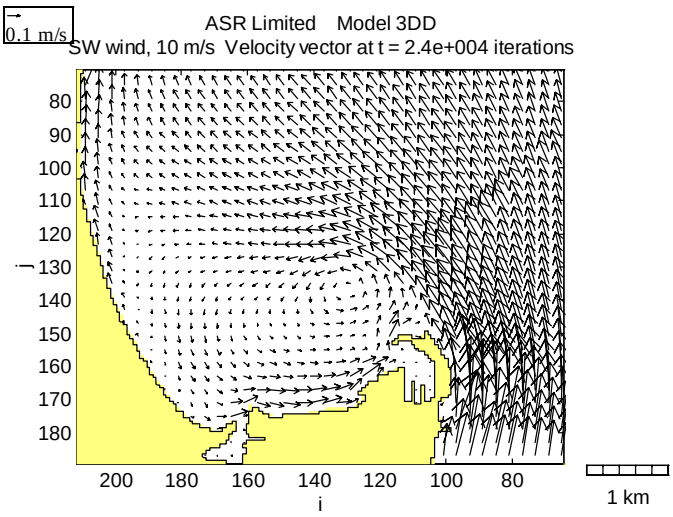

Figure 6.12. SW wind of 10 m/s (~20 kts), at mid-tide.

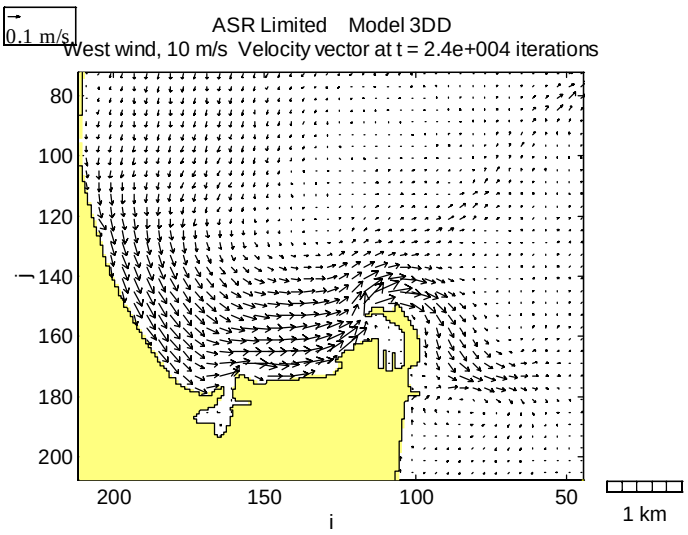

Figure 6.13. W wind of 10 m/s (~20 kts), at mid- tide.

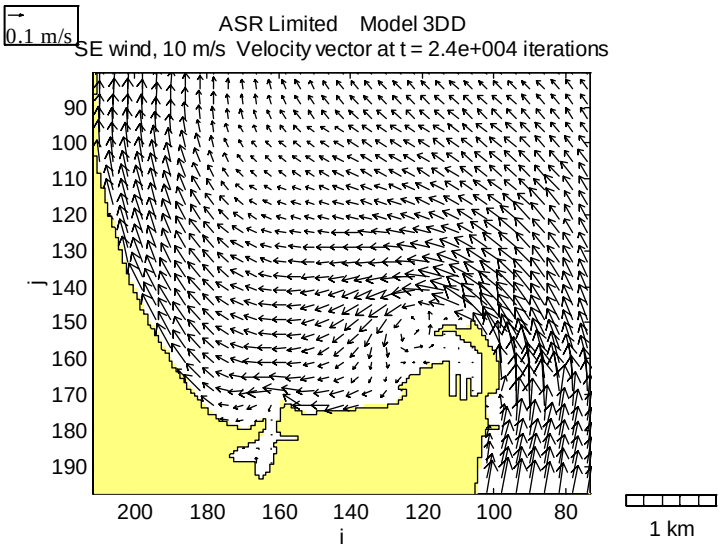

Figure 6.14. SE wind of 10 m/s (~20 kts), at mid-tide.

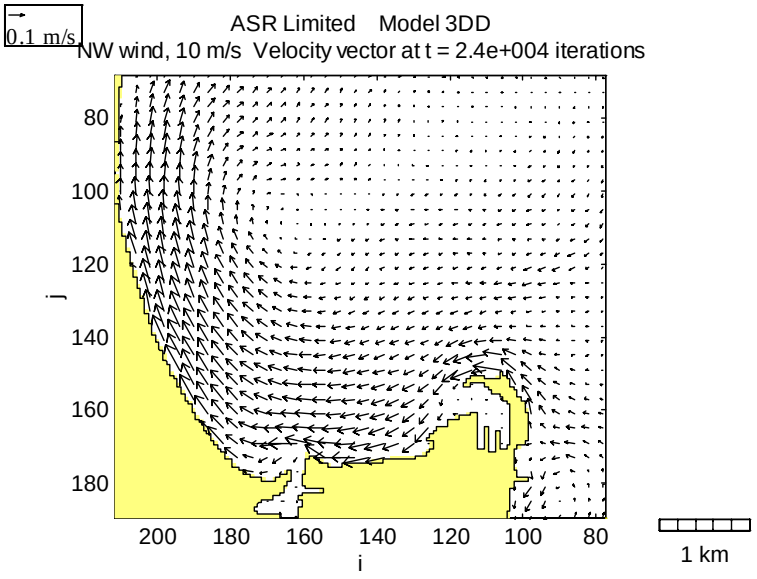

Figure 6.15. NW wind of 10 m/s (~20 kts), at mid-tide.

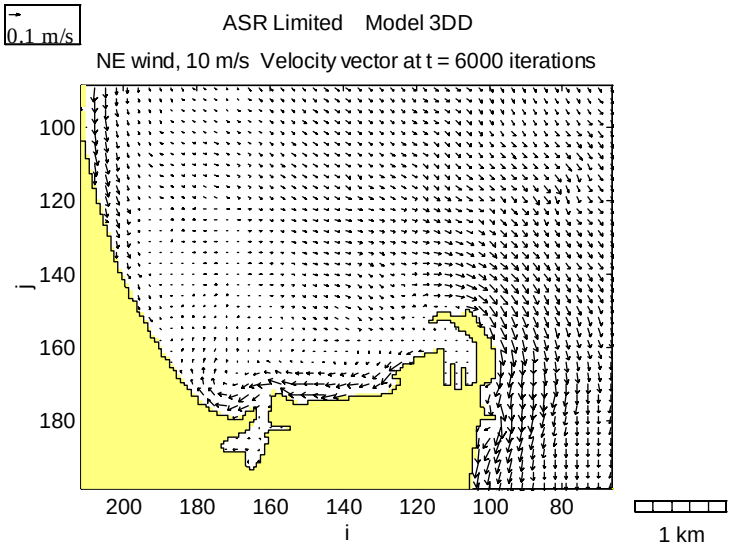

Figure 6.16. NE wind of 10 m/s (~20 kts), at mid-tide.

Thus, a third important mechanism is as follows

- **The presence of the port diverts sand from its natural pathway around the coast, redirecting the sediment pathway into deeper water and therefore away from Westshore beach. Sand is deposited in deeper water and cannot easily find its way back to the beach due to the presence of the headland eddy directing flows offshore. The port disrupts the continuous recirculating sediment pathway over the Westshore sand fillet.**

The idealized drawing of this mechanism is presented in Figure 6.17. We present two cases, with a clockwise and anti-clockwise gyre. The clockwise gyre is seen to be open with the port present, but closed with the port removed.

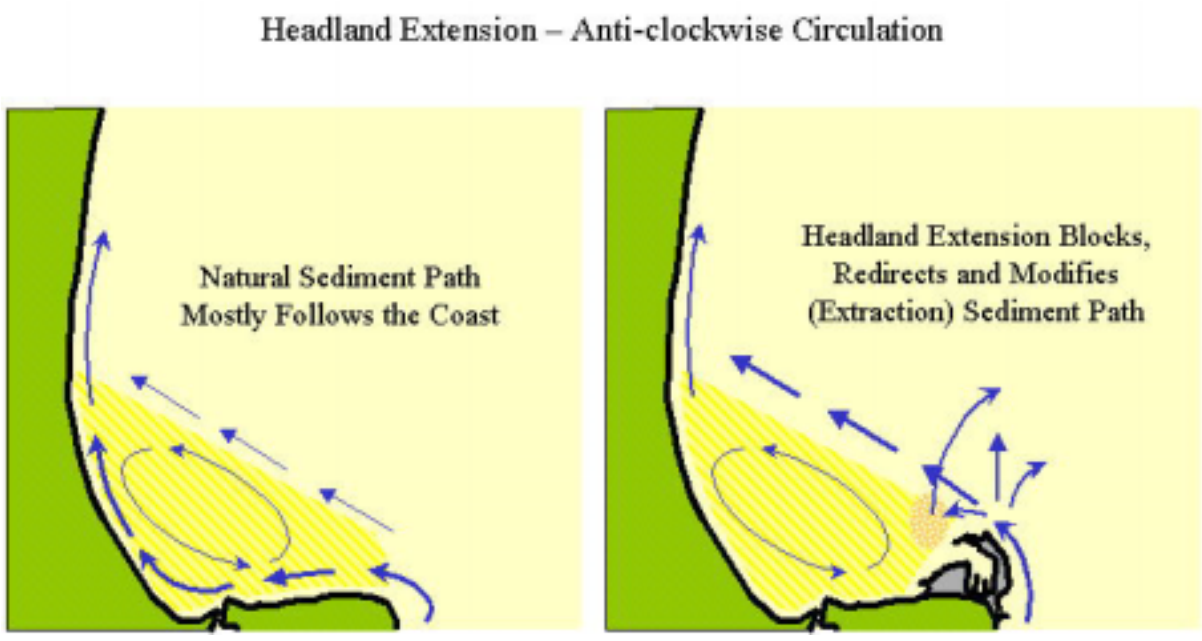

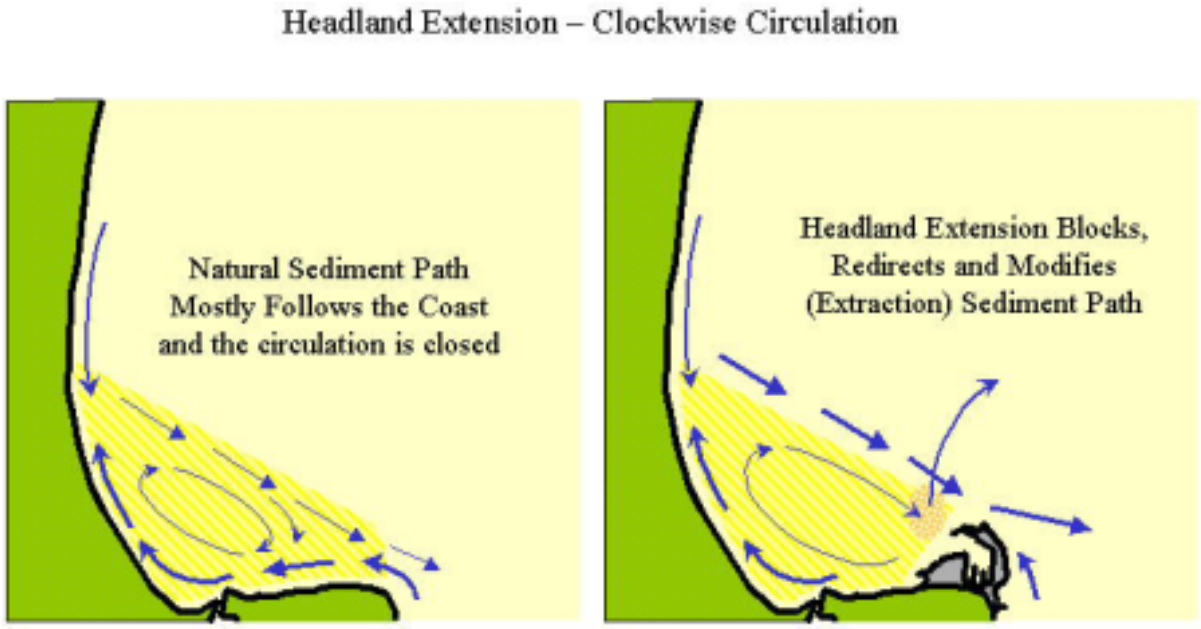

Figure 6.17. Idealised diagram of the effects of the headland extension (Port development) at Westshore Bay – Mechanism #3.

6.6 Volume calculations

Mechanisms 2 and 3 at Westshore Bay indicate that sediment is constantly being lost out of the Westshore sand fillet (Figs. 6.6 and 6.17). In order to verify this, comparisons of existing nautical charts were used. While charts pre-dating the 1931 Hawke's Bay Earthquake exist (e.g. the 1855 chart of Ahuriri Road and Port Napier was used to reproduce the Scinde Island headland in the absence of the Port of Napier – Fig. 6.18), only the 1954 and 1981 nautical charts cover the whole of the Westshore Bay area, and so these were used for comparison. In addition, the changes to the bathymetry caused by the Earthquake and the continued extension of the Port (Section 3.4) would confound volume calculations of the area – although the inner Port was not reclaimed to the same extent in 1954 as it was by 1981, the outer breakwater was the same length and shape at the time both charts were produced. For the purposes of the volume comparison of these two charts, which are

separated by a period of 27 years, only the Westshore fillet was compared. Differences between the two charts were found in deeper regions covered by the Napier Roads charts, however, an assessment of the causes of these changes are beyond the scope of the present study.

In addition, two smaller regions were compared to the 1981 chart bathymetry using soundings provided by the Port of Napier of the inshore spoil ground (1996) and the north of the Fairway (2000) (Fig. 6.18).

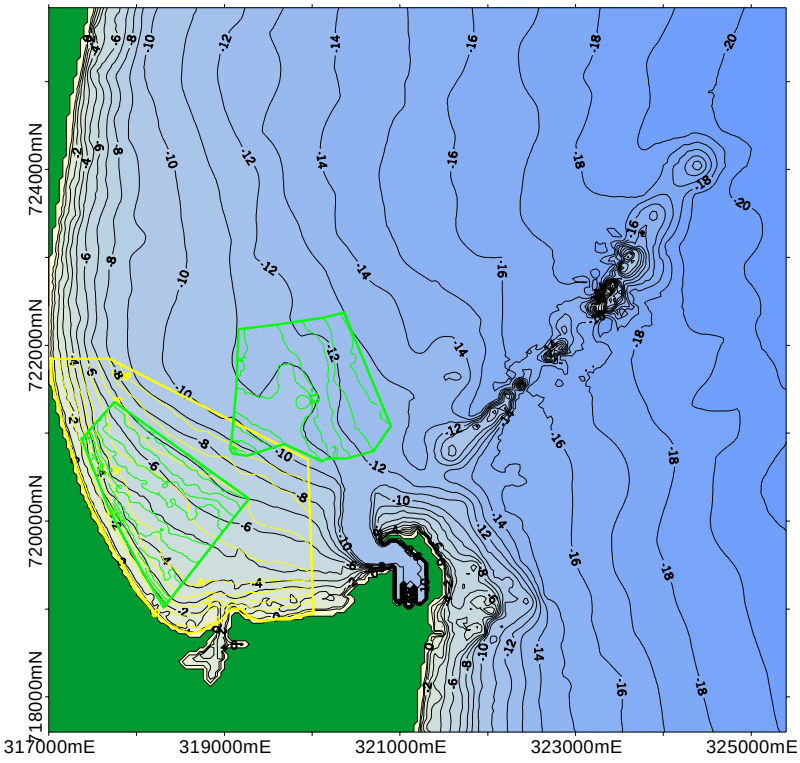

Figure 6.18. Location map of the areas used to compare volume changes between bathymetry surveys of Westshore Bay. The main chart is 1981 NZ 517, the yellow section is extracted from 1954 57 and the two green sections are from Port of Napier soundings (lower left 1996 and upper right 2000).

Table 6.2 summarises the calculated volume changes. In all cases the comparisons show significant decreases in volume, i.e. a loss of sediment and deepening of Westshore Bay. Although the area compared between the 1954 and 1981 charts is around twice as big as the areas compared between 1981 and 1996/2000, the results indicate that the rate of sediment loss was greater in the former period. This may be due to a number of reasons including the residual effects of the 1931 uplift and short-term differences in the metocean conditions between periods. Indeed, observations by many people who had input into this study suggest that the past 10 years was a period of calm weather in comparison to earlier periods (P. Frizzel, pers. comm.) and thus lower sediment flux.

Table 6.2. Calculated volume changes in Westshore Bay.

Area	Period	Area Compared (m^2)	Total Volume Difference (m^3)	Change/Yr (m^3)
Westshore Fillet	1954-1981	4,634,000	3,553,570	-131,613
Spoil Ground 'R'	1981-1996	1,930,500	352,353	-23,490
North Fairway	1981-2000	2,750,000	522,785	-27,515

6.6.1 The Beach Compartment

A volume comparison of the sediment difference between 1954 and 1981 was also carried out for the 'beach compartment', which is the area along Westshore Beach between 0.5 and 4 m deep (Figure 6.19). In this case, a total volume of 808,067 m^3 of sand had depleted over an area of 1,099,200 m^2. This represents an annual sediment loss of 29,928 m^2.

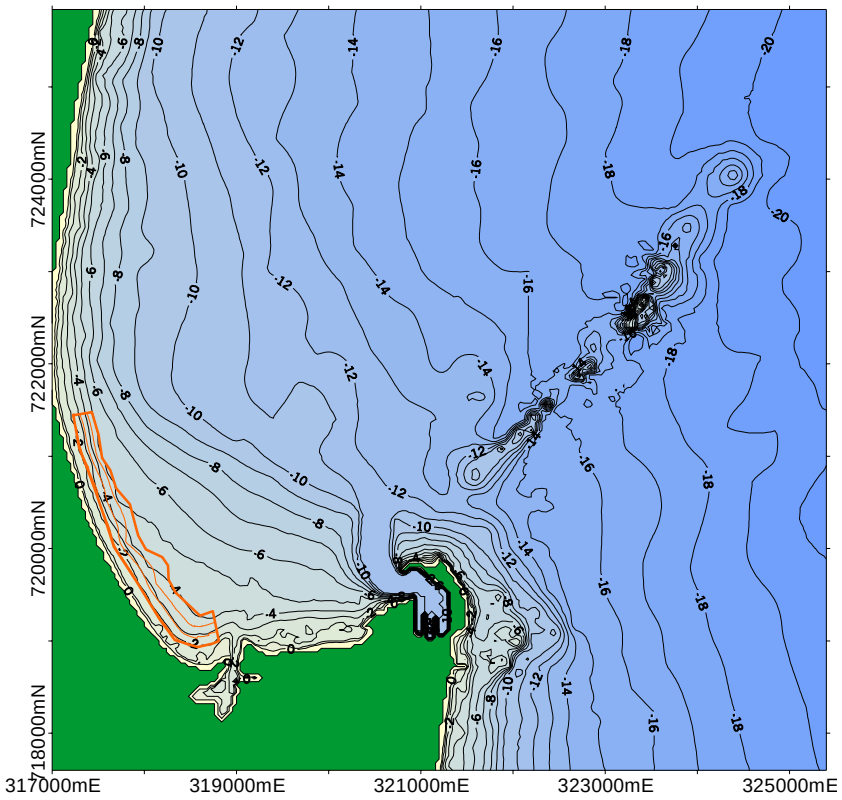

Figure 6.19. Location map of the area used to compare volume change in the beach compartment.

We conclude from this analysis that:

- **the beach erosion is symptomatic of a much larger problem, with volumes of around 131,000 m^3/yr being lost from the Westshore sand fillet. A new complete survey of the region is needed to confirm these findings and to record changes over the fillet in the last 20 years. However, the existing data shows a consistent erosionary trend. Mechanisms causing the losses of sediment in the Westshore sand fillet have been identified, and the losses in the fillet explain the beach erosion that has been observed along Westshore Beach.**

7 RECOMMENDATIONS FOR REMEDIAL WORKS

7.1 Introduction

The study has shown that both the beach and the sub-tidal parts of the Westshore sand fillet are eroding. The volume changes derived during the study are summarised in Figure 7.1 and the rates of loss are relatively large in comparison to the present-day beach nourishment of 12,000 m^3/yr.

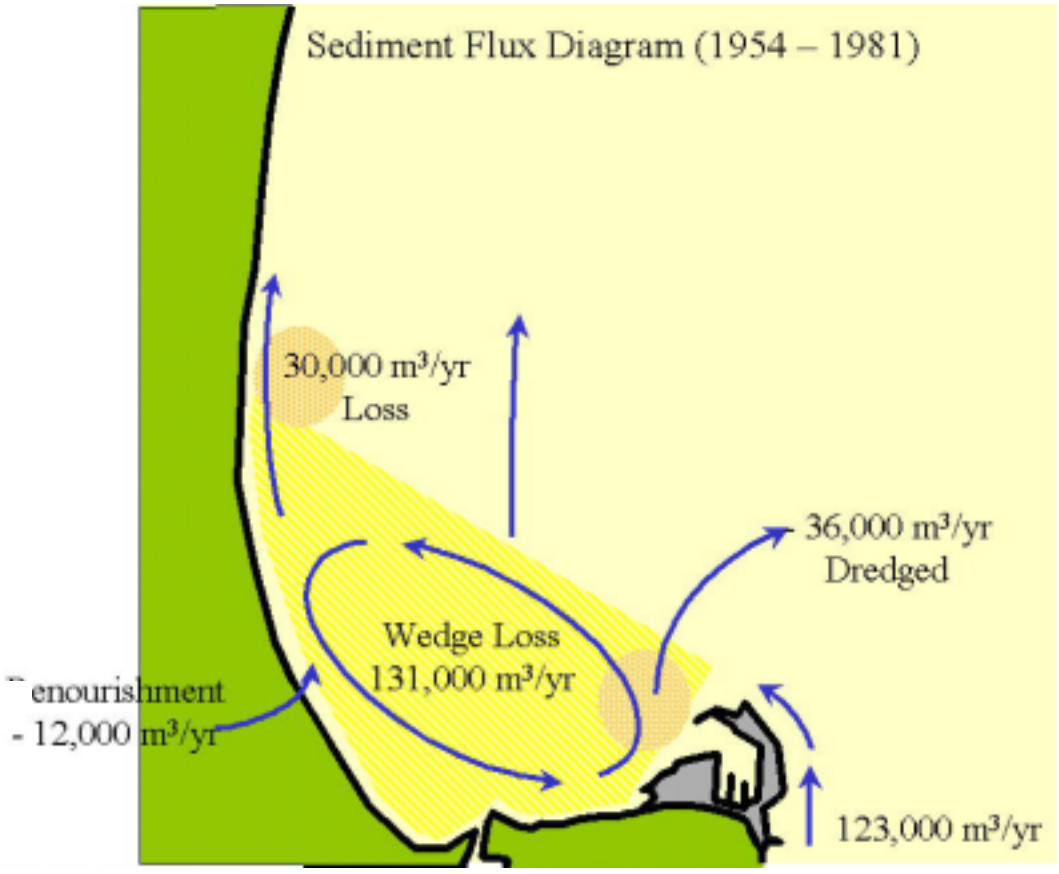

Figure 7.1. Summary of the sediment fluxes in Westshore Bay.

In future, the port will be using an inshore dump ground that is likely to positively impact on the beach erosion. Thus, a critical question to be addressed is:

- will the inshore dumping be sufficient to protect the beach without construction of shore protection devices?

The Westshore sand fillet is eroding at an estimated total rate of about 140,000 m^3/yr, prior to 1981 and, although bay-wide bathymetry surveys have not been undertaken over the last 20 years, surveys of smaller regions have indicated that this trend appears to be continuing.

However, while the total volume losses are very large, the volume of dredged sand to be dumped in the beach compartment is very similar to the amount of sand presently being lost. That is, the port's dredging has, on average, been about 36,000 m^3/yr. Our comparison in Chapter 6 indicates that the "beach compartment" out to the 4 m depth contour lost an average of 32,300 m^3/yr over the 25-year period prior to 1981.

Thus, the port's dumping operations will have a major beneficial impact on the beach erosion if the port's dredged sand is deposited as close as possible to the beach, and preferentially at the southern end of the beach in the allowable zone. This will ensure maximum benefit on the beach itself, even though offshore erosion is expected to continue. In order for the port's dredging to provide optimal benefit, we recommended that:

- **The port's dredged sand be preferentially placed within the beach compartment (shallower than the 5 m contour) in the zone marked in Figure 7.2.**

The orientation of the offshore side of this region is not parallel to the beach, but is set at an angle in order to rotate the waves as they cross the artificial sand bar and encourage longshore transport to the south.

- **To gain further insight into whether the port's operations alone will eradicate the beach erosion, the dredged sand will need to be monitored after placement, through bathymetric survey and using physical oceanographic methodologies.**

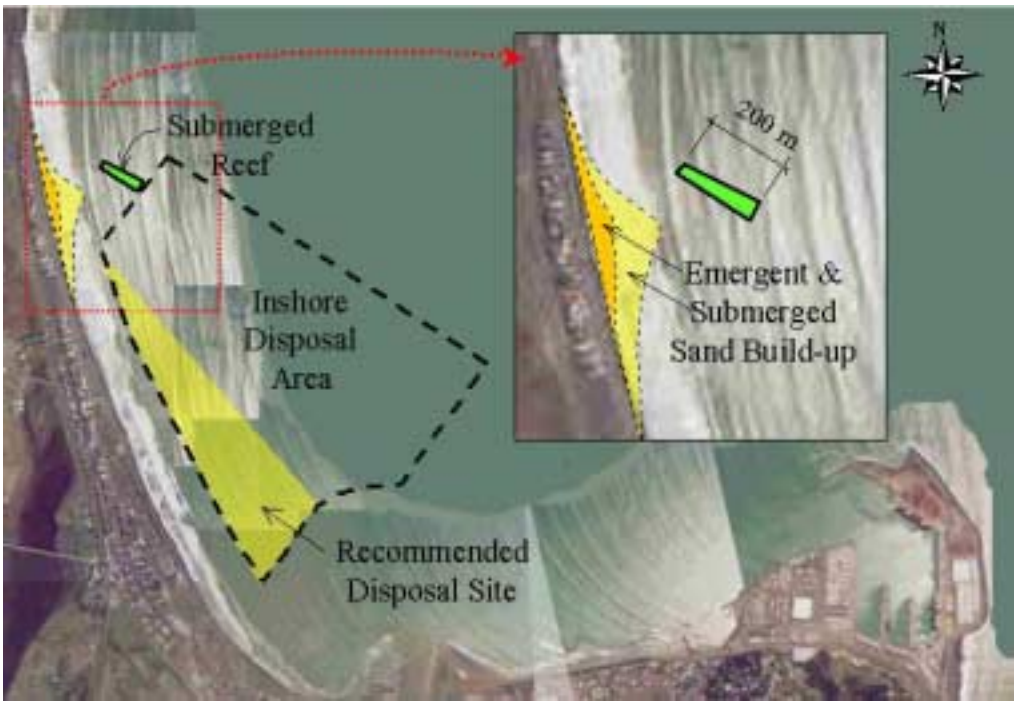

Figure 7.2. Recommended strategy for erosion remediation at Westshore.

With respect to mitigation, the port's inshore placement of dredged sand will provide security against severe erosion. However, the port's dredging operations are sporadic. Indeed, the port has not dredged for several years due to the "unusually calm" weather (P. Frizzell, pers. comm.). When dredging is finally undertaken, volumes as large as 150,000 m^3 may be removed. Thus, the beach protection cannot be guaranteed. In some years, the offshore dump mound will create a broad "over-full" sand bar (approximately 0.4-0.5 m above natural bed level if deposited evenly) that is likely to erode more rapidly than a beach with an equilibrium profile. Also, only a fraction of the sand will move onto the beach. In other years with no nourishment, the beach will be fully exposed to erosion.

In this context, more permanent protection would be beneficial to:

- Act as a coastal control point;
- Smooth out the sporadic nature of the dredging events;

- Capture the sediment in a salient to act as a reservoir in the lean years;
- Optimise the benefits of the port's "on-demand" dredging program; and
- Provide a sustainable solution to the beach erosion.

We consider the various coastal protection options below and ultimately recommend an offshore, submerged reef at the northern end of the port's inshore dump ground. A position, volume and cost of the reef is provided, although detailed design studies would be needed to optimise the reef's benefits. We recommend that the reef be constructed of geotextile tubes, filled with sand from the port's channels. By bagging the sand in geotextile, the reef acts like nourishment, but the sand is not washed away during storms. By storing sand and protecting the beach in the form of a salient, the bagged reef thereby acts to smooth out the irregular nature of the port's dredging operations and to sustain the beach through the lean years. More detailed description various erosion control options and the submerged reef are given below.

To successfully protect a coastline from erosion, it is always very important to first identify the processes that are causing the problem and then address the cause, rather than the effect. As a variety of options can be used to protect coastal developments, we consider each of the key options in the light of the understanding of coastal processes operating in Westshore Bay that has been developed in this study. Beach nourishment, dune rehabilitation, seawalls, groynes, artificial headlands, detached breakwaters and submerged reefs are considered.

7.2 Protective Works Options

7.2.1 Beach Nourishment

Where there is insufficient sediment on a beach to meet storm erosion or long-term sediment loss, additional sediment can be placed by mechanical means, as is presently done at Westshore. Beach nourishment involves the artificial placement of sand onto a beach to

replace sand that has been lost through erosion. The nourishment forms a buffer against storm erosion, with periodic topping up to satisfy the natural erosion processes. To be successful, nourishment is best undertaken over the whole beach profile including the part of the beach below the water out to depths where storm waves are breaking (in Westshore Bay this would be up to 5-6 m deep – Section 4.4.3.1), not only the beach above the low-water mark. This approach of profile nourishment has been used successfully on the Gold Coast for many years (Jackson & Tomlinson, 1990).

Beach nourishment is a favoured means of beach protection for resort and high amenity beaches because it promotes amenity and, unlike some other structural measures, generally it does not have adverse effects on adjacent areas of the coastline. Provided sufficient sand is used, beach nourishment can provide total protection. However, it may be an expensive means of control. To prevent excessive offshore losses of the placed material, the nourishment sand should be similar in size or, preferably, slightly coarser than the natural beach material (Nielsen, 2001). The sand grain size of the fairway dredge material (Hume *et al*., 1989) is of a similar size to that currently found in Westshore Bay (Section 4.4.1).

At Westshore, the granting of the resource consent for the inshore dumping of dredge spoil will increase the volume of sediment placed in the beach compartment (up to 36,000 m^3/yr), but only a fraction of this will move onto the beach. The exact fraction will depend on the cross-shore location of dumping, the size of the mound and prevailing weather in the following months. In addition, the port's dredging operations are irregular and so the nourishment will not be provided every year. Thus, nourishment is not an assured method of coastal protection, as discussed above, although inshore dumping of dredge spoil is highly encouraged.

7.2.2 Sea Walls

Seawalls are shore parallel structures, that are put in place to impose a landward limit to coastal erosion and to provide protection to the area behind it. Seawalls are commonly built

of many materials including timber, steel, concrete, rock, gabions, geotextiles and specially designed armour units and have a face that is either vertical, curved, stepped or sloping.

Seawalls need to cover the full length of coast to be protected, that is, with the ends of the walls beyond the erosion zone, because erosion around the ends of the wall can lead to collapse – this is commonly known as the 'end effect'. In addition, isolated sections of seawall may exacerbate erosion on unprotected sections of a beach by denying sediment down coast during storms and by deflecting wave energy (Nielsen, 2001).

A seawall is not a feasible option for erosion protection at Westshore Bay because:

1. It does not address the causes of erosion;
2. The large length of coastline being eroded (almost 3 km) means the construction cost would be prohibitive, and;
3. It has a negative impact on the beach amenity, access and aesthetics.

7.2.3 Groynes and Artificial Headlands

Groynes and their massive relatives, artificial headlands, are coastal structures built of similar materials as seawalls, but oriented approximately shore-normal. They form a cross-shore barrier that traps sand that moves alongshore, thereby increasing the width of the beach on the upstream side.

For groynes to be effective there must be a longshore supply of sand which is trapped on the updrift side of the groyne and accretes. This reduces sand supply downdrift of the groyne and erosion can result. Downdrift erosion can be reduced by filling the groyne embayment under a beach nourishment program, and dune management measures can be used both up drift and down drift to accommodate changes in the beach and dune systems (Nielsen, 2001).

Groynes do not reduce the cross-shore movement of sand during storms. Therefore, groynes are not effective as a means of managing short-term erosion in the form of cross-shore sediment transport, other than their effect in building up a sand buffer.

A groyne(s) is not a recommended option for erosion protection at Westshore Bay because:

1. It/they do not address all the causes (partially address the northerly loss of sediment in mechanism #3 by causing a barrier).

2. It/they cause down-coast erosion (in this case on the northern side).

3. Although the predominant littoral drift is to the north, the alongshore sediment transport has been found to move both up and down the coast. However, a groyne can act as a "one-way valve", or a major blockage to the natural shoreline movement. Because a groyne significantly imposes on the sedimentary system, and a large groyne may be needed to have a significant impact on the shoreline erosion, very detailed modelling and predictive studies would be needed before considering this option.

7.2.4 Detached Breakwaters

Detached breakwaters are oriented approximately parallel to the beach but, unlike a seawall, are some distance offshore. They protrude above water level and can be continuous or consist of a series of segments and can be built of similar materials as the previously mentioned coastal protection works. While these kinds of structures have not been used for coastal protection in New Zealand, they have been used extensively for a number of years in Japan, the USA, Singapore and in Europe (Fig. 7.3). Overseas, detached breakwaters, typically, have been used along coastlines with small tidal fluctuations to control the cross-shore sand transport processes (Nielsen, 2001).

Figure 7.3. An example of a detached breakwater project in East Anglia, Great Britain. Note the formation of tombolos in the lee of the breakwaters. The sand was placed as nourishment, not trapped from the natural system.

In general, detached breakwaters are suited to coastlines that require higher levels of protection at sensitive points and do not have sensitive downdrift beaches, as detached breakwaters may cause downdrift erosion on a beach where there is a strong nett transport of littoral drift.

Detached breakwaters provide protection by reducing the energy in their lee and thereby, reducing the wave-driven currents that cause coastal erosion. Material is deposited in the zone of reduced wave energy forming a salient (a bulge in the coast) or tombolo (a connection between the coast and the offshore obstacle). However, like a groyne, a tombolo will block alongshore sediment transport and cause erosion on the down drift side of the structure. Eventually, sediment transport may resume along the seaward face of the detached breakwater. This situation may be desirable if the intention is to create a pocket

beach or to reclaim part of the foreshore. However, it requires a large and continuous sediment supply, which is not present in Westshore Bay, as well as accompanying renourishment on the downdrift side until equilibrium has been reached.

Conversely, a salient allows sediment to pass between the offshore obstacle and the coast, and so the 'one-way valve' effect doesn't occur and sediment can move in both directions without causing long-term depletion on the downdrift side. The beach is protected in the lee without totally blocking sediment movement. It is therefore critical to place the detached breakwater of the correct length at the correct distance offshore to achieve a salient and not a tombolo.

A well-designed detached breakwater could provide a control at Westshore Bay to help retain Port dredge material placed to the south. However, such a structure cannot rotate waves to an alignment closer to shore parallel and therefore the breakwater is not as sophisticated as a submerged reef and does not provide as much opportunity for subtle adjustment of structure's geometry and position to achieve design criteria. A detached breakwater is not a recommended option for Westshore Bay erosion control because.

1. It does not address all the causes of erosion (e.g. no ability to rotate waves to a more favourable alignment);

2. Detached breakwaters protrude above water level in the surf zone and so are prone to damage and hence maintenance, and are also more difficult to construct than land based solutions, both of which makes them expensive to construct, and;

3. Because they protrude above the water level, they negatively impact on the aesthetics of the beach.

4. Very little additional amenity is provided by the structure.

7.2.5 Submerged Reefs and Surfing Reefs

Offshore, submerged reefs are a relatively new coastal zone management concept that is being very well received by the public (Nielsen, 2001). The concept attempts to blend the socio-economics with the coastal protection imperatives, thereby offering the opportunity for coastal engineers to act on the community's requests and aspirations (Black, 2000) (Appendix 4).

While the concept of blending coastal amenity and coastal protection is new, there are many examples of coastal structures in the form of natural reefs and islands that provide protection to the shoreline in their lee. Andrews (1996) identified several hundred such cases around the New Zealand and New South Wales, Australia coastlines. Figure 7.4 is a classic example of a protective reef that has created a natural widening of the beach in the form of a salient. Indeed, the Mahia Peninsula is actually a local classic example of a sandy tombolo formed in the lee of the Island by these same processes (Fig. 6.1).

Figure 7.4. A salient formation in the lee of a natural submerged reef.

Salient growth in the lee of a reef leads to enhanced shoreline stability and protection. Recreational and public amenity can be incorporated through surfing, diving, sheltered swimming, water games, fishing and/or marine habitat. The inclusion of amenity, however, requires the amalgamation of different purposes in the reef design and, consequently, can make the design more difficult than that which may be required for coastal protection only.

Offshore, submerged reefs can provide shoreline protection with low environmental impact. Because the structure is underwater, the visual amenity is not impaired. Further, submerged offshore reefs can lead to eliminating the need for rock works on beaches. The reef may:

- unify coastal protection and amenity benefits into a single structure placed offshore;
- enhance the coastal amenity value by incorporating multiple use options of surfing, diving, marine habitat, water games and sheltered swimming; and
- preserve the beach amenity.

The depth of the reef, its size and its position relative to the shoreline determine the level of coastal protection that may be provided by the reef. This ability to vary the protection level as part of the reef design is a feature of the offshore reefs.

Offshore reefs allow sand to pass over their crest and between the reef and the shoreline. Thus, offshore reefs may be used when:

- a partial blockage to sand is required;
- hard-rock construction on the beach is not wanted or may not be suitable;
- the natural character of the beach is to be preserved; or
- an improved recreational and environmental amenity value is required.

Two artificial surfing reefs (ASR's) have been constructed recently in Australia. The first reef was designed specifically to improve surfing conditions at Cottesloe in Perth, WA, and was constructed from rock. The second reef (designed by K. Black, ASR Ltd) has been constructed on Australia's eastern seaboard at Narrowneck on the Gold Coast, Qld, using very large sand-filled geotextile bags. This structure was the first to be designed for the dual purpose of providing beach protection as well as surfing amenity. The shape is novel as the reef is the first to be oriented primarily cross-shore, while prior reefs and breakwaters solely for coastal protection have been aligned longshore.

Submerged reef structures can be used for coastal protection, though their effectiveness at reducing wave energy may be limited, particularly on macro-tidal shores subject to storm surge. In these cases, a reef may be designed to change the orientation of the wave crests as they pass over the structure. This may lead to an altered wave angle at the breakpoint and a reduction in surf zone currents, leading to reduced nett sand transport and improved beach stability (Black, 2000). Such a device may act even when waves are not breaking on the reef, and so may be suitable for regions with large tidal ranges. Such a reef has been designed for Noosa Beach (Black *et al*., 2001) and is planned to be constructed in late 2001.

Studies of the Gold Coast, Bournemouth (UK) and sites in New Zealand (Raybould and Mules, 1998; Black *et* al., 2000; Gough, 1999) have indicated that surfing reefs can be a viable economic proposition, which have positive cost/benefit ratios. The community of Westshore Bay has actively supported the concept of a surfing reef for coastal protection.

Geotextile containers are a low cost alternative for coastal construction, especially when there is a ready supply of clean sand for fill, as is the case with the Port of Napier's fairway maintenance dredging. Cost estimates using other common construction materials have been found to be over 3 times as expensive (Headley, 2001). Even in New Plymouth where large quarry rocks are readily available, geotextiles still proved to be the most cost effective option (Black *et al*., 1999).

A submerged reef at Westshore Bay is the recommended option for remediating erosion because:

1. It would address one of the critical causes of erosion along Westshore Beach by locally neutralising longshore currents and forming a coastal control point that still allows free passage of sand after the salient has stabilised;

2. There are no negative aesthetic impacts (indeed, the visual rhythm of waves breaking on an offshore submerged reef may be considered an aesthetic enhancement that compliments the seascape);

3. Construction materials and methods have low environmental impact, as they provide habitat for marine life (Fig. 7.5) and construction is carried out from the water;

4. Construction costs are relatively low, and;

5. Amenity value can also be enhanced.

Figure 7.5. After 18 months on the seabed, the geotextile containers that comprise the Narrowneck Reef on the Gold Coast are a flourishing habitat in a relative 'desert' of mobile sand.

7.2.6 Dune Management

Dune management measures are needed to accommodate the increased sand volume that will occur initially in the lee of the submerged reef and eventually back into Westshore Bay. During storms, sand is removed from the beach to form an offshore bar and, during intense storms, a demand for dune sand is created which involves the sand buffer reserves held in the dunes. The maintenance of a sufficient sand storage relies on effective dune management, which is based on maintenance of a satisfactory primary, secondary and tertiary vegetative cover (Chapman, 1989). This requires the introduction of appropriate plant species and defined access/walkways over the dunes to maintain their health.

Beach vegetation, such as Spinifex and Pingao, stabilise the sand that returns within a few weeks of the return of fine weather following storms. Secondary species have an important function of stabilising seaward of the permanent dune crest, and permanent tertiary species on and behind the crest of the foredune that are slow growing, provide shelter to the secondary species and, most importantly, act to modify locally the onshore wind field favourably for aeolian sand deposition onto the dune field (O'Callaghan, 1986; Nielsen, 2001). Secondary and tertiary species should not be considered at Westshore Beach until the dune has sufficiently widened to ensure that the loss of the back dune is a rare event.

7.3 Recommended Option For The Mediation of the Erosion Occurring Along Westshore Beach

The large volume of sediment already lost from the Westshore Bay area, and the disruption to the re-circulating sediment pathway over the Westshore sand fillet associated with the port, make a 'quick-fix' to the erosion problems a difficult task. However, the placement of dredge spoil on an inshore dumpsite will have major beneficial impacts, albeit irregular and insecure. To overcome these deficiencies, an offshore, submerged reef is recommended as a 'control point' to retain sediment and thereby smooth out the irregular nature of the port's dredging operations and to sustain the beach through the lean years.

The most appropriate position for the reef is at the northern end of the inshore dredge dumpsite, in order to capture and store the sand leaking northwards from this site. The position is also centred on the area of worst erosion along the shoreline. Design of the submerged reef should also consider multi-purpose options such as optimising surfing conditions and incorporation of habitat enhancement, which can greatly enhance the amenity and environmental values of coastal structures (Jackson *et al.*, 2000; Gough, 1999; Black *et al.*, 1998).

It is also recommended that the dredge spoil be dumped within a narrower coastal region shorewards of the 4-5 m contour, an area of 400,000 m^2 (Fig. 7.2). In a typical dredging campaign of 150,000 m^3, the seabed would be raised by an average of about 0.37 m in this region.

Recommended additional data collection and design studies are as follows:

- A detailed bathymetric survey of the sand fillet and environs at Westshore to determine the rates of bed level adjustment over the last 20 years.
- Wave/current and sediment transport measurements at the proposed site of the ASR. Similar techniques to those used in the present study, amalgamated with the technical methods of Black and Vincent (2001), could be adopted.
- Monitoring of the dredge spoil and beach after placement, possibly including tracer experiments at the mound and around the port.
- Detailed optimisation and design of the ASR. The estimated volume of the reef is 12,250 m^3 and the estimated inclusive cost of construction and additional studies is $1.1 million, based on a geotextile construction method and utilisation of the Port's dredge sand.

ACKNOWLEDGEMENTS

ASR would like to thank all the local people that gave assistance during this study. Peter Frizzel and the Port of Napier for provision and discussion of metocean information and many other aspects that were relevant to this study. Mark Dunnett of Survey Services, Kamen Ganev from Hawke's Bay Regional Council, and others that supplied technical data and discussion.

REFERENCES

Andrews, C. J., 1997. *Sandy Shoreline Response to Emerged and Submerged Offshore Obstacles*. Unpublished MSc Thesis. Centre of Excellence in Coastal Oceanography and Marine Geology, Earth Sciences Department, University of Waikato.

Barrow, S., 2000. *Geomorphological, Palaeoenvironmental and Managerial Implications for the conservation of the fossil forest at Titahi Bay*. A report prepared for the Porirua City Council, July, 2000.

Beca Carter-Caldwell Connell, 1980. *Moa Point Wastewater Treatment Plant and Outfall Study*. Report prepared for the Wellington City Corporation, January 1980.

Black, K. P. & S. L. Gay, 1987. Eddy Formation in Unsteady Flows. *Journal of Geophysical Research*, 92 (C9): 9514-9522.

Black, K.P., 1995. *The numerical hydrodynamic model 3DD and support software.* Occasional Report No. 19. Department of Earth Sciences, University of Waikato, New Zealand. 53 pp.

Black, K.P. and Rosenberg, M.A., 1992a. Natural stability of beaches around a large bay. *Journal of Coastal Research*. 8(2): 385-397.

Black, K.P. and Rosenberg, M.A., 1992b. Semi-empirical treatment of wave transformation outside and inside the breaker line. *Coastal Engineering.* 16: 313-345.

Black, K.P., Beamsley, B., Gorman, R., 1997a. *Wave refraction model confirmation in the Poverty Bay, Gisborne, New Zealand*. Report to the Port of Gisborne, Earth Sciences Coastal Marine Group, University of Waikato.

Black, K. P., C. Andrews, M. Green, R. Gorman, T. Healy, T. Hume, J. Hutt, S. Mead and A. Sayce, 1997b. Wave Dynamics and Shoreline Response On and Around Surfing Reefs. *Proceedings of the 1st International Surfing Reef Symposium*, Sydney, Australia. March, 1997.

Black, K. P., J. A. Hutt & S. T. Mead, 1998. *Narrowneck Reef Report 2: Surfing Aspects*. Technical Report prepared for the Gold Coast City Council, June, 1998.

Black, K. P., 1999. Designing the shape of the Gold Coast Reef: sediment dynamics. *Proceedings of the Coasts & Ports '99 Conference*, 14-16 April 1999, Perth, Australia. Pp.58-63.

Black, K. P., 2000. *Artificial surfing reefs for erosion control and amenity: theory and application*. International Coastal Symposium (ICS2000) Invited paper. Rotorua, April, 2000.

Black, K. P., J. A. Hutt, S. Mead, A. Jackson, J. McGrath, 2000a. Design of the Gold Coast Artificial Reef: Surfing aspects. Special Issue of the *Journal of Coastal Research* on Surfing. (in press).

Black, K. P., S. Mead and A. Jackson, 2000b. *Beach Amenity Options and Coastal Protection at Bournemouth*. Technical Report Prepared for Leisure and Tourism Services, Bournemouth Borough Council, May, 2000.

Black, K. P., and C. J. Andrews, 2000a. Sandy Shoreline Response to Offshore Obstacles: Part 1: Salient and tombolo geometry and shape. Special Issue of the *Journal of Coastal Research* on Surfing. (in press).

Black, K. P., and C. J. Andrews, 2000b. Sandy Shoreline Response to Offshore Obstacles: Part 2: Discussion of Formative Mechanisms. Special Issue of the *Journal of Coastal Research* on Surfing. (in press).

Black, K.P., and C.E. Vincent, 2001. High-resolution field measurements and numerical modelling of intra-wave sediment suspension on plane beds under shoaling waves. *Coastal Engineering* 42: 173-197.

Black, K. P., S. T. Mead and J. Mathew, 2001. *Design and Approvals for an Artificial Reef for Protection of Noosa Main Beach: Detailed Investigations and Modelling*. Final report for Noosa Council and ICM Ltd, June 2001.

Bohnsack, J. A. & D. L. Sutherland, 1985. Artificial Reef Research: a review with recommendations for future priorities. *Bulletin of Marine Science* 37: 3-10.

Brunn, P., 2000. Coastal Protection Structures. *Proceedings Coastal Structures '99*, Losada (ed.), Balkema, Rotterdam. Pp. 737-746.

Bush, D. M., O. H. Pilkey Jr., and W. J. Neal, 1996. *Living by the Rules of the Sea*. Duke University Press, Durham and London, 1996. Pp. 179.

Carter, L., 1992. Acoustical Characteristics of seafloor sediments and its relationship to active sedimentary processes in the Cook Strait, New Zealand. *New Zealand Journal of Geology and Geophysics* 35:289-300.

Carter, L., I. C. Wright, N. Collins, J. S. Mitchell and G. Win, 1991. Seafloor stability along the Cook Strait power cable corridor. *Coastal Engineering – Climate for Change. Proceedings of the 10th Australasian Conference on Coastal and Ocean Engineering*, Auckland 2-6 December 1991. Pp. 565-570.

Carter, L and Lewis, K., 1995. Variability of Modern Sand Cover on a tide and storm driven inner shelf, south Wellington, New Zealand. *New Zealand Journal of Geology and Geophysics*, 38:451-470.

CE, 1976. *Wellington Airport Runway Extension, Environmental Audit.* Commission for the Environment, Wellington, 1976.

Golden Software, Inc., 1996. *Surfer Surface Mapping System, Version 6.03.* Golden Software, Incorporated, Colorado, USA.

Hsu, J. R. C., and R. Silvester, 1990. Accretion Behind Single Offshore Breakwaters. *Journal of Waterway, Port, Coastal and Ocean Engin*eering 116(3); 362-381.

Hutt, J. A., 1997. *Bathymetry and wave parameters defining the surfing quality of five adjacent reefs.* MSc. Thesis, University of Waikato, New Zealand. 170 pp.

Komar, P., 1976. P. D., 1976. *Beach Processes and Sedimentation*. Prentice-Hall Inc., New Jersey.

Lewis, K. B., and J. S. Mitchell, 1980. *Cook Strait Sediments.* 1:200,000 New Zealand Oceanographic chart coastal series.

LINZ, 2000. *Wellington Harbour – Nautical Chart NZ 4632.* Scale 1:25,000. Published by Land Information New Zealand, July 2000.

Mathew, J., K. P. Black, S. T. Mead & G. Cox, 2000. *Waitakere and Hunua Ranges Lake Surveys*. Report and Software prepared for WaterCare Services Ltd, June 2000.

McComb, P.J., Black, K.P., Atkinson, P.N., Healy, T.R. and Bell, R.G., 1997. High-resolution wave transformation on a coast with complex bathymetry. *Pacific Coasts and Ports'97*, Christchurch, 7-11 September 1997.

McComb, P.J., Gorman, R.G., Black, K.P., and Kun, A. 2001. Measuring directional wave spectra using the 3D ACM-WAVE on fixed and taut-wire moorings. *Journal of Oceanic Engineering,* (in press).

Mead, S., Black, K. and Hutt, J., 1998a. Surfing Reef Morphological Components Combine To Create World-Class Surfing Breaks. *2nd Annual International Artificial Surfing Reef Symposium*. San Diego. April, 1998.

Mead, S., Black, K. and Hutt, J., 1998b. An Artificial Offshore Reef at Tay Street – Mount Maunganui Beach. *Annex IIIC: Reef Design and Physical and Biological Processes.* Report submitted to Environment Bay of Plenty, July, 1998.

Mead, S. T. and Black, K.P., 1999. Configuration of Large-Scale Reef Components at a World-Class Surfing Break: Bingin Reef, Bali, Indonesia. *Proc. Coasts & Ports '99*, Vol. 2:438-443.

Mead, S. T. & K. P. Black, 2000a. Field Studies Leading to the Bathymetric Classification of World-Class Surfing Breaks. Special Issue of the *Journal of Coastal Research* on Surfing. (in press).

Mead, S. T. & K. P. Black, 2000b. Functional Component Combinations Controlling Surfing Wave Quality at World-Class Surfing Breaks. Special Issue of the *Journal of Coastal Research* on Surfing. (in press).

Mead, S. T. & K. P. Black, 2000c. Predicting the Breaking Intensity of Surfing Waves. International Coastal Symposium (ICS2000) Rotorua, New Zealand. Special Issue of *Journal of Coastal Research* (in press).

Middleton, J.F. and Black, K.P., 1994. The low frequency circulation in and around Bass Strait: a numerical study. *Continental Shelf Research* 14 (13/14): 1495-1521.

Ministry of Transport, 1975. *Wellington Airport Runway Extension Environmental Impact Report*. Prepared by the Civil Aviation Division, Ministry of Transport.

Morton, J. E. & M. C. Miller, 1968. *The New Zealand Seashore*. William Collins Sons and Co. Ltd, Glasgow, Great Britain.

NZ MetService, 1982. *The Climatology of Napier Airport*. NZ Meterological Service Publication No. 171 (20), ISSN 0110-6937.

Pickrill, R. A., 1979. *Beach and Nearshore Morphology, Lyall Bay, Wellington*. NZOI Oceanographic Report, No. 13, April 1979.

Pickrill, R. A., and J. S. Mitchell, 1979. Ocean Waves Characteristics Around New Zealand. *New Zealand Journal of Marine and Freshwater Research*, 13(4): 501-520.

Pilarczyk, K. W. & R. B. Zeidler, 1996. *Offshore Breakwaters and Shore Evolution Control*. A. A. Balkema, Rotterdam. 560p.

Pratt, J. R., 1994. Artificial habitat technology and ecosystem restoration: managing for the future. *Bulletin of Marine Science* 55(2-3):268-275.

Rowe, T. W., 1999. *An Investigation into the Viability of Lyall Bay, Wellington, as a Suitable Location for an Artificial Surfing Reef*. Unpublished BSc Thesis, Massey University, 1999.

Saito, K., 1992. Japan's Sea Urchin Enhancement Experience. *Proceedings, Sea Urchin, Kelp and Abalone Conference, Sea Grant Extension Programme*. University of California, Bodega Bay Marine Laboratory, Bodega Bay, California, March 18-21 1992.

Walker, 1997. Surfing Reef Fundamentals. *1st International Surfing Reef Symposium.* Sydney, Australia, March 1997.

Young, I.R., Black, K.P. and Heron, M.L., 1993. Circulation in the ribbon reef region of the Great Barrier Reef. *Continental Shelf Research*. 14 (2/3): 117-142.

Aagaard, T. & Greenwood, G., (1994). Suspended sediment transport and the role of infragravity waves in a barred surf zone. *Marine Geology*, 118: 23-48.

Antsyferov, S. & Kos'yan, R.D. (1990). Study of suspended sediment distribution in the coastal zone. *Coastal Engineering*, 14: 147-172.

Black, K.P. (1994). Suspended sediment load during an asymmetric wave cycle over a plane bed. *Coastal Engineering*, 23: 95-114.

Black, K.P. & Rosenberg, M.A. (1991). Suspended sediment load at three time scales. Coastal Sediments '91 Proceedings Specialty Conference/WR Div./ASCE.

Black, K.P., Gorman, R.M. & Symonds, G., (1995). Sediment transport near the break point associated with cross-shore gradients in vertical eddy diffusivity. *Coastal Engineering*, 26: 153-175.

Goda, Y. (1970). Numerical experiments on wave statistics and spectral estimates. Report of the Port and Harbour Research Institute, 9(3): 3-57.

Green, M.O. & Black, K.P. (1999). Suspended-sediment reference concentration under waves: Field observations and critical analysis of two predictive models. *Coastal Engineering, in press.*

Green, M.O. & Vincent, C.E. (1990). Wave entrainment of sand from a rippled bed. *Coastal Engineering*, Proceedings, Vol 3: 2200-2212.

Greenwood, B., Osborne, P.D., Bowen, A.J. & Hazen, D.G. (1990). Nearshore sediment flux and bottom boundary dynamics: The Canadian Sediment Transport Programme (C-Coast). Coastal Engineering, Proceedings, Vol 3: 2227-2240.

Hutt, J.A. and Black, K.P. (1997). Vertical attenuation of wave-induced pressure. Pacific Coasts and Ports '97 Conference, Christchurch, 7-11 September 1997. P.965-970.

Jonsson, I.G. (1966). Wave boundary layers and friction factors. Proc. 10th Conf. Coastal Engng, Tokyo, Am. Soc. Civ. Engrs, New York, , 127-148.

Lee, T. T. & Black, K. P. (1978) The energy spectra of surf waves on coral reefs. 16th International Conference on Coastal Engineering, Hamburg, ASCE, 588-608.

M^{c}Comb, P.; Black K.; Healy, T. & Atkinson, P. (1999). Coastal and sediment dynamics at Port Taranaki, New Zealand: a large, multi-faceted, field experiment. Proceedings of Coastal Structures '99 Conference, Santander, Spain. Vol. 2: 823-832.

M^{c}Comb, P.; Gorman, R.; Black K. & Kun, A. (2000a). Measuring directional wave spectra with the 3D-ACM WAVE. IEEE Journal of Oceanic Engineering, 26 (2), 171-180.

M^{c}Comb, P.J. & Black, K.P. (submitted). "Measuring time-averaged suspended sediment concentrations by sediment trap and automated water sampler: a comparative study under wave-dominated flow".

Mocke, G.P. and Smith, G.G., (1992). Wave breaker turbulence as a mechanism for sediment suspension. Coastal Engineering, Vol 2: 2279-2292.

Nielsen, P. (1986). Suspended sediment concentrations under waves. *Coastal Engineering*, 10: 23-31.

Nielsen, P. (1992). Coastal bottom boundary layers and sediment transport. Advanced Series on Ocean Engineering - Volume 4. World Scientific. 324 p.

Osborne, P.D. & Greenwood, B. (1992a). Frequency dependent cross-shore suspended sediment transport. 1. A non-barred shoreface. *Marine Geology*, 106: 1-24.

Osborne, P.D. & Greenwood, B. (1992b). Frequency dependent cross-shore suspended sediment transport. 2. A barred shoreface. *Marine Geology*, 106: 25-51.

Osborne, P.D. & Vincent, C.E. (1992) Timescales of bed response in a low energy surf zone. *Coastal Engineering*, Proceedings, Vol 2: 2321-2331.

Ribberink, J.S. & Al-Salem, A.A. (1995). Sheet flow and suspension of sand in oscillatory boundary layers. *Coastal Engineering*, 25: 205-225.

Swart, D.H., (1974). Offshore sediment transport and equilibrium beach profiles. Pub. No. 131. Delft Hydr. Lab.

1933

1933

1937

APPENDICES

Appendix 1: Wave Refraction Model WBEND

A1.1 List of notation

x,y,z	orthogonal space dimensions
F	wave power (Wm^{-1})
θ	wave angle (radians)
F_D	combination of bed friction (F_f) and wave breaking (F_b) dissipation terms
F_f	bed friction coefficient
E	wave energy (Jm^{-2})
Cg	wave group speed (ms^{-1})
ρ	fluid density (kgm^{-3})
g	gravitational constant (9.81 m^2s^{-1})
H	wave height (m)
k	wave number (m^{-1}) = $2\pi/L$, L = wavelength (m)
ω	wave radian frequency (Hz)
Ψ	smoothing function for wave height or wave angle
ε	eddy viscosity coefficient (m^2s^{-1})
φ	wave height (m) or wave angle (°)
C_f	friction coefficient
H_L	friction term expressed as wave height loss per unit path length s
s	unit path length (m)
f	frequency (Hz)
H_f	wave height associated with spectrum band of frequency f (m)
H_{rms}	root-mean-square wave height (m)
Δf	spectral bandwidth (Hz)
$S(f)$	spectral density ($m^2.s$)
N_f	number of frequencies in the spectrum
ω_{av}	average radian frequency (Hz)
k_{av}	average wave number (m^{-1})
γ	breaking ratio

A1.2 General description

Model WBEND (Black and Rosenberg, 1992a, Black, 1997) is a 2-dimensional numerical wave refraction model for monochromatic waves or a wave spectrum over variable topography. The model applies a fast, iterative, finite-difference solution of the wave action equations to solve for wave height, wave period, breakpoint location and longshore sediment transport. WBEND provides for:

- variable bathymetry;
- time-varying boundary conditions;
- the wave spectrum;

- options to “enhance” the wave shoaling to overcome the limitations of linear theory;
- a range of friction formulae for different physical conditions;
- third-order differential approximations to eliminate grid scale “wiggles”;
- a “diffusion” scheme to parameterize diffraction;
- longshore sediment transport on beaches;
- continuity of style throughout the suite of linked models and support software;
- software tools for data input, model output manipulation and graphical presentation;
- graphical output using the Matlab routine Plot3DD[1].

A1.3 Model equations

WBEND is a two-dimensional wave propagation model that uses, as a basis for refraction, the wave action equation for the conservation of wave power in two dimensions given by,

$$\frac{\partial}{\partial x}(F\cos\theta)+\frac{\partial}{\partial y}(F\sin\theta)=-F_D \qquad \text{(A1.1)}$$

where x and y are orthogonal co-ordinates, θ is the wave angle and F_D $(=F_f+F_b)$ is a combination of the bed friction (F_f) and wave breaking (F_b) dissipation terms. F is the wave power which, for Airy waves, is

$$F = EC_g = \frac{1}{8}\rho g H^2 C_g \qquad \text{(A1.2)}$$

where E is the wave energy, C_g is the group speed, ρ is the fluid density, g is gravitational acceleration and H is the wave height.
The wave angle is obtained from the equation for conservation of wave number

$$\frac{\partial}{\partial x}(|k|\sin\theta)-\frac{\partial}{\partial x}(|k|\cos\theta)=0 \qquad \text{(A1.3)}$$

The model solves equations A4.1 and A4.3 for wave power and wave angle respectively using a shoreward marching iterative scheme (Black and Rosenberg, 1992b). Height and angle are directly obtained on a regular finite difference grid, which eliminates the need for interpolation, as required when a ray tracking procedure is used.

To obtain the wave number k, the dispersion relation for linear waves,

[1] Plot3DD, Gorman, R.M. (1995)

$$\omega^2 = gk \tanh(kh) \qquad \text{(A1.4)}$$

is solved using an iterative *Newton-Raphson* technique, given the radian frequency ω and depth *h*.

A formulation based on the horizontal eddy viscosity in the hydrodynamic model 3DD (Black, 1995) is used to smooth the height and angle solutions. This has the effect of spreading energy along the wave crests, similar to the process of diffraction. While solving the wave action and conservation of wave number equations, heights and angles are smoothed by the function ψ given by,

$$\psi = \varepsilon\left(\frac{\partial^2 \varphi}{\partial y^2}\right) \qquad \text{(A1.5)}$$

where ε is the eddy viscosity coefficient and φ is either wave height or angle. The dominant wave direction is along the model's *x*-axis, and so the term acts primarily along the wave crests. The eddy viscosity coefficient is set by calibration. Simulations of several different environments (e.g. Black and Rosenberg, 1992b; Hutt, 1997; McComb et al., 1997) have indicated that appropriate values are in the range $0.02 < \varepsilon < 0.06$.
For monochromatic cases, the wave-energy frictional dissipation term is given by,

$$F_f = \frac{\rho C_f}{6\pi}\left(\frac{H\omega}{\sinh(kh)}\right)^3 \qquad \text{(A1.6)}$$

where C_f is the friction coefficient.

For a wave spectrum, mean bed orbital velocity is obtained from the variance in the spectrum, using the linear theory transform function to relate sea surface wave height and period to bed orbital motion. The transform function is applied to each spectral estimate and then the spectrum is re-constituted to obtain total bed orbital variance. The friction term adopted in the model, expressed as a height loss H_L per unit path length *s*, becomes,

$$\frac{\partial H_L}{\partial s} = \frac{2.83 C_f H_f H_{rms} \omega_f^2 \omega_{av}}{3\pi g C_g \sinh^2(k_f h)\sinh(k_{av} h)} \qquad \text{(A1.7)}$$

where H_f is the height of the wave associated with the spectral band of frequency *f*, radian frequency ω_f and wave number k_f given by,

$$H_f = 2.83(S_f \Delta f)^{1/2} \qquad \text{(A1.8)}$$

where S_f is the spectral energy density of the band with frequency f, and Δf is the bandwidth.

H_{rms} is the root-mean-square wave height calculated from the total variance in the spectrum as,

$$\langle \eta^2 \rangle = \sigma^2 = \int_0^\infty S(f)df = \sum_0^{f_n} S_f \Delta f$$
$$H_{rms} = 2.83\sigma \qquad \text{(A1.9)}$$
$$H_s = 4\sigma$$

while the average radian frequency ω_{av} is given by,

$$f_{av} = \frac{\sum H_f f}{\sum H_f} \qquad \text{and} \qquad w_{av} = 2\pi f_{av} \qquad \text{(A1.10)}$$

The summations are across all N_f frequencies in the spectrum. The corresponding wave number k_{av} is defined by the dispersion relation as,

$$\omega_{av}^2 = g k_{av} \tanh(k_{av} h) \qquad \text{(A1.11)}$$

The group speed C_g is the speed coinciding with the frequency ω_{av} and wave number k_{av}.
When solving in the model, the wave path length is assumed to consist of a series of straight line segments across each cell of width Δx for a wave travelling at angle θ. Thus the path length is

$$\Delta s = \Delta x / \cos\theta \qquad \text{(A1.12)}$$

The total height loss is summed across the model grid, row-by-row, after initially solving eqn A4.1, assuming $F_D = 0$.

Wave breaking is assessed by checking if height exceeds a depth limitation, that is if,

$$H > \gamma h \qquad \text{(A1.13)}$$

where γ is user selected and is typically of order 0.6-0.8.

A1.4 Model Grids and files

The model adopts a rectangular grid for bathymetry. The *x*-direction is positive to the east and corresponds with increasing '*I*', while the *y*-direction is positive northwards and corresponds with increasing '*J*'. The cell (1,1) is located at the bottom left corner of the grid and the maximum coordinate cell (I_{max} , J_{max}) is at the top right corner. The model assumes the shoreline is at the eastern side of the grid (maximum *I*). Wave angle is defined relative to the left ("east") of the grid and is positive anti-clockwise (Cartesian axes).

Model WBEND requires three input files which are:

1. Information file
2. Wave height, period and angle file, or spectrum file
3. Bathymetry file

One information file controls the model by providing the input data and output file names. More information on the options used in the information file can be found in the WBEND user's manual (Black, 1997).

WBEND has three types of boundary condition that can be used: the probability file listing wave events and their probability of occurrence; the spectrum file containing spectral densities and frequencies for a sea surface spectrum; and the sediment transport contour file for calculation of surf zone littoral drift. WBEND produces several output files, outlined in detail in the user's manual. The binary file, *filename.out*, was the main file used for the present study. This contains depths, wave heights, wave periods, and bottom orbital motion over the full grid for each simulated event.

A1.5 Previous applications of the model and selected references

Model WBEND has been used for a range of applications since its original development in 1991. The broad categories of study include:

- investigations for proposed marina developments;
- beach, bay and shelf sediment dynamics studies;
- artificial surfing reef investigations;
- surf zone wave transformations.

A selection of publications which have arisen from these applications are summarised below:

Black, K.P.; Rosenberg, M.A. (1992a). Natural stability of beaches around a large bay. *Journal of Coastal Research*. 8(2): 385-397.

Black, K.P.; Rosenberg, M.A. (1992b). Semi-empirical treatment of wave transformation outside and inside the breaker line. *Coastal Engineering.* 16: 313-345.

Black, K.; Rosenberg, M.; Symonds, G.; Simons, R.; Pattiaratchi, C.; Nielsen, P. (1995) *Measurements of wave, current and sea level dynamics of an exposed coastal site.* Chapter 2 in "Mixing Processes in estuaries and coastal seas". C. Pattiaratchi (ed.). American Geophysical Union. p.29-58.

Black, K.; Andrews, C.; Green, M.O.; Gorman, R.M.; Healy, T.R.; Hume, T.M.; Hutt, J.; Mead, S.; Sayce, A. (1997). Wave dynamics and shoreline response on and around surfing reefs. Ist International Surfing Reef Symposium, Sydney, March 1997.

Black, K.P. (1997) *Wave refraction model WBEND*. Occasional Report, Centre of Excellence in Coastal Oceanography and Marine Geology, Department of Earth Sciences, University of Waikato, New Zealand. (in prep.)

Hutt, J.A. (1997) Bathymetry and wave parameters defining the surfing quality of 5 adjacent reefs. MSc thesis. Centre of Excellence in Coastal Oceanography and Marine Geology, Earth Sciences Department, University of Waikato. 170 pp.

McComb, P.; Black, K.P.; Atkinson, P. (1997). High-resolution wave transformation on a coast with complex bathymetry. Pacific Coasts and Ports'97, Christchurch, 7-11 September 1997.

Appendix 2: Hydrodynamic and Advection/Dispersion Model 3DD

A2.1 List of notation

u	velocity in the x direction (m / s)
v	velocity in the y direction (m / s)
w	velocity in the z direction, positive upward (m / s)
t	time (s)
dx	size in the x-direction of an averaging region (m)
dy	size in the y-direction of an averaging region (m)
dz	size in the z-direction of an averaging region (m)
A_H	horizontal eddy viscosity coefficient (m^2s^{-1})
f	Coriolis parameter
N_Z	vertical eddy viscosity coefficient (m^2s^{-1})
P	pressure (hPa)
S_b	represents Boussinesq terms and other forcing terms including radiation stress
ρ	fluid density (kgm^{-3})
h	water depth (m)
z	vertical distance above seabed (m)
P_{atm}	atmospheric pressure (hPa)
g	gravitational constant (9.81 m^2s^{-1})
T	temperature (°C)
S	salinity (psu)
K_H	horizontal eddy diffusivity coefficient (m^2s^{-1})
K_Z	vertical eddy diffusivity coefficient (m^2s^{-1})
τ_x	wind stress in the x direction
τ_y	wind stress in the y direction
ξ	sea level
γ	wind drag coefficient
ρ_a	density of air
W	wind speed
W_x	wind speed in x direction
W_y	wind speed in y direction
$S(0)$	surface salinity
E_l	net evaporation
P_l	net precipitation
Q	net ocean heat flux
c	water heat capacity
τ^b_x	bottom stress in the x direction at seabed
τ^b_y	bottom stress in the y direction at seabed
u_h	bottom current in x direction
v_h	bottom current in y direction
C	Chezy's C
D	net depth (m)
i	cell number in i direction

j cell number in j direction

A2.2 General description

Model 3DD (Black, 1995) is a 3-dimensional circulation, advection / dispersion and heat transfer model, for application to vertically-stratified or homogeneous ocean, continental shelf and shallow water environments. An explicit finite difference (Eulerian) solution is used to solve the momentum and continuity equations for velocity and sea level, while the temperature and salinity advection / dispersion equations are solved using either Eulerian or Lagrangian particle techniques. Shallow water wave simulations use a Boussinesq approximation, solved with a semi-implicit iterative method (Gorman and Black, 1997). Heat transfers between the ocean and atmosphere are accommodated so that thermocline development can be simulated.

3DD has a number of common and novel features, including:

- a complete momentum equation for both deep or shallow barotropic and baroclinic environments.
- flooding and drying of inter-tidal zones
- a wide range of open boundary options, e.g. currents, sea levels, volumes, radiation conditions and sponges

In addition:

- the model can be operated in 2 or 3 dimensions using the same input files in both cases, thereby ensuring an effortless transition
- “side-view” (2-dimensional) simulations are catered for, so that vertical stratification can be simulated with high resolution.
- the side-view operation provides for a simplified longshore momentum balance for continental shelves
- 3DD is supported by a range of software tools for data input, model output manipulation and graphical presentation
- the procedures to specify the open boundaries are both simple to use and comprehensive
- third-order accurate derivative approximations eliminate grid-scale zig-zagging
- a body force can be applied to simulate large-scale pressure gradients associated with coastal trapped waves, other continental shelf waves or geostrophic gradients
- shallow-water form of the Boussinesq equations provide for simulations of finite-amplitude waves around ports, beaches or harbours
- a zero up-crossing technique is applied to find the wave heights
- radiation stress terms are calculated within the model and can be optionally included in the simulation to model wave-driven currents
- a special inter-tidal flooding and drying scheme prevents the development of velocity spikes on the sand banks when flooding first occurs
- an "effective depth" formulation prevents excessive frictional resistance in very shallow water

- a boundary slip parameter eliminates the problem of excessive damping of currents in narrow channels due to horizontal diffusion
- a variety of vertical eddy viscosity formulations are selectable
- barometric pressure and wind conditions, entered as time series from a number of locations, will be interpolated by the model
- heat inputs to the water body and thermocline formation can be simulated
- enhanced bed friction due to wave / current interaction can be selected
- hot starts are possible so that new runs can commence at any time during a prior simulation
- 3DD provides for nested simulations
- bathymetry can be represented on the cell walls (rather than cell mid-points) thereby maximising bathymetric resolution without increasing CPU requirements
- advection / dispersion can be treated using either a Eulerian scheme or Lagrangian scheme which is coupled to the hydrodynamics. Alternatively, these simulations can be separately undertaken with the Lagrangian model POL3DD
- model results are presented to the screen at run-time as a diagnostic aid to allow rapid assessment of model behaviour

A2.3 Model equations

3DD (Black, 1995) is a layered 3-dimensional hydrodynamic and transport / dispersion model which incorporates the vertically-averaged model hydrodynamic Model 2DD (Black, 1983). The 3-dimensional equations are,

$$\frac{\partial u}{\partial t}+\frac{u\partial u}{\partial x}+\frac{v\partial u}{\partial y}+\frac{w\partial u}{\partial z}-fv=-\frac{g\partial \varsigma}{\partial x}-\frac{1\partial P}{\rho\partial x}+A_H\left(\frac{\partial^2 u}{\partial x^2}+\frac{\partial^2 u}{\partial y^2}\right)+\frac{\partial}{\partial z}\left(N_z\frac{\partial u}{\partial z}\right)+S_b \quad \text{(A1.1)}$$

$$\frac{\partial v}{\partial t}+\frac{u\partial v}{\partial x}+\frac{v\partial v}{\partial y}+\frac{w\partial v}{\partial z}+fu=-\frac{g\partial \varsigma}{\partial y}-\frac{1\partial P}{\rho\partial y}+A_H\left(\frac{\partial^2 v}{\partial x^2}+\frac{\partial^2 v}{\partial y^2}\right)+\frac{\partial}{\partial z}\left(N_z\frac{\partial v}{\partial z}\right)+S_b \quad \text{(A1.2)}$$

$$w=-\frac{\partial}{\partial x}\int_{-h}^{z} u\,dz-\frac{\partial}{\partial y}\int_{-h}^{z} v\,dz \quad \text{(A1.3)}$$

t is the time, u, v are velocities in the x, y directions respectively, w the vertical velocity in the z direction (positive upward) at the top of each layer, h the depth, g the gravitational acceleration, ζ the sea level above a horizontal datum, f the Coriolis parameter, P the pressure, ρ the density of water, A_H the horizontal eddy viscosity coefficient, and N_Z the vertical eddy viscosity coefficient. S_b represents Boussinesq terms, discussed below, and other forcing terms including radiation stress calculated from the wave height spatial gradients and body forces.

The pressure at depth z is:

$$P = P_{atm} + g\int_{z}^{o} \rho \, dz \qquad \text{(A1.4)}$$

where P_{atm} is the atmospheric pressure. The conservation equations for temperature and salinity may be written as:

$$\frac{\partial T}{\partial t} + \frac{u\,\partial T}{\partial x} + \frac{v\,\partial T}{\partial y} + \frac{w\,\partial T}{\partial z} = \frac{\partial}{\partial z}\left(K_z \frac{\partial T}{\partial z}\right) + K_H\left(\frac{\partial^2 T}{\partial x^2} + \frac{\partial^2 T}{\partial y^2}\right) \qquad \text{(A1.5)}$$

$$\frac{\partial S}{\partial t} + \frac{u\,\partial S}{\partial x} + \frac{v\,\partial S}{\partial y} + \frac{w\,\partial S}{\partial z} = \frac{\partial}{\partial z}\left(K_z \frac{\partial S}{\partial z}\right) + K_H\left(\frac{\partial^2 S}{\partial x^2} + \frac{\partial^2 S}{\partial y^2}\right) \qquad \text{(A1.6)}$$

where T is temperature, S is salinity, and K_H, K_Z are the horizontal and vertical coefficients of eddy diffusivity.

Using the temperature and salinity, the density is computed according to an equation of state of the form,

$$\rho = \rho(T,S,z) \qquad \text{(A1.7)}$$

that is,

$$\begin{aligned} T_K &= T + 2.7 \\ \rho &= 1000(1 - 3.7\times10^{-6} T_K^2 + 8.13\times10^{-4} S) \end{aligned} \qquad \text{(A1.8)}$$

Surface boundary conditions at $z = 0$ are:

$$\rho N_z \frac{\partial u}{\partial z} = \tau_x^s$$

$$\rho N_z \frac{\partial v}{\partial z} = \tau_y^s \qquad \text{(A1.9)}$$

$$\frac{\partial \varsigma}{\partial t} + u\frac{\partial \varsigma}{\partial x} + v\frac{\partial \varsigma}{\partial y} = w^s$$

where τ_x^s, τ_y^s denote the components of wind stress and

$$\tau_x^s = \frac{\rho_a}{\rho}\gamma |W|\ W_x$$
$$\tau_y^s = \frac{\rho_a}{\rho}\gamma |W|\ W_y \qquad \text{(A1.10)}$$

ρ is the water density, W the wind speed at 10 m above sea level with W_x and W_y its x and y components, $\gamma$is the wind drag coefficient, ρ_a the density of air.

Surface boundary conditions for temperature and salinity are,

$$\rho\ N_z \frac{\partial S}{\partial z} = S_l \qquad \text{(A1.11)}$$
$$\rho\ N_z \frac{\partial T}{\partial z} = T_l$$

where

$$S_l = S(0)\ (E_l - P_l)/\rho \qquad \text{(A1.12)}$$
$$T_1 = Q/c$$

and $S(0)$ is the surface salinity, E_1 is the net evaporation, P_1 is the net precipitation mass flux of fresh water, Q is the net ocean heat flux and c is the water heat capacity.

At the sea bed, $z = -h$, we have

$$\rho\ N_z \frac{\partial u}{\partial z} = \tau_x^h \qquad \text{(A1.13)}$$
$$\rho\ N_z \frac{\partial v}{\partial z} = \tau_y^h$$

where τ_x^h, τ_y^h denotes the components of bottom stress. Applying a quadratic law at the sea bed,

$$\tau_x^h = g u_h (u_h^2 + v_h^2)^{1/2} / C^2 \qquad \text{(A1.14)}$$

$$\tau_y^h = g v_h (u_h^2 + v_h^2)^{1/2} / C^2$$

with u_h, v_h being the bottom currents and C is Chezy's C. For a logarithmic profile,

$$C = 18 \log_{10}(0.37 h/z_o) \qquad \text{(A1.15)}$$

where z_o is the roughness length.

Also,

$$\frac{\partial S}{\partial z} = 0$$

$$\frac{\partial T}{\partial z} = 0 \qquad \text{(A1.16)}$$

$$w_h = -u_h \frac{\partial h}{\partial x} - v_h \frac{\partial h}{\partial y}$$

to ensure no transport of mass, salinity or temperature through the bed.

The form of the horizontal eddy viscosity term results when the depth is presumed constant before taking the derivative of the horizontal shear stresses. The term, as presented, behaves as a velocity smoothing algorithm. The horizontal eddy viscosity coefficient is a variable in space in the model.

A staggered finite difference grid is utilised similar to that applied by Leendertse and Liu (1975) which places the v and u components on “north” and “east” walls respectively. w is located in the centre of the "top" wall. The sea level replaces w in the top layer. The solution is found by time stepping with an explicit scheme.

A2.4 Boussinesq terms

For short surface wave applications, the momentum equations for depth-averaged velocity require additional ("Boussinesq") terms. Including these terms, the 2-dimensional form of equations A1.1 and A1.2 may be written

$$u_t = F^{(u)} + \frac{D}{2}\Big[(hu_t)_x + (hv_t)_y\Big]_x - \frac{Dh}{6}\Big[u_{xt} + v_{yt}\Big]_x \qquad \text{(A1.17)}$$

$$v_t = F^{(v)} + \frac{D}{2}\Big[(hu_t)_x + (hv_t)_y\Big]_y - \frac{Dh}{6}\Big[u_{xt} + v_{yt}\Big]_y \qquad \text{(A1.18)}$$

where $F^{(u)}$ and $F^{(v)}$ represent the terms previously considered, and h is the mean still-water depth. Subscripts x, y, t denote partial derivatives. In the original form (Peregrine, 1967), $D = h$, but following McCowan (1985), a version in which D is the net depth $h + \zeta$ is also considered; both forms are supported for 2-dimensional modelling in 3DD.

On the eastern wall of cell (i,j), the depth $h^{(u)}{}_{i,j}$ and the x component of velocity $U_{i,j}{}^{(n)}$ at time step n are defined, while the depth $h^{(v)}{}_{i,j}$ and the y component of velocity $V_{i,j}{}^{(n)}$ at time step n are located on the northern wall. Defining the velocities at the next step as the standard 3DD prediction (ie. solving (A1.17, A1.18) with $\vec{S}$ = 0), plus a Boussinesq correction:

$$U_{i,j}{}^{(n+1)} = U_{i,j}{}^{(n)} + F^{(u)}{}_{i,j}\delta t + \hat{U}_{i,j}\,, \qquad \text{(A1.19)}$$

$$V_{i,j}{}^{(n+1)} = V_{i,j}{}^{(n)} + F^{(v)}{}_{i,j}\delta t + \hat{V}_{i,j}\,, \qquad \text{(A1.20)}$$

the momentum equations may be written in difference form as

$$\hat{U}_{i,j} - \frac{D_{i,j}}{\delta x^2}\Big[\tfrac{1}{2}(h^{(u)}{}_{i+1,j}\hat{U}_{i+1,j} - 2h^{(u)}{}_{i,j}\hat{U}_{i,j} + h^{(u)}{}_{i-1,j}\hat{U}_{i-1,j}) - \tfrac{1}{6}h^{(u)}{}_{i,j}(\hat{U}_{i+1,j} - 2\hat{U}_{i,j} + \hat{U}_{i-1,j})\Big]$$

$$= \frac{D_{i,j}}{\delta x^2}\Big[\tfrac{1}{2}(h^{(u)}{}_{i+1,j}F^{(u)}{}_{i+1,j} - 2h^{(u)}{}_{i,j}F^{(u)}{}_{i,j} + h^{(u)}{}_{i-1,j}F^{(u)}{}_{i-1,j}) - \tfrac{1}{6}h^{(u)}{}_{i,j}(F^{(u)}{}_{i+1,j} - 2F^{(u)}{}_{i,j} + F^{(u)}{}_{i-1,j})\Big]$$

$$- \frac{D_{i,j}}{\delta x\,\delta y}\Big[\tfrac{1}{2}(h^{(v)}{}_{i+1,j}\hat{V}_{i+1,j} - h^{(v)}{}_{i,j}\hat{V}_{i,j} - h^{(v)}{}_{i+1,j-1}\hat{V}_{i+1,j-1} + h^{(v)}{}_{i,j-1}\hat{V}_{i,j-1}) - \tfrac{1}{6}h^{(u)}{}_{i,j}(\hat{V}_{i+1,j} - \hat{V}_{i,j} - \hat{V}_{i+1,j-1} + \hat{V}_{i,j-1})\Big]$$

(A1.21)

and

$$\hat{V}_{i,j} - \frac{D_{i,j}}{\delta y^2}\Big[\tfrac{1}{2}(h^{(v)}{}_{i,j+1}\hat{U}_{i,j+1} - 2h^{(v)}{}_{i,j}\hat{V}_{i,j} + h^{(v)}{}_{i,j-1}\hat{V}_{i,j-1}) - \tfrac{1}{6}h^{(v)}{}_{i,j}(\hat{V}_{i,j+1} - 2\hat{V}_{i,j} + \hat{V}_{i,j-1})\Big]$$

$$= \frac{D_{i,j}}{\delta y^2}\Big[\tfrac{1}{2}(h^{(v)}{}_{i,j+1}F^{(v)}{}_{i,j+1} - 2h^{(v)}{}_{i,j}F^{(v)}{}_{i,j} + h^{(v)}{}_{i,j-1}F^{(v)}{}_{i,j-1}) - \tfrac{1}{6}h^{(v)}{}_{i,j}(F^{(v)}{}_{i,j+1} - 2F^{(v)}{}_{i,j} + F^{(v)}{}_{i,j-1})\Big]$$

$$-\frac{D_{i,j}}{\delta x\,\delta y}\left[\tfrac{1}{2}(h^{(u)}{}_{i,j+1}\hat{U}_{i,j+1}-h^{(u)}{}_{i,j}\hat{U}_{i,j}-h^{(u)}{}_{i-1,j+1}\hat{U}_{i-1,j+1}+h^{(u)}{}_{i-1,j}\hat{U}_{i-1,j})-\tfrac{1}{6}h^{(v)}{}_{i,j}(\hat{U}_{i,j+1}-\hat{U}_{i,j}-\hat{U}_{i-1,j+1}+\hat{U}_{i-1,j})\right]$$

(A1.22)

To solve these, $\hat{U}$ and $\hat{V}$ are first set to zero, and (A1.21) is solved for $\hat{U}$ by a tridiagonal algorithm along each row of constant *j*. $\hat{V}$ is found similarly from (A1.22). This process is iterated with updated $\hat{V}$ terms in the $\hat{U}$ equation and vice-versa until convergence is reached. Typically around 5 iterations are required for 1% precision.

A2.5 Previous applications of the model and selected references

Model 3DD and its predecessors (Model 2DD, Model 1D2D) have been applied to a wide variety of applications since original development in 1983. The broad categories of study include:

* investigations for proposed port developments,
* continental shelf tidal and sub-tidal hydrodynamics,
* scientific investigations of sediment dynamics,
* estuarine salinity-intrusion studies,
* hot water discharges,
* larval dispersal studies.

A selection of publications which have arisen from these applications are summarised below:

Black, K.P. (1984). *Sediment Transport. Tauranga Harbour Study.* Consulting Report to the Bay of Plenty Harbour Board, New Zealand. Volume 1 (Text) 159 pp. and Volume 2 (Fig.s and Tables).

Black, K.P. (1987). *A numerical sediment transport model for application to natural estuaries, harbours and rivers.* In: 'Numerical modelling applications to marine systems'. ed.: J. Noye. North Holland / Elsevier. Mathematics Studies No. 145, pp. 77-105.

Black, K.P. and Gay, S.L. (1987). Eddy formation in unsteady flows. *Journal of Geophysical Research.* 92 (C9): 9514-9522.

Black, K.P.; Healy, T.R. (1988). Formation of ripple bands in a wave convergence zone. *Journal of Sedimentary Petrology*, 58: 195-207.

Black, K.P.; Healy, T.R.; Hunter, M. (1989). Sediment dynamics in the lower section of a mixed sand and shell-lagged tidal estuary. *Journal of Coastal Research.* 5(3): 503-521.

Black, K.P. et al. (1989). *Influences on the marine environment of cooling water discharged to Bream Bay from a proposed 1000 MW power station - physical aspects. Volume 1 - Main Report.* Prepared for GHD -Black and Veatch Pty Ltd. Victorian Institute of Marine Sciences. 133 pp.

Black, K.P.; Colman, R.; Chidgey, S. (1989) *The water quality and flushing of a proposed canal development at Safety Beach "Martha Cove"*. Report for Watsons Pty Ltd. Victorian Institute of Marine Sciences. 39 pp.

Black, K.P. and McShane, P.D. (1990) The influence of surface gravity waves on wind-driven circulation in intermediate depths on an exposed coast. *Australian Journal Marine Freshwater Research.* 41:353-363.

Black, K.P.; Gay, S.L.; Andrews, J.C. (1990). Residence times of neutrally-buoyant matter such as larvae, sewage or nutrients on coral reefs. *Coral Reefs.* 9: 105-114.

Black, K.P.; Hatton, D.N.; Colman, R.S. (1990). *Prediction of extreme sea-levels in northern Port Phillip Bay and the possible effects of a rise in mean sea level.* Report to the Board of Works Melbourne. Victorian Institute of Marine Sciences. 48 pp.

Black, K.P.; Moran, P.J. (1991) The influence of hydrodynamics on the passive dispersal and initial recruitment of larvae of the crown-of-thorns starfish on the Great Barrier Reef. *Marine Ecology Progress Series*. 69: 55-65.

Black, K.P.; Moran, P.J.; Hammond, L.S. (1991) Numerical models show coral reefs can be self-seeding. *Marine Ecology Progress Series.* 74: 1-11.

Black, K.P. (1992) Evidence of the importance of deposition and winnowing of surficial sediments at a continental shelf scale. *Journal of Coastal Research.* **8**(2): 319-331.

Black, K.P. (1992) The relative importance of local retention and inter-reef dispersal of neutrally-buoyant material on coral reefs. *Coral Reefs*. In press.

Black, K.P. (1992) *The dynamics of Port Phillip Bay and adjacent Bass Strait.* Victorian Institute of Marine Sciences Report for the Port Phillip Bay Model Consortium. Victorian Institute of Marine Sciences Technical Report No. 18. 120 pp.

Black, K.P. (1993) *Assessment of the proposed expansion of the port facilities for an existing ferry at Queenscliff - Hydrodynamics and sediment transport.* Report for the Borough of Queenscliffe. 21 pp.

Black, K.P.; Sokolov, S. (1993) New Plymouth power station consent renewal thermal plume studies. *Vict Inst Mar Sci.* 232 pp.

Black, K.P.; Hatton, D.J. (1993) Two and three-dimensional numerical hydrodynamic and dispersal models of an open coastal site. *11th Australasian Conference on Coastal and Ocean Engineering.* Townsville, August, 1993. (in press).

Black, K.; Hatton, D.; Rosenberg, M. (1993) Locally and externally-driven dynamics of a large semi-enclosed bay in southern Australia. *Journal of Coastal Research*. In press.

Black, K.P.; Hatton, D.N. (1993) Two and three-dimensional numerical hydrodynamic models of an exposed coastal site. *11th Australasian Conference on Coastal and Ocean Engineering. Coastal Engineering - A Partnership with Nature.* Townsville, 23-27 August, 1993.

Black, K.P.; Gorman, R.M.; Burrage, D. (1995) Broad-scale numerical model boundary conditions assimilating a 25-year current hindcast: Central Great Barrier Reef. *Continental Shelf Research* (to be submitted).

Colman, R.S.; Black, K.P. (1988). Use of numerical models in port design and management. *2nd Australasian Port, Harbour and Offshore Engineering Conf.* Brisbane. Inst of Engineers. ACT, Australia. pp. 32-36.

Gorman, R.; Black, K.; Sokolov, S. (1995) *Physical processes and sediment transport study for proposed modifications to the Port of Taranaki*, Victorian Institute of Marine Sciences consulting report.

Gorman, R.M.; Sokolov, S.; Turnbull, J. (1995) *Marsden A Power Station consent renewal thermal plume studies*, Victorian Institute of Marine Sciences consulting report.

Greilach, P.; Easton, A.; Black, K.; Colman, R. (1991). *The interpolation of currents within the Great Barrier Reef for use in the On-Scene Spill Model (OSSM).* Report to the Australian Maritime Safety Authority, Canberra.

Healy, T.R.; Black, K.P.; de Lange, W.P. (1987). Field investigations required for numerical model studies of port developments in large tidal inlet harbours. *International Geomorphology*. pp.1099-1112.

Jenkins, G.P; Black, K.P. (1993) Temporal variability in settlement of a coastal fish, the King George whiting, Sillaginodes punctata, is determined by hydrodynamic factors. *Bulletin Marine Science*

McShane, P.E.; Black, K.P.; Smith, M.G. (1988). Recruitment processes in Haliotis rubra (Mollusca:Gastropoda) and regional hydrodynamics in south-east Australia imply localised dispersal of larvae. *Journal of Experimental Marine Biology and Ecology*. 124: 175-203.

Middleton, J.F.; Black, K.P. (1994) The low frequency circulation in and around Bass Strait: a numerical study. *Continental Shelf Research* 14(13 / 14): 1495-1521.

Appendix 3: Sediment Transport Model GENIUS

A3.1 MODEL DESCRIPTION AND OPERATION

Model **GENIUS** predicts refraction, break point wave conditions and longshore sediment transport on beaches. The results are obtained by assuming that the longshore variability in bathymetry is small so that Snell's Law is applicable. When this assumption is not acceptable, predictions are made using WBEND. GENIUS is similar to the better-known model GENESIS (Hanson and Kraus, 1989) but with some improvements including the addition of frictional attenuation of wave height and a more physically-based treatment of wave transmission factors across submerged reefs.

The model accepts a time series of wave conditions to find net sediment fluxes. Offshore wave heights are brought into a shallow water site using linear wave relationships to find the refraction and shoaling coefficients. Frictional attenuation is applied by approximating the methods adopted by WBEND. Breakpoint height and angle are obtained by iteration around the breakpoint of the linear wave refraction and shoaling relationships while longshore sediment transport is calculated using the CERC formula applied in GENESIS. Input data to the model is in the file **LONG.DAT** which is presented as Table A3.1.

Table A3.1: Example of the information file used to control GENIUS

```
LONG.DAT     LONGSHORE SEDIMENT MODEL DATA
K:\BLACK\BRIS.TOT
2        NUMBER OF HEADER LINES IN WAVES FILE
1        TIME COLUMN IN WAVES FILE
1        WAVE HEIGHT COLUMN IN WAVES FILE
3        WAVE PERIOD COLUMN IN WAVES FILE
4        DIRECTION COLUMN IN WAVES FILE
0       MINIMUM PERIOD IN REFRACTION STAGE
-65,85    ALLOWABLE ANGLE RANGE
11.5      MAGNETIC NORTH CORRECTION TO BOUNDARY ANGLES
80        OFFSHORE WATER DEPTH (m)
7.1       INSHORE WATER DEPTH (m)
10        SHORELINE ANGLE RELATIVE TO N/S (degrees)
0.02      INNER SHELF FRICTION COEFFICIENT CF
0.04      BREAKPOINT FRICTION COEFFICIENT CFB
27000     CROSS-SHORE DISTANCE FROM OFFSHORE TO INSHORE SITES (m)
0.23      D50 GRAIN SIZE (mm)
0.02      AVERAGE SEA BED SLOPE
0.58      K1 LONGSHORE SEDIMENT TRANSPORT PARAMETER
1.0       TRANSMISSION COEFFICIENT
100.0     MAXIMUM WAVE HEIGHT ABLE TO CROSS OFFSHORE REEF (m)
90.       ANGLE WINDOW OF WAVES AFFECTED BY OFFSHORE OBSTACLE
```

The first line is any ID and second line is the name of the file containing the waves data. All other lines are self explanatory, expect for the last three. The transmission coefficient is the fraction of wave height which is able to pass across an offshore structure. While the structure is not specifically represented, its presence is felt by this value. Alternatively, the maximum wave height able to cross the stucture can be set in the second last line. For long, thin structures or submerged breakwaters, energy can reach the beach when the wave angle is greater than a minimum value. This minimum value is set in the last line. 90^o means that all waves are affected by the maximum height coefficient, while 10^o indicates that only those waves approaching with angles less than +/- 10^o are affected. For the friction, typical C_f values are 0.01-0.09. However, the approximation for friction can cause heights to be severely dissipated if the friction coefficient is set too high in shallow water. The longshore transport coefficient K_1, is normally in the range 0.58-0.77.

Two output files are written:
LONG.OUT containing offshore and inshore wave parameters
QB.OUT containing breakpoint wave parameters and net sediment flux

Note: The model expects significant heights as inputs, not mean or rms heights.

A3.2 MODEL EQUATIONS

The Model GENIUS adopts the CERC formula for longshore sand transport rate given by,

$$Q = (H^2 C_g)_b \left[a_1 \sin(2\theta_{bs})\right]_b \qquad \text{(A3.1)}$$

where

H = wave height
C_g = wave group speed given by linear wave theory
b = subscript denoting wave breaking condition
θ_{bs} = angle of breaking waves to the local shoreline

the non-dimensional parameter a_1 is given by

$$a_1 = \frac{K_1}{16(\rho_s / \rho - 1)(1 - P)(1.416)^{5/2}} \qquad \text{(A3.2)}$$

where

K_1 = empirical coefficient, treated as a calibration parameter
ρ_s = density of sand (taken as 2650 kg.m^{-3} for quartz sand)
ρ_w = density of water (taken as 1025 kg.m^{-3} for seawater)
P = porosity of sand on the bed (taken to be 0.4)

In accordance with the strategy adopted by GENESIS, the factors involving 1.416 are used to convert from significant height to root-mean-square (rms) wave height.

To calculate the height of inshore or breaking waves that have been transformed by refraction and shoaling,

$$H_2 = K_R K_S K_f H_0 \qquad \text{(A3.3)}$$

where

H_2 = inshore wave height
K_R = refraction coefficient
K_S = shoaling coefficient
K_f = frictional coefficient

The refraction coefficient is given by

$$K_R = (\cos\theta_0 / \cos\theta_2)^{1/2} \qquad \text{(A3.4)}$$

where

θ_0 = wave angle in deep water relative to the shoreline orientation
θ_2 = wave angle at the inshore site

The shoaling coefficient is given by

$$K_s = (C_{g0} / C_{g2})^{1/2} \qquad \text{(A3.5)}$$

where

C_{g0} = group speed offshore
C_{g2} = group speed inshore

The group speed is obtained using a Newton Raphson iterative solution of the linear wave dispersion relation

$$\sigma^2 = gk \tanh(kh) \qquad \text{(A3.6)}$$

where

σ = radian frequency
g = gravitational acceleration (9.81 $m.s^{-2}$)
k = wave number
h = water depth

The equation for depth limited breaking is given by

$$H_b = \gamma d_b \qquad \text{(A3.7)}$$

where

γ = breaker index often taken as 0.78

The wave angle transformation is calculated by Snell's Law

$$\frac{\sin\theta_0}{C_0} = \frac{\sin\theta_2}{C_2} \qquad \text{(A3.8)}$$

where

C_o = phase speed offshore

C_2 = phase speed inshore

Appendix 4: Submerged Reefs For Coastal Protection

Marine and Freshwater Consultants
P O Box 13048, Hamilton, New Zealand.
Ph. +64 7 834 8180, fax. +64 7 834 8188
E-mail s.mead@asrltd.co.nz Website www.asrltd.co.nz

Submerged structures for coastal protection: A short summary of what they are, why we need them and how they work

January 1999

What's special about offshore reefs

Offshore, submerged reefs provide a shoreline protection solution with low environmental impact. Visual amenity is not impaired, the reef is constructed offshore and there is no requirement for rock emplacement along the shoreline. Salient growth in the lee of the reef leads to enhanced shoreline stability and protection. *Recreational and public amenity can be incorporated through surfing, diving, sheltered swimming, water games, fishing and/or marine habitat.* The inclusion of amenity, however, requires the amalgamation of different purposes in the reef design and consequently the designed reef and interstitial substrate needs much more sophistication than that required for coastal protection only.

Figure 1: Raglan, New Zealand

Why we need them

The present situation in coastal protection is well described as a modern-day hiatus. Quite correctly, there has been a strong negative public reaction to rock emplacement along the coast. This has led to uncertainty by regulators and local government authorities about how to treat shoreline erosion. Many are resorting to “planned retreat” where houses are simply removed and the coast is left to erode. However, planned retreat can be expensive, unnecessary and sometimes impossible, especially in highly modified environments. While permission to modify or develop the frontal dune should never be given, coastal erosion and threats to property cannot be easily eradicated and so a solution is required.

Offshore, submerged reefs eliminate the need for rock emplacement on beaches and overcome the modern-day hiatus in shoreline protection by:

- unifying coastal protection and amenity benefits into a single structure placed offshore;
- enhancing coastal amenity value by incorporating multiple use options of surfing, diving, marine habitat, water games and sheltered swimming; and
- preserving existing beach amenity.

Most importantly, natural character is retained. The reef simply enhances wave breaking. When the swell is large, quality waves for surfing are available while, in calm seas, the reef provides recreation for divers and fishers. At all times, the reef provides shoreline protection and marine habitat.

Thus, offshore, submerged reefs are needed because other coastal protection solutions do not offer the same overall value to the community. They cater for the growing demand for more positive coastal amenity development and environmentally-friendly solutions to coastal protection. They achieve this by unifying coastal protection and amenity benefits into a multi-faceted structure. There is no need for any hard structure along the beach and the reef can be submerged at all times.

The use of offshore reefs

Offshore reefs can be permanently submerged, emerged or inter-tidal. In each case, the depth of the reef, its size and its position relative to the shoreline determine the coastal protection level provided by the reef. This ability to vary the protection level as part of the reef design cannot be achieved with hard rock structures like rock walls or groynes and breakwaters. These latter structures cannot be easily adjusted to the environment because they form impermeable barriers. On the contrary, offshore reefs allow sand to pass over their crest and between the reef and the shoreline.

Thus, offshore reefs are used when:

a partial blockage to sand is required;

hard-rock construction on the beach is not wanted or not suitable;

natural character is to be preserved; or

improved recreational and environmental amenity value is required.

Three case studies from the Artificial Reefs Program

To illustrate the use of Artificial Reefs, three reef designs developed for coastal protection and recreational amenity in physically-contrasting environments are presented and compared. The first is a large shore-normal submerged reef for the Gold Coast (Australia), on a sandy shoreline experiencing littoral sediment drift exceeding 450,000 $m^3.yr^{-1}$. The second is on the rocky New Plymouth coast (New Zealand) where littoral sediment supply is smaller and the design combined a submerged reef with an impermeable rock wall. In the third case, Port Gisborne (New Zealand) requested a surfing reef and enhanced marine habitat on new port walls as part of a major port expansion.

At all three sites, shoreline stabilisation and coastal protection were primary project goals but incorporation of recreational amenity was an essential additional requirement.

Reef design was undertaken using refraction/diffraction, wave-driven circulation and sediment transport numerical models. These were supplemented and calibrated by field data collected at the sites including deployments of wave-recording current meters, an instrumented sea sled hauled through and beyond the surf zone, sediment trapping and an automated video beach monitoring system. The surfing aspects were underpinned by bathymetry surveys of 38 of the world's best surfing reefs from around the Pacific Basin and Indonesia.

Gold Coast nourishment and coastal control

On the Gold Coast, a “double-sided” headland was designed which consisted of two arms extending 450 m offshore to the reef toe in 10.4 m depth. The reef was submerged at low tide and a large lagoon was placed in the lee of the two arms to provide sheltered swimming at low tide. World-class surfing waves were included on the offshore side of the two arms, providing “left” and “right” hand breaking waves. Wave interference patterns due to diffraction and refraction provided an inshore segment of “wedge-like” waves at the cross-over points for water games and all forms of surf craft. With the high longshore sediment transport on this coast, the inshore end of the reef was placed on the 2 m depth contour, leaving a gap between the reef and beach for sediment by-passing. Sediment is also expected to pass over the submerged reef crest. The ratio of cross-shore to longshore reef dimensions and the wave penetration into the lee of the reef by refraction and diffraction determined the size of the salient growth in the lee.

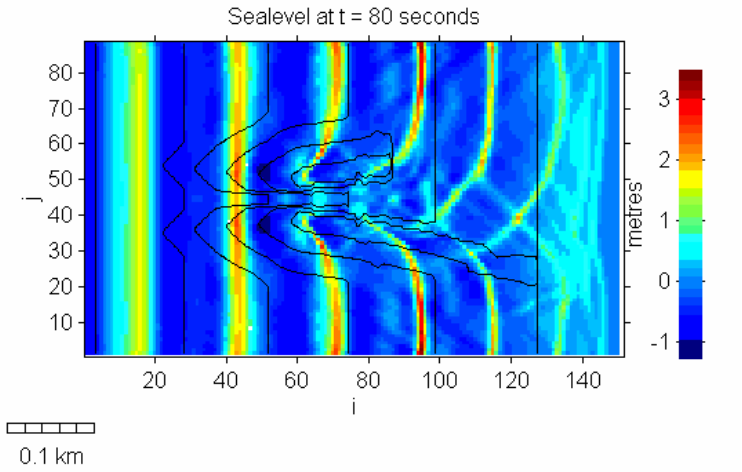

Figure 2: Waves crossing the bathymetry of the submerged reef designed for Australia’s Gold Coast.

New Plymouth City Foreshore

At New Plymouth, onshore facilities were merged with a multi-purpose structure offshore. Contrary to the Gold Coast case where littoral drift is large, much of the sediment transport at New Plymouth takes place offshore within the complex reef and sand topography. Natural sedimentation within the structure was predicted to be slow, requiring beach creation by initial nourishment and a design that retains this sand.

A curving rock wall, constructed of local rock, was adopted with an attached surfing reef. The reef dissipated wave energy, allowing wall height to be reduced while providing recreational amenity. Interstitial rock structure was chosen to enhance shellfish habitat. The sedimentary impact on downstream beaches was assessed in conjunction with a large field and modelling study being undertaken on behalf of the local port.

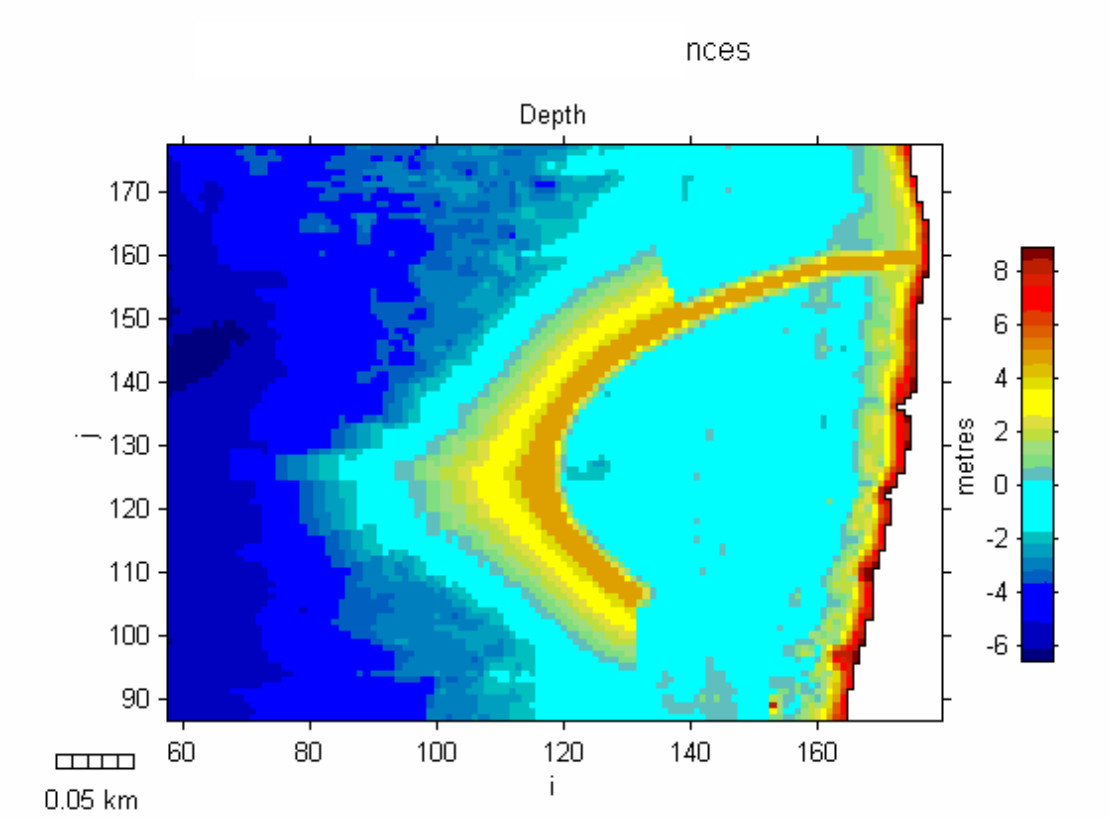

Figure 3: A feasibility design of the New Plymouth Reef. The surfing reef bathymetry is preliminary and subject to a detailed design phase.

Port Gisborne

At Gisborne, the surfing reef was added purely for its amenity value as part of the desire by the port to enhance local recreational facilities and tourism, and to mitigate for the effects of port expansion. The reef reduces wave impacts and its cost is partially compensated for by a reduction in wall height.

How they work to protect the coast

Most commonly, an offshore obstruction, such as a reef or island, will cause the shoreline in its lee to protrude in a smooth fashion, forming a salient or a tombolo. This occurs because the reef reduces the wave height in its lee and thereby reduces the capacity of the waves to transport sand. Consequently, sediment moved by longshore currents and waves builds up in the lee of the reef. The level of protection is governed by the reef's size and offshore position and so the size of the salient or tombolo varies in accordance with reef dimensions.

While considerable research has been done on shoreline response to emerged offshore breakwaters, very little qualitative work has been done on the effect of submerged offshore reefs, particularly beyond the laboratory. Thus, within the Artificial Reefs Program, Andrews (1997) examined aerial photographs seeking cases of shoreline adjustment to offshore reefs and islands. All relevant shoreline features in New Zealand and eastern Australia were scanned and digitised, providing123 different cases. A range of other statistics, particularly reef and island geometry, were also obtained. Andrews discovered that the size of salients (including length, offshore amplitude and shape) behind submerged reefs was predictable. For example, Fig. 6 shows that the distance between the tip of the salient and the offshore reef (X) can be predicted from the longshore dimension of the offshore reef (B) and its distance from the undisturbed shoreline (S). The relationship defined by the data is not totally consistent with previous studies of offshore breakwaters.

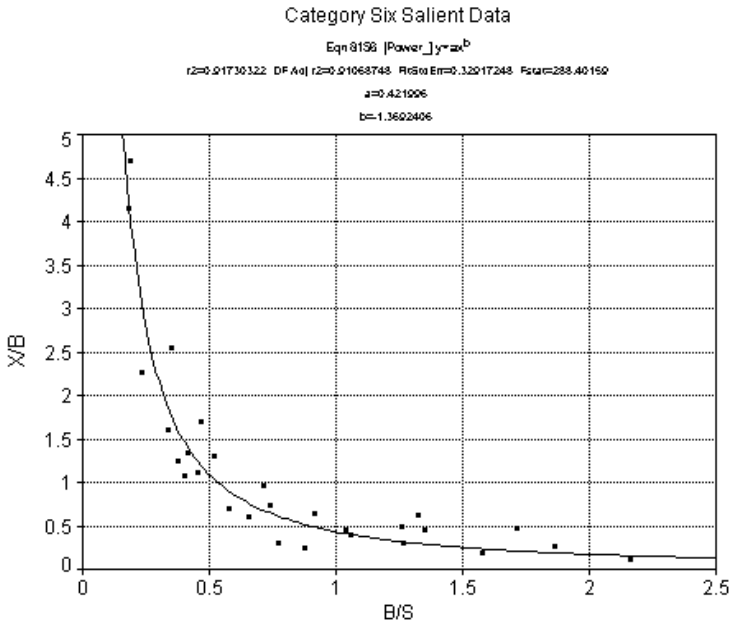

Figure 4: X/B versus B/S for submerged offshore reefs, where X is the distance of the tip of the salient from the offshore reef, B is the longshore dimension of the reef and S is the distance of the reef from the undisturbed shoreline.

Conclusions

Rock walls, breakwaters or groynes usually serve their purpose of protecting land from erosion and/or enabling safe navigation into harbours and marinas, but these same structures could also have recreational and commercial value. By incorporating multi-purpose recreational and amenity enhancement objectives can be incorporated into coastal protection and coastal development projects. Research and practical design is the focus of the "Artificial Reefs Program" (Fig. 5).

Figure 5: The Artificial Reefs Program at the Centre of Excellence in Coastal Oceanography and Marine Geology